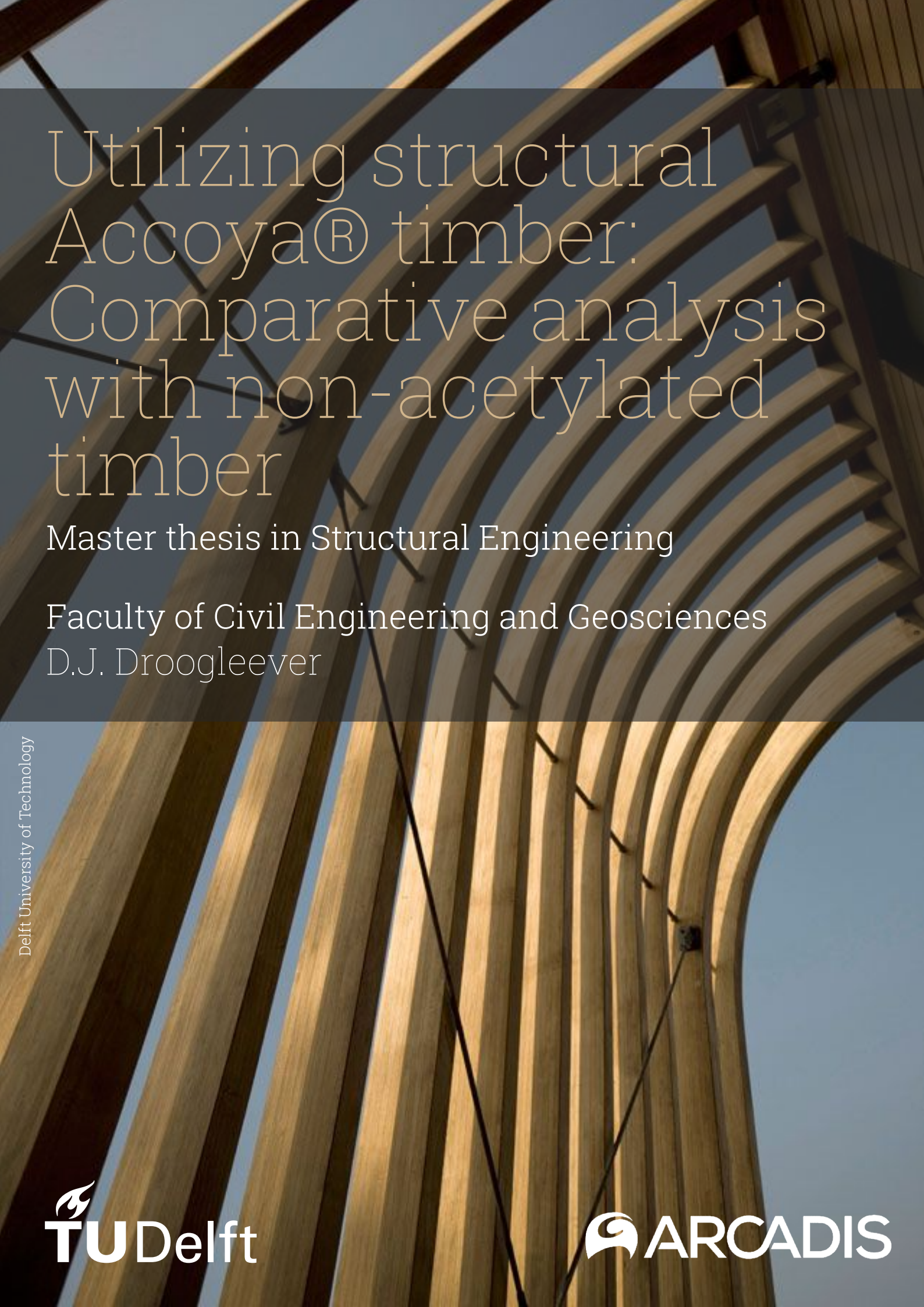

Utilizing structural Accoya® timber: Comparative analysis with non-acetylated timber

Master thesis in Structural Engineering

Faculty of Civil Engineering and Geosciences
D.J. Droogleever

Delft University of Technology

TU Delft

ARCADIS

Utilizing structural Accoya® timber: Comparative analysis with non-acetylated timber

Master thesis in Structural Engineering

by

D.J. Droogleever

4644204

Chairman:	Prof.dr.ir. J.W.G. van de Kuilen
Supervisor:	Dr.ir. P.A. Korswagen Eguren
Supervisor:	Drs. W.F. Gard
Supervisor:	Prof.dr.ir. M.A.N. Hendriks
Arcadis supervisor:	Ir. L. Alfrink
Arcadis supervisor:	BEng P. de Bliek
Faculty:	Civil Engineering and Geosciences, TU Delft

Cover: 'The Haven' boathouse, Norfolk (United Kingdom), Accoya® 2024.

TU Delft

Abstract

This research focuses on comparing Accoya® with unmodified wood and investigates Accoya®'s structural performance in environments with varying relative humidity levels. The wood's moisture content, and consequently its swelling and shrinking behavior, fluctuates on an annual basis due to these varying relative humidity levels, especially when exposed to outdoor conditions. FEM analyses were conducted to investigate physical properties and the performance of moment-resistant connections, with their implementation aimed at incorporating rotational stiffness into a structural portal frame. Accoya® demonstrates excellent moisture resistance and an increase in dimensional stability of approximately 80%, based on Dutch climate conditions. The reduction in swelling alleviates internal stresses within the connections, enhancing the strength and stiffness of moment-resisting connections. Specifically, a clamped connection and a circular dowel connection were analysed using a linear elastic static FEM model, revealing internal stress reductions of 81% and 52%, respectively. This reduction was observed during the simulated initial annual swelling cycle that the wood may undergo. With the use of Accoya®, significantly less plastic deformation is expected in connections due to swelling issues compared to unmodified wood and reduced deflection in structures is expected. An increase of 219% and 58% in rotational stiffness was observed for the respective cases. To evaluate the impact on overall stiffness, these observed values were implemented in a portal frame structure. A reduction in horizontal displacement was observed ranging from 31% to 66%. This opens up new possibilities in structural wood design, allowing for slimmer and lighter wood constructions. Due to Accoya®'s lower property degradation and more stable structural performance in high-humidity conditions, an adjustment of the k_{mod} and k_{def} factors is suggested; however, this is not sufficiently substantiated in the current study. Future research could explore long-term performance factors with experiments such as creep and fatigue to validate Accoya®'s structural reliability further.

Preface

This master's thesis was written to fulfill the requirements for obtaining my Master's degree in Structural Engineering at Delft University of Technology. I am a student with a Bachelor's degree in Architecture, Urbanism, and Building Sciences, who sought a technical challenge by transitioning to the Faculty of Civil Engineering and Geosciences.

When searching for a thesis topic, my primary criterion was its novelty, something that had not been done before and addressed a current and relevant problem. This project has taught me what it is like to work independently over an extended period, especially due to the lack of relevant expertise available during the first phase of my thesis.

I would like to express my gratitude to Arcadis for initiating the topic and providing intensive guidance throughout the process, with special thanks to Luuk Alfrink. I would also like to thank the entire committee for their guidance throughout my project. I have gained valuable insights through the process of writing my thesis and consider it an honor to have been mentored by esteemed experts with such extensive experience and knowledge.

D.J. Droogleever
December 2024

Contents

1

Introduction

Research context

Timber is, after concrete and steel, the third most commonly used material for structural frames, and its popularity is rising as sustainability becomes a key factor in material choices (Ramage et al., 2017). Accoya®, a brand of acetylated wood introduced in 2007, shows promise for structural applications due to its high durability, resistance to moisture, and dimensional stability. These improved properties, created through a chemical acetylation process that reduces moisture retention within the wood, make it suitable for outdoor applications. However, engineers and contractors are less familiar with heavy structural uses of Accoya® timber, and its potential in load-bearing applications is still largely unexplored.

Research problem

While Accoya® has been used primarily in non-structural applications, there is increasing interest in its structural potential due to its unique properties. Designing in wood is approached differently from the outset compared to designing in steel. This is due to wood's anisotropic properties, sensitivity to moisture, (unpredictable) (long-term) deformations, and high maintenance requirements. If some of these negatively influencing properties can be reduced, it opens up new possibilities for designing with wood. Currently, Accoya® timber lacks comprehensive European certification for structural glulam applications, and it is not yet included in the Eurocode for laminated beams, with only a certified strength classification of C22. Furthermore, there is limited data on its performance in large structural projects which will be the focus of this study.

Research objective

The objective of this research is to investigate Accoya®'s structural advantages and determine to what extent it could be a more suitable material than unmodified wood for outdoor structures, with a particular focus on the positive impact of its improved dimensional stability. The use of Accoya® in a train station canopy is employed as a case study for this purpose. The aim is to provide evidence for Accoya®'s performance in structural use, specifically in relation to key factors like rotational stiffness, dimensional stability, and moisture-induced stresses, which may support favorable calculation methods in international standards. This study will also investigate the potential of Accoya® in terms of increased lifespan, reduced CO_2 emissions, and low maintenance requirements by conducting a comprehensive literature review on the existing knowledge regarding Accoya®.

Research scope

This study focuses on the use of Accoya® timber for structural applications, with train station canopies serving as a case study. Accoya®'s performance will be analysed in the context of moment-resisting (doweled) timber connections using linear elastic static models. A comparative analysis will be conducted with non-acetylated timber of similar strength classifications but different swelling behavior to investigate how Accoya® might offer advantages in terms of strength and stiffness of timber load-bearing structures.

Research questions

Following from the research problem, objective and scope, the main research question with its sub-questions have been formulated. The sub-questions are designed to help answer the main research question. Underneath the questions, an explanation is given on how these questions will be answered.

How does Accoya® timber compare to non-acetylated timber in terms of structural performance?

- What are the characteristic properties of Accoya® and glulam Accoya®, and how is this certified?
- How do rigid clamped and circular dowel connections perform in Accoya® compared to unmodified Radiata pine?
- What role does the enhanced dimensional stability of Accoya® timber play in mitigating the effects of rotational stiffness variability in portal frame structures?
- How can Accoya® be utilized more advantageously in terms of strength and stiffness calculations considering adjustments to the k_{def} and k_{mod} factors compared to non-acetylated timber?

Research theory and methods

To address the first sub-question, a literature review will be conducted, detailing current understanding of Accoya®'s structural properties and certification standards. For the second sub-question, FEM analysis will be employed to investigate the behavior of (doweled) moment-resisting connections. This includes internal stresses, deflection, possibilities for plastic deformation and calculations for rotational stiffness. Simple models will be used initially for validation purposes, followed by more complex simulations to better represent real-world applications. The third sub-question is addressed by implementing found rotational stiffness values for different materials and connection types into a portal frame structure model. From this model, moment distributions and displacements are analysed. The fourth sub-question will explore potential adjustments to the k_{def} and k_{mod} factors, based on the observed behavior of Accoya® in numerical models and literature findings.

Hypothesis

Given Accoya®'s reduced shrinking and swelling, we hypothesize that this material will exhibit lower internal stresses and more stable stiffness properties compared to non-acetylated timber, even under fluctuating humidity conditions. The increased dimensional stability of Accoya® potentially makes it more suitable for structures requiring minimal deformation. It is anticipated that the enhanced dimensional stability of Accoya® will have varying effects on the resulting internal stresses and rotational stiffness, depending on the specific type of connection, but will in all cases have a positive influence.

Stakeholders

Prorail, on behalf of *Nederlandse Spoorwegen* is directly responsible for the implementation and maintenance of train station structures. Their values include ensuring the safety, reliability, and efficiency of train stations and the railway network. The introduction of Accoya® timber could enhance the sustainability and durability of these structures. If Accoya® proves to be a highly suitable material for train station structures, it could lead to more sustainable construction practices, potentially reducing the carbon footprint associated with railway infrastructure projects.

Arcadis is essential for the practical implementation of research findings in construction projects together with other construction and engineering firms. These firms value innovation, efficiency, and safety in construction practices. Engineering firms will apply the research findings directly to design and construct train station structures. This could result in more sustainable construction designs, improved project timelines, and enhanced structural performance.

Users of train stations are directly affected by the quality and safety of the infrastructure. They value safety and comfort in public transport facilities. Additionally, the sustainable appearance can enhance public satisfaction and support for sustainable infrastructure investments.

Technische Universiteit Delft, together with other research institutions, will be focused on advancing knowledge and innovation in structural engineering and materials science. It will possibly continue to research and validate the properties of Accoya® timber, potentially leading to further innovations and improvements. Successful implementation in train stations could provide valuable case studies and data for future research, driving further advancements in sustainable construction.

2

Case study

In this thesis, the principle of a station platform canopy is used as a case study to investigate the potential benefits of structural Accoya®. Given that such a canopy requires a specific shape, it entails particular design requirements for the load-bearing structure. Since specific dimensions and typologies are required for the design of station canopies or platform canopies, with fixed requirements and loads, the general design of station structures can be standardized by following the *Ontwerpvoorschrift perron- en sporenkappen (OVS)* (Prorail, 2012).

Portal frames

Figure 2.1 shows three typical possible cross-sections of solutions for timber portal frames. A platform canopy will contain such portal frames perpendicular to the length of the platform with cantilevers on either side added. Type (c) avoids moment-resisting connections by creating triangular columns. However, this type is not preferred for a platform canopy as it takes up more space in the walking area on the platform. This triangle would be perpendicular to the main walking direction of platform users and could reduce passenger flow and create dangerous situations. The *OVS* prefers vertical columns on the platforms without bracing. This requires moment-resistant connections at the top or bottom of vertical columns. Or by adding a horizontal strut in the portal frame, the moment can be transferred in the form of compressive force into the column and tensile force into the strut.

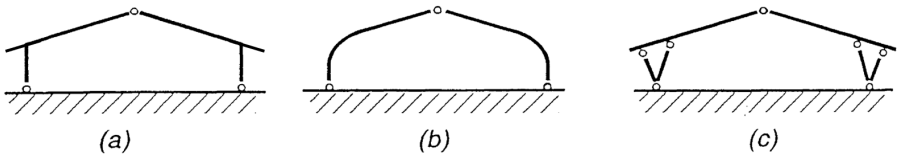

Figure 2.1: Three typical types of portal frames.

Moment-resisting connections are avoided in the design of timber structures in general and are more feasible in steel. If moment-resisting connections must be implemented in wood, steel components are often used to support critical points. Implementing moment-resisting connections in wood presents various challenges due to its anisotropic properties and higher sensitivity to environmental factors.

Prorail canopies design regulation

In the *OVS00213* (Prorail, 2012), functional and performance requirements are described. A distinction is made between a platform canopy; a structure that covers (part of) a platform to provide shelter for passengers in the waiting and circulation zones, and a track canopy; a structure that covers multiple platforms and tracks. This research will focus on the platform canopy.

Constructional requirements: Regarding safety, usability, and durability, the platform canopy must meet the requirements set forth in NEN-EN 1990. For railway junctions with more than 25,000 passengers per day (as of 2020), Consequence Class CC3 with a design life of 100 years (Design Service Life 4) is applied. For all other situations, Consequence Class CC2 with a design life of 50 years (Design Service Life 3) is used. The loads that the structure must withstand are described in Eurocode 1 (NEN-EN 1991 and NEN-EN 1991-2). For architectural loads, a vertical point load of 2.0 kN can be assumed, which can occur at any point on the supporting structure. However, the area is limited to 3 meters from the centerline of the adjacent track. A vertical distributed load of 0.1 kN/m² over the entire roof surface can be assumed.

Geometric requirements: The clear height between the top of the platform floor and the underside of any fixtures attached to the canopy structure must be at least 2.50 meters. The minimum height of the canopy structure at the platform must be 3.50 meters. The use of supporting structures beside or between the tracks should be avoided. The document also outlines how the structure should be built, taking into account the movement directions of platform users. Elevation points are identified as obstacles and should not impede the flow of passengers. This precludes the use of diagonal vertical connections.

Sustainability requirements: The only requirement concerning sustainability is that a LCC (Life Cycle Cost) analysis must be performed with multiple variants, from which the most suitable option can be selected. Materials, whether with or without a finish, must be resistant to copper and iron filings. Sustainable and environmentally friendly materials should be used.

Nijmegen platform 5-6 canopy

Platform canopy 5-6 at the station in Nijmegen is a real-world example that will be analysed (figure 2.2). This station is in the execution phase in 2024. It is partially constructed in steel and partially in timber. The roof structure is made of timber, while the columns and beams running along the platform are made of steel. Arcadis owns all designs for this station. If the station were to be constructed entirely in timber, this consideration would need to be integrated from the beginning of the design process. This would have resulted in changes to the appearance of the design. The current design includes moment-resistant connections and integrated piping and water drainage systems within the load-bearing structure, which are not feasible in wood in the same manner. Other relevant designs in timber, such as Ede-Wageningen station (Netherlands), Assen station (Netherlands), Sangubashi station (Japan), and the Chicago Horizon Pavilion (USA), will also be examined to ensure the connections under investigation are relevant.

Figure 2.2: Nijmegen platform 5-6 canopy (Prorail, 2024).

The wooden beams of the roof in this design are clamped to steel beams using a mortise and tenon principle. In this setup, the tenon is made of wood and the mortise of steel. To maintain the rigidity of this connection, it is crucial that the wood does not expand or contract excessively. This connection will be modeled in both Accoya® wood and non-acetylated wood.

Standardized case

Figure 2.3 shows a standardized model for a portal frame. This simple model was chosen because it represents the standard form of platform canopies and avoids introducing unnecessary modeling complexities. This approach allows the focus to remain on highlighting the differences between Accoya® and non-acetylated timber.

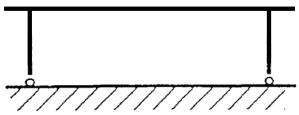

Figure 2.3: Standardized portal frame used as case study.

In this model, two pinned connections are used at the base plate, and two rigid connections are applied between the columns and the beam. However, a stable frame like this can also be designed with rigid connections at the base and pinned connections at the tops of the columns, or with only rigid connections. This principle is further explained in the methodology chapter. (Semi-)rigid connections can be implemented in various ways and will be modeled in Abaqus. In SCIA, the influence of different rotational stiffnesses of these connections will be analysed in a frame model. The portal frame will be tested under a vertical distributed roof load and a horizontal point load at the roof edge.

3

Literature review

In this literature review, the parameters influencing rigid timber connections are discussed. Following this, the properties of (glulam) Accoya® are researched. Finally, the review highlights the advantageous properties of Accoya® that are crucial for designing robust rigid timber connections.

3.1. Design parameters rigid timber connections

In addition to strength classes, creep, laminating and size effects, and connection types, emphasis is placed on the anisotropic movement properties of wood and the impact of reduction factors in strength and stiffness calculations. These considerations are crucial for designing robust and reliable timber connections.

Strength classes

In structural applications, wood is classified into different strength classes based on its mechanical properties. The primary strength classes are divided into three categories. These strength classes are determined based on standardized testing methods and criteria, including factors such as bending strength, modulus of elasticity, and density. Classes are designated by a letter followed by a number (NEN, 2024).

- Softwood strength classes (’C’)
- Hardwood strength classes (’D’)
- Glued laminated strength classes (’GL’)

Softwood strength classes are used for softwood species derived from gymnosperm trees. Softwoods are widely available and generally more cost-effective than hardwoods. Many softwood species grow quickly and can be harvested from sustainably managed forests. Softwoods are generally easier to cut, shape, and join compared to hardwoods due to their lower density and softer texture, which can simplify certain construction processes (Antonsson et al., 2009).

Hardwood strength classes are used for hardwood species derived from angiosperm trees. Hardwoods are known for their high strength and durability, making them suitable for high-stress applications. Due to their higher density and hardness, hardwoods are more resistant to wear, abrasion, and impact. Hardwoods generally exhibit less shrinkage and swelling compared to softwoods, which enhances their stability in varying environmental conditions (Ross, 2021).

Glued laminated strength classes or glulam classes are made by bonding together individual layers of timber with adhesives. The GL-h classification indicates that all the laminations in the glulam member are of the same strength class. The GL-c classification indicates that the glulam member is made from laminations of different strength classes. Combination glulam optimizes timber use by positioning higher strength laminations in high-stress areas (often outer layers) and lower strength laminations in low-stress areas (Studiengemeinschaft Holzleimbau e.V., 2012).

Creep

Creep is the time-dependent deformation under constant load. Timber fibers can slowly deform, leading to increased strain over time. Factors such as moisture content, temperature, and the duration of the load contribute to the creep behavior of timber (Armstrong and Christensen, 1961). The deformation occurs at both the microstructural level (cell walls and fibers) and the macroscopic level (overall structural dimensions).

It can lead to a reduction in the stiffness of timber connections. Over time, this can result in increased deflections and rotations at the joints. As the material deforms, its ability to resist further loads diminishes. Additionally, in rigid timber connections, such as those using dowels, bolts, or glued and mortise and tenon joints, the reduction in stiffness due to creep can cause misalignment and increased rotational movements. Internal stress distribution within the material and at the connections changes. This can create localized stress concentrations that further accelerate the degradation of the material and the connection (Fridley, Soltis, and Rammer, 1992). Timber with higher moisture content is more susceptible to creep. Additionally, fluctuations in moisture levels can accelerate creep deformation (Dinwoodie, 2000).

Ensuring that timber is properly dried and protected from moisture is crucial, as moisture content significantly influences creep behavior. Glulam exhibits less creep compared to solid timber. Additionally, adding reinforcement, such as steel plates or additional fasteners, can help distribute loads more evenly and reduce the impact of creep on timber connection performances.

Fiber directions & humidity

Wood is an anisotropic material, its properties vary based on the direction relative to the grain. The three principal directions in wood are longitudinal, radial and tangential with respect to fiber direction and annual rings (figure 3.1). The tensile strength of wood in radial direction is lower than in longitudinal direction. This has an impact on the potential uses of wood in construction applications since it requires designs to align major stresses with the wood grain. Additionally, the shrinkage and swelling behavior of wood differ based on the direction. For unmodified wood, in the tangential direction, wood shrinks and swells the most. Generally, wood deforms 2 to 3 times less in the radial direction. In the longitudinal direction, wood deforms the least, and is having a much better dimensional stability in that direction (Sargent, 2019).

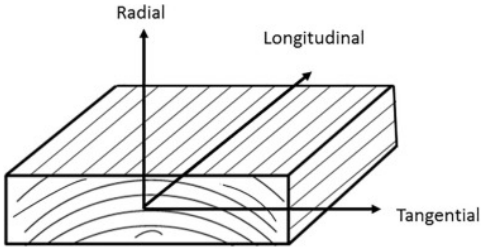

Figure 3.1: Three principal directions of wood (Sotayo, Green, and Turvey, 2016).

Changes in moisture content, driven by variations in relative humidity and temperature, result in wood deformation. The cells tend to expand and contract when they absorb or lose water. So-called bound and free water occur in wood. Bound water is chemically bound to the cell walls. Free water is found in the hollow spaces. If all positions where moisture can bind to the cell walls are occupied, the wood is called saturated. Dimensional instability of wood affects how wood joints perform, especially in environments with fluctuating humidity (Lanata, 2015). Improper drying or repeated moisture cycles can lead to internal stresses and cracks, particularly in the tangential direction. These cracks can compromise the load-bearing capacity and durability of the structure.

In moment-resisting connections, tangential and radial movements can cause misalignment and stress concentration around fasteners or connectors or gaps and misalignments in mortise and tenon joints, potentially compromising joint integrity. Where large beams and columns are connected, swelling can cause bolts to loosen or wood to split around fasteners. While longitudinal movements occur to a lesser extent and have less impact, they can still be important for ensuring that the overall structure remains

true to its designed geometry. Properly orienting the grain in structural members can reduce the impact of timber movements. An uneven moisture distribution in the wood can also cause disproportionate deformation. For example, if only the side of a beam becomes moist while the middle remains dry, it can lead to uneven warping.

In the Netherlands, the daily average relative humidity generally fluctuates between 70% and 90% on a yearly basis (figure 3.2). Especially in outdoor air, large fluctuations are possible due to changing precipitation and temperature. Extremes can drop as low as 35% during the summer and spring months or rise as high as 100% during rain or wet snow (KNMI, 2024). Certain areas of a structure may experience higher humidity levels than the surrounding air due to placement behind glass or poor ventilation. Wood will exhibit the greatest swelling in early summer during periods of frequent and prolonged condensation and the greatest shrinking in winter during dry, cold conditions with low absolute humidity. Colder air has a reduced capacity to retain moisture.

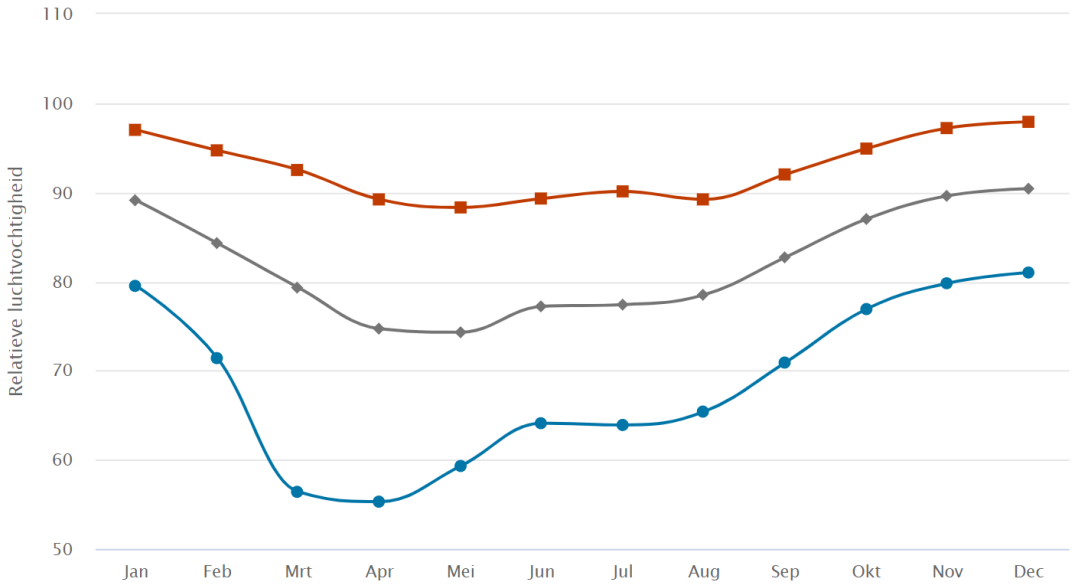

Figure 3.2: Relative humidities based on observations in the Netherlands over the past 10 years. Blue: minimum values, grey: average values, red: maximum values (Meteovista, 2024).

Figure 3.3 illustrates how the absolute humidity (the actual water content in the air) varies with temperature. It demonstrates that at higher temperatures (such as in summer), the air can hold significantly more moisture, even at lower relative humidity levels. As a result, the absolute moisture content in the air can be higher in summer than in winter, despite the lower relative humidity. This explains why wood tends to expand more during the summer.

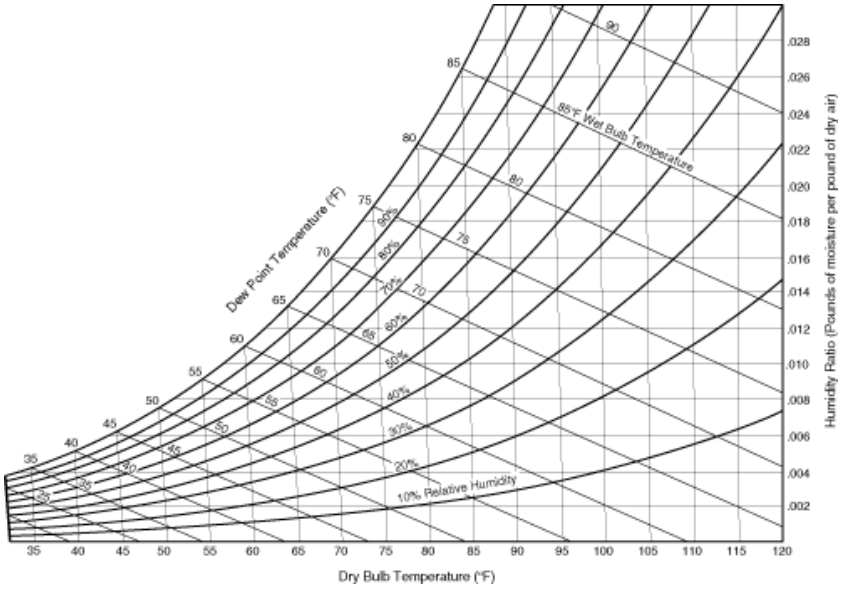

Figure 3.3: Psychrometric chart: Temperature, humidity, and moisture content relationship (John, 2023).

When vapour pressure changes, the wood moisture content also changes. However, the rate at which the wood moisture content adjusts depends on the dimensions of the wood. Additionally, there is not only a delay in the response of moisture content to changes in vapour pressure, but also a difference in behaviour depending on whether the wood is adsorbing or desorbing moisture. This phenomenon, illustrated by the hysteresis graph in figure 3.4, shows that during desorption, the wood retains more moisture at a given vapour pressure than during adsorption. This cyclic dependency highlights the inherent asymmetry in moisture uptake and release, known as hysteresis, which varies across cycles.

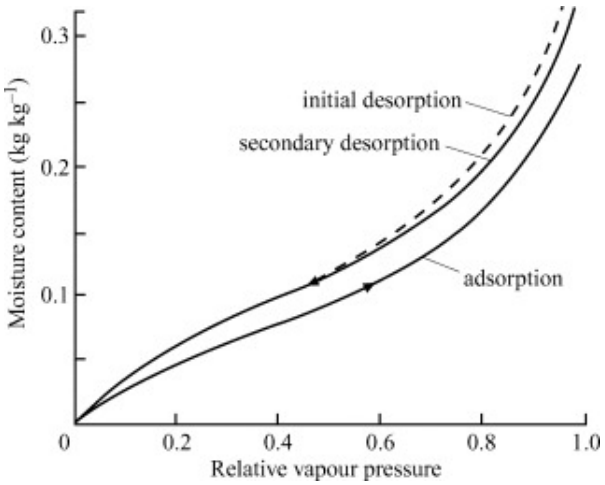

Figure 3.4: Hysteresis moisture absorption/desorption with changing relative vapour pressure (Hartley and Hamza, 2001).

Rigid timber connections

Moment resisting connections in wood can be applied in various ways and at different locations within a structure. For this thesis, the focus will be on connections that could be suitable for use in portal frames, connecting a column to a beam.

A possibility for a rigid connection without the use of steel is the cross-lapped glued connection or the mitred finger jointed connection (figure 3.5). Glued connections have good fire resistance but often need to be glued in-factory, resulting in transportation problems. These connections often tend to exhibit sudden brittle failures.

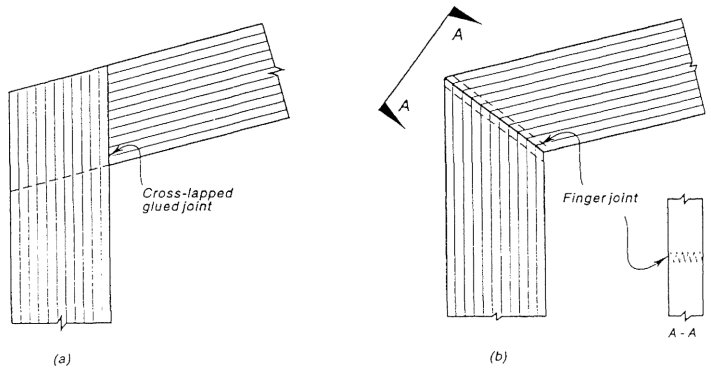

Figure 3.5: Glued connections (Buchanan and Fairweather, 1993).

Steel or plywood plates connected with nails along joints can be added to distribute stresses and prevent splitting (figure 3.6). The plates distribute the stresses across the connection and reduces the effect of dimensional instability. A large side surface is needed for these connections to accommodate the plates.

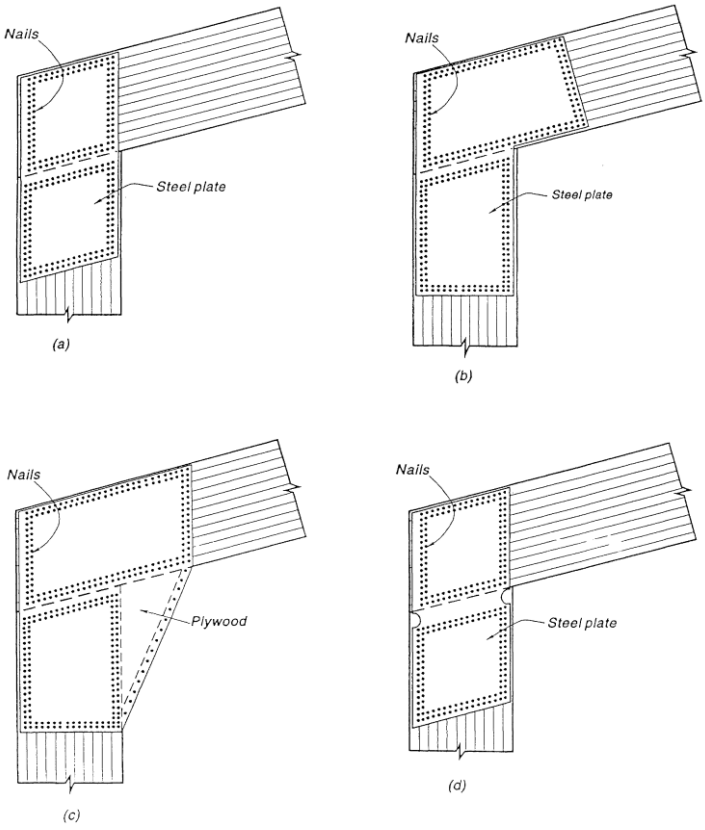

Figure 3.6: Nailed plate connections (Buchanan and Fairweather, 1993).

Another type of connections is a circle of (often steel) dowels connecting a double column to a single rafter. The circle of dowels can be either single or double. Figure 3.7 shows a single circle. Dowels can also be arranged in a grid pattern. A connection using a steel plate between wooden parts, secured with bolts, follows a similar principle. However, when using a steel plate connecting two wooden columns/beams, two dowel circles or dowel patterns should be used. These will both have their own rotational stiffness and will automatically make the connection half as stiff. Timber around the dowels can split due to the concentration of stress, particularly when there is differential shrinkage and swelling

in the radial and tangential directions. This failure is exacerbated by the stiffness mismatch between steel and timber (Rebouças et al., 2021).

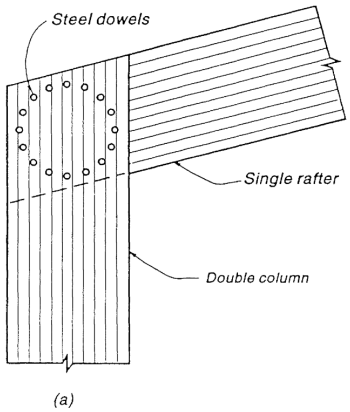

Figure 3.7: Single circle dowel connection (Buchanan and Fairweather, 1993).

Using slotted holes can accommodate dimensional changes without compromising the joint's integrity. However, this slotted hole can only take dimensional changes in one direction. Therefore, this is a limited solution when connecting two wooden elements perpendicular to each other. Flexible connectors can accommodate dimensional changes as well but will result in a connection with reduced moment capacity. Another option to distribute stresses and prevent splitting are additional fasteners.

Connections with epoxied steel rods have gained popularity at a later stage in time (figure 3.8). These connections gain good rotation capacity and high ultimate moments by the influence of steel rods. However, failures occur when the adhesive bond between the steel rods and the timber is compromised. This bond can degrade due to moisture-induced dimensional changes in the timber, such as swelling and shrinkage, which lead to stress concentration and eventual failure of the adhesive layer (Rebouças et al., 2021).

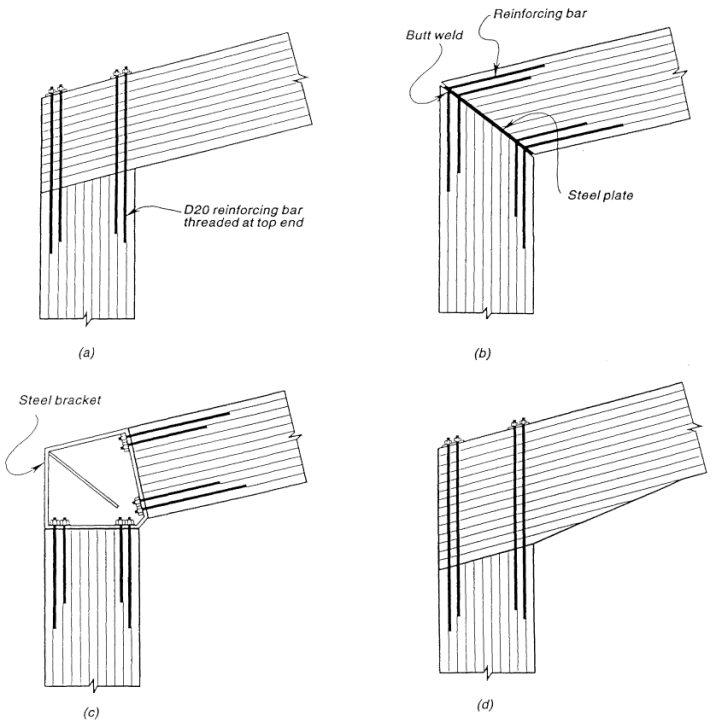

Figure 3.8: Epoxied steel rods connections (Buchanan and Fairweather, 1993).

The mortise and tenon joint is a traditional and reliable method for joining two pieces of wood, especially at right angles. The same principle is used when a tenon is placed into a wooden or metal sleeve. It requires precise cutting and fitting to ensure a tight and strong connection. Many other rigid connections, often seen in traditional Japanese woodworking, are possible without using steel, where wooden joints are tightly interlocked.

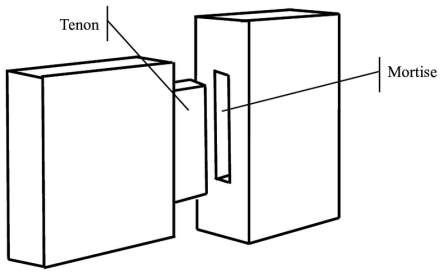

Figure 3.9: Mortise and tenon joint principle (Zaliha and Awang, 2018).

In portal frames, joints are typically classified as either rigid or pinned. However, joints that use mechanical fasteners are actually semi-rigid, exhibiting a stiffness K_r. This stiffness is influenced by several factors, including the arrangement and number of fasteners, the types of fasteners used, and the properties of the connected members. The stiffness of these joints affects the deformation behavior of the structure and, in statically indeterminate systems, also impacts the distribution of internal forces and moments (Leijten, 1988). Figure 3.10 shows the course of the bending moment for pinned (a), rigid (b) or semi-rigid joints (c).

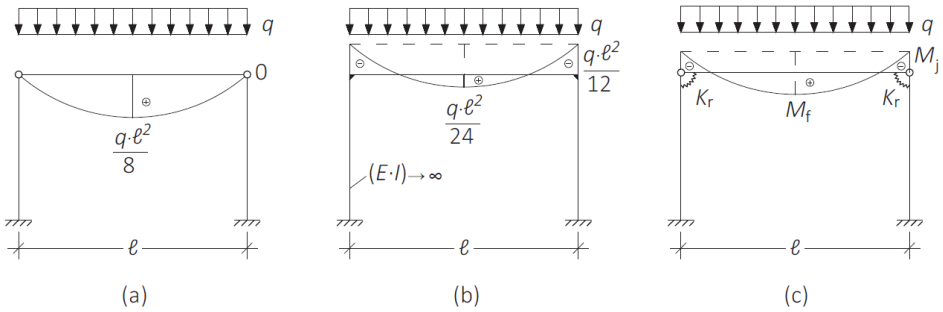

Figure 3.10: Bending moment diagrams for three joint types (Blaß and Sandhaas, 2017).

Dowel failure modes

For dowel connections, potential failure modes are highlighted here, with a focus on the failure mechanisms of the wood surrounding the dowels. This analysis excludes the use of steel components and does not emphasize dowel failure. Instead, the primary emphasis is on how the wood around the dowels may fail under different loading conditions.

Figure 3.11 illustrates common failure modes in dowel connections of surrounding timber. It includes five primary types of failure.

- (a) Embedment: The wood deforms under pressure from the dowels. This is the only ductile failure mode in this image. The rest are brittle.
- (b) Splitting: The wood splits along the grain due to stress concentration near the dowels.
- (c) Row Shear: Shear failure occurs along a row of dowels.
- (d) Block Shear: A block of wood shears off, affecting multiple dowels.
- (e) Net Tension: Tension forces cause a fracture through the wood, often in cases of axial loading.

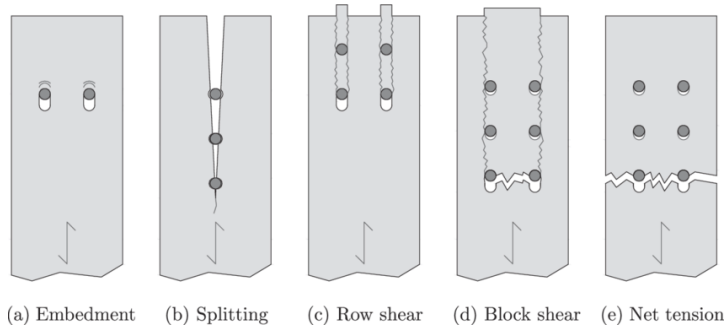

Figure 3.11: Possible failure modes of surrounding timber (Yurrita and Cabrero, 2021).

Figure 3.12 illustrates various failure patterns in dowel joints. Each subfigure (a through k) demonstrates a distinct dowel and load arrangement, emphasizing failure modes under single or double shear conditions, as well as mixed loading scenarios. This highlights how specific loading types directly impact the nature of failure in dowel connections.

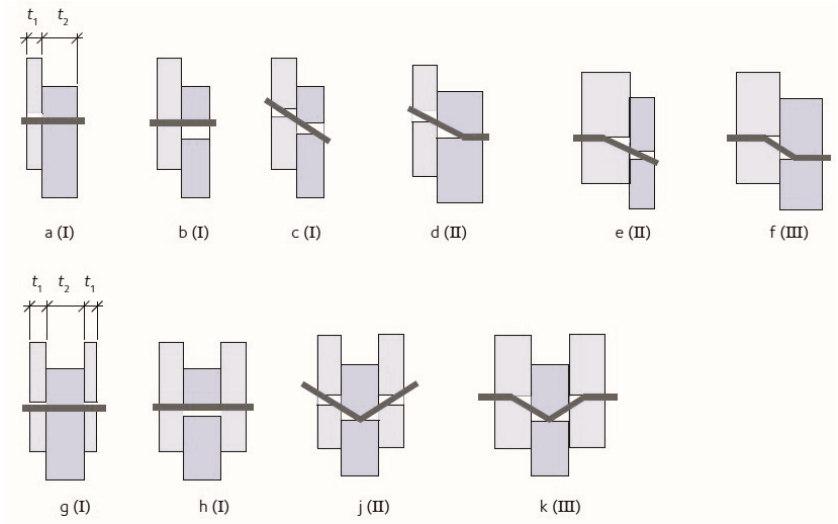

Figure 3.12: Failure modes in single and double shear (Augustino and Antwi-Afari, 2018).

Although these failure modes are often caused by external forces, certain failure modes can also arise from internal stresses due to wood swelling.

Calculation adjustment factors

The design value X_d of a material property with the characteristic value X_k is defined as follows in timber construction:

$$X_d = k_{mod} * \frac{X_k}{\gamma_m}$$

Where

- γ_m is the partial safety factor for the material property.
- k_{mod} is the modification factor, which takes into consideration the impact of the load duration and moisture content on the strength properties.

The material factor γ_m depends on the accuracy with which the characteristic values of the material properties can be determined. Industrially manufactured products such as laminated timber, plywood, and LVL exhibit less variation than sawn timber. For this reason, a differentiation in material factors is

applied. Material factors for steel are generally lower than those for wood due to the more homogeneous and predictable nature of the material. Material factors for concrete and masonry are typically higher than those for wood.

Table 3.1: Material factors γ_m (EN 1995-1-1).

Material	Material factor γ_m
Sawn timber	1,3
Laminated timber	1,25
LVL, plywood, OSB	1,2
Connections	1,3
Metal connector plates	1,25

The k_{mod} factor depends on the service class and the load-duration class of the structure. The average equilibrium moisture content in most softwoods does not exceed 12% in service class 1 (internally) and 20% in service class 2. For service class 3 (externally), however, no limit value is determined for wood moisture content. The wood moisture content is calculated using the formula below. It represents the mass of the water present in the wood, expressed as a percentage of the mass of the dry wood.

$$\omega = \frac{m_\omega - m_{\omega=0\%}}{m_{\omega=0\%}} \times 100\% \tag{3.1}$$

Table 3.2 shows all k_{mod} factors for different service classes and load durations. The k_{mod} values are determined through extensive experimental research and statistical analysis of wood and wood products under various loading conditions and environmental factors. The environmental factors that influence this value include moisture content, temperature, and relative humidity. This factor is also intended to account for the effects of shrinkage and swelling behavior on the mechanical properties in strength calculations.

Table 3.2: k_{mod} factors for sawn timber sections and glulam (EN 1995-1-1).

Load duration class	More than 10 years (Permanent)	6 months to 10 years (Long)	1 week to 6 months (Medium)	Less than one week (Short)	(Inst.)
Service class 1 & 2	0.6	0.7	0.8	0.9	1.1
Service class 3	0.5	0.55	0.65	0.7	0.9

For calculating deflections, a k_{def} factor is included to account for the long-term effects of creep. This factor does not influence the strength calculations of wood structures. However, k_{def} also is dependent on moisture content and changes in moisture content, load durations, temperature, and level of stresses. k_{mod} and k_{def} are not dependent on the type of wood in calculations. Additionally, there is currently no distinction made in the Eurocode for modified wood.

Laminating effects

Laminating effects that demonstrate how glulam could achieve higher performance values than their separate boards are as follows (Colling and Falk, 1993), (Tian et al., 2024):

- Dispersion effect
- Reinforcing effect
- Test procedure effect
- Dimensional stability effect

Due to the *dispersion effect* there is a small chance that low-quality boards will significantly reduce the strength of the glulam beam. There is a possibility that a low-quality board might be placed as an outer lamella. However, due to the compensatory positioning higher quality boards adjacent to it, the glulam beam is unlikely to fail. The limited strength of these boards will therefore not affect the

characteristic bending strength of the glulam beam. A weak board from a batch in bending will fail at a lower bending moment compared to a glulam lay-up with the same weak board in the outer lamination of the tension zone. This results in a smaller standard deviation for glulam beams than for individual boards.

The *reinforcing effect* can be explained by comparing a single board to a layered composition. In a single board, defects like knots cause failure due to the lack of alternative load paths. In a layered composition, such as a glulam beam, the higher stiffness of adjacent boards reinforces the defects, creating alternative load paths for stresses. This increases the overall strength of the GLT beam (Colling and Falk, 1995).

The *test procedure effect* impacts the results of testing procedures. In tension tests, uncentered defects like edge knots cause cracks leading to lateral deformation, which is not restrained, reducing tensile strength. In contrast, in a glulam beam, the boards provide lateral support to each other, resulting in higher tensile strength compared to individual board tested by the procedure according to EN 408.

The *dimensional stability effect* refers to its enhanced resistance to moisture-induced swelling and shrinking. This effect is primarily due to the layered structure and the adhesive used in lamination, which minimize moisture absorption and prevent deformation. As a result, laminated wood demonstrates higher durability and is more suited for environments with fluctuating moisture levels compared to non-laminated wood.

Size effects

Besides laminating effects, the size effect can play an important role as well. It is addressed in European standards and highlights how timber strength increases with decreasing size. This effect, covering length, width, and depth, is incorporated into NEN-EN 384, 2013 and NEN-EN 14080, 2013.

For tension tests, NEN-EN 384, 2013 adjusts strength for a standard width of 150 mm using a factor k_h:

$$k_h = \text{Min}\left(\left(\frac{150}{h}\right)^{0.2}, 1.3\right)$$

For glulam bending tests, NEN-EN 14080 adjusts for a standard height of 600 mm:

$$k_h = \text{Max}\left(\left(\frac{h}{600}\right)^{0.1}, 0.90\right)$$

The length factor for glulam bending tests considers a standard length l equal to 18 times the depth of the beam:

$$k_l = \left(\frac{48h}{l_{et}}\right)^{0.2}$$

$$l_{et} = l + 5a_f$$

The standards also specify procedures for tensile tests to account for length and local critical defects. Size effects are important as they influence the mechanical properties and design values of timber and glulam beams, affecting their strength and reliability in practical applications. Studies based on Weibull's weakest link theory demonstrate that timber strength decreases with increasing size due to a higher probability of encountering defects (Weibull, 1939).

3.2. Accoya®

This section provides an overview of Accoya®, focusing on its known properties and performance in structural applications. Key aspects include its enhanced durability, dimensional stability, and resistance to moisture-related issues due to the acetylation process. This background offers essential context for evaluating Accoya®'s performance and reliability in structural environments.

Acetylation

Acetylation is a wood treatment method that is well known for increasing the resistance of wood against wood-decaying fungi and destructive insects, as well as improving dimensional stability in moist conditions. This process also creates opportunities to enhance the utilization of low-value softwood and hardwood species (Bongers and Uphill, 2019). Through acetylation with acetic acid, the water-binding hydroxyl group is replaced by an acetyl group (figure 3.13), resulting in the wood absorbing less moisture while also letting it swell during the acetylation process (Hill, 2006). This wood modification is distinguished from others by the alteration of the wood's molecular structure. During the acetylation process, the cell walls become bulked due to the reaction between the hydroxyl groups of the cell wall and the acetic anhydride. The waste product of acetylation is acetic acid, which must then be recycled.

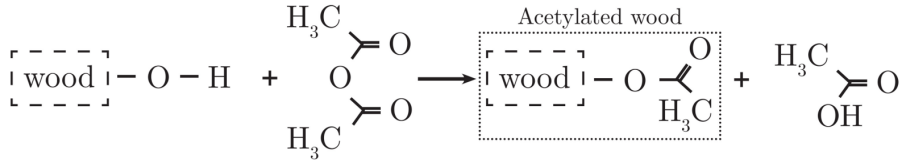

Figure 3.13: Acetylation process of wood.

The volume-to-surface ratio greatly influences the ease of the acetylation process. The smaller the volume per surface area, the more easily the acetylation process proceeds. The acetylation process might not be entirely uniform across various treated boards and can be affected by the board's position within the original log. Boards from the core of the log often have a denser structure and may respond differently to the acetylation process than boards from the outer parts of the log.

An important characteristic of these is that their dimensional stability; after treatment, results in a significant reduction of shrinking and swelling (SHR, 2007; SHR, 2018). Stichting Hout Research conducted research on the swelling and shrinking behavior of Accoya® and non-acetylated Radiata pine at different relative humidities. The results for Accoya® and non-acetylated Radiata pine swelling and shrinking in longitudinal, radial, and tangential directions are presented in table 3.3 and 3.4. Unacetylated Radiata pine had higher moisture content change percentages than Accoya®, reflecting its greater dimensional instability. A significant advantage of Accoya's lower moisture absorption is that it exhibits reduced creep. Based on the possible conditions in the Netherlands, a range of 35% to 90/95% has been shown in table 3.3 and 3.4. What is not shown in these tables are the differences in distortion between 0% and 35%. However, the largest differences are seen in this range and can be seen in Appendix A and B. The 90% and 95% distinction is due to the difference in available data.

Table 3.3: Accoya® and unacetylated Radiata pine swelling, between brackets standard deviation (SHR, 2007; SHR, 2018).

Swelling	Relative humidity		
from to	65% 35%	90% 65%	95% 65%
Longitudinal Accoya® [mm/m]	0,15 (0,05)	0,27 (0,10)	-
Longitudinal Radiata pine [mm/m]	0,26 (0,07)	0,36 (0,15)	-
Radial Accoya® [%]	0,16 (0,03)	-	0,34 (0,08)
Radial Radiata pine [%]	0,56 (0,15)	-	1,72 (0,37)
Tangential Accoya® [%]	0,28 (0,05)	-	0,81 (0,13)
Tangential Radiata pine [%]	1,07 (0,14)	-	3,73 (0,29)

Table 3.4: Accoya® and unacetylated Radiata pine shrinking, between brackets standard deviation (SHR, 2007).

Shrinking	Relative humidity		
from to	65% 35%	90% 65%	95% 65%
Radial Accoya® [%]	-0,15 (0,10)	-	-0,27 (0,07)
Radial Radiata pine [%]	-0,72 (0,45)	-	-1,14 (0,25)
Tangential Accoya® [%]	-0,36 (0,17)	-	-0,60 (0,10)
Tangential Radiata pine [%]	-1,34 (0,68)	-	-2,50 (0,51)

The results for Accoya® and unactylated Radiata pine longitudinal swelling and shrinking are median values based on 10 individual samples from 1 batch. The results for Accoya® radial and tangential swelling and shrinking are average values based on 3 batches of each 15 samples. The results for unacetylated Radiata pine radial and tangential swelling and shrinking are average values based on 1 batch of 10 samples. A more extensive study with additional batches and samples would yield more reliable results. Notably, the results from SHR show some extreme outliers with deformations over ten times greater than the median. However, the standard deviation indicates that these are exceptions. Moreover, the principle of the *dispersion effect*, as described in the laminating effects chapter, ensures that these deviations are mitigated by surrounding boards when the board is incorporated into glulam timber.

Lahtela and Karki, 2015 conducted research on the swelling behavior differences between Accoya® and other wood modification types. Accoya® exhibited the least swelling behavior. The only wood modification technique that came close in performance was Kebony®, a technique that uses furfuryl alcohol to impregnate hardwood cells. Kebony® still showed twice as much swelling in the radial direction and three times as much swelling in the tangential direction.

Pinus Radiata

For the initial commercial production of acetylated timber, Accsys Technologies® utilized the acetylation technology on Radiata pine (Pinus Radiata D. Don), marketed under the name Accoya®. This Dutch company has been marketing this product since 2007 for use in decking, cladding, window frames, and doors. In 1999 a pilot plant was built in the Netherlands that was able to produce acetylated wood. Hereafter, research started and the material proved potential for commercialization. The company focuses on the non-structural market due to the more consistent demand for volume in this sector. Additionally, there have been issues with the European certification of load-bearing Accoya®. However, the timber is classified for structural applications (Bongers and Uphill, 2019).

Figure 3.14: Acetylated batch of Radiata pine (Accoya, 2024).

In general, wood species that are easily dried, possess good liquid impregnability, and have low intermediate density (300 to 700 kg/m³) have high potential to be suitable for acetylation. Accsys Technolo-

gies® has also conducted research on acetylation for wood species other than Pinus Radiata, such as pine and beech growing in Europe. However, only Pinus Radiata is used in production.This pine species is imported from New Zealand due to the favorable market conditions and growth conditions in that country. After 30 years, the tree is harvested. The choice of this wood species is because of the good balance between fast growth and high yield (Accoya, 2024).

Accoya® properties

Based on several studies, the mechanical properties of acetylated Radiata pine have been determined. Along with the effects of safety factors and service classes, load-bearing structures appear to be feasible, particularly when uitilized as glued laminated timber. The German Institute for Structural Engineering (Deutsche Institut für Bautechnik, 2022) stated the following allowable properties for 'Accoya sawn wood' (table 3.5).

Table 3.5: General construction technique permit (Bautechniek, 2022).

Width	100 mm up to 250 mm
Thickness or height	25 mm up to 100 mm
Minimum density (ρ)	440 kg/m^3

A distinction is made between A1 and A2 grading classes, where A1 has four sides that are primarily clear, and A2 is primarily clear on three sides. The characteristic strength, stiffness, and density values of strength class C22 of DIN EN 338 apply to the design of members made of grading class A1. The characteristic strength, stiffness, and density values of strength class C16 of DIN EN 338 apply to the design of members made of grading class A2. Certain requirements are specified for these grading classes with respect to knots, bark or resin pockets, surface cracks, splits, warps, and wanes.

Accoya® wood demonstrates enhanced thermal properties, making it an suitable material for external applications in hot climates. Thermographic imaging studies conducted by Lankveld et al., 2014 have shown that the surface temperature of Accoya® wood is significantly lower than that of thermally modified wood and Wood-Plastic Composites (WPC). Under ambient conditions of 32°C, the surface temperature of Accoya® was approximately 46°C, whereas thermally modified pine ranged from 51°C to 54°C, and WPC exceeded 55°C.

The acetylation of Radiata pine affects the properties of the wood. Jorissen et al., 2005 conducted research on the effect on density, moisture content, modulus of elasticity (MOE) and bending strength (MOR). It does not appear to influence the MOE significantly. It does not alter the relationship between modulus of elasticity in bending and the MOR. The bending strength of the tested material are lower for the acetylated wood compared to the untreated wood. The mean value of MOR is only slightly lower for the acetylated material, however, due to an increase in variation, the characteristic value drops significantly. Table 3.6 shows the average results before and after acetylation. The standard deviation is given in brackets. There are two test groups for acetylated Accoya® because the MOR cannot be determined before and after treatment since the wood breaks during this test.

Table 3.6: Test results before and after acetylation, between brackets standard deviation (Jorissen et al., 2005).

Treatment	Oven dried density [kg/m^3]	Moisture content [%]	MOE [N/mm^2]	MOR [N/mm^2]
Untreated	417 (25)	12.2 (1.3)	9664 (2130)	43 (10)
Acetylated (before treatment)	411 (38)	13.1 (1.5)	9064 (2268)	-
Acetylated (after treatment)	492 (48)	5.2 (3.1)	8788 (2320)	39 (13)

Figure 3.15 shows the relative change in material properties after acetylation, including the change in swelling behavior. The relative change presented for swelling (in red) represents the change observed within a relative humidity range of 65% to 90/95%.

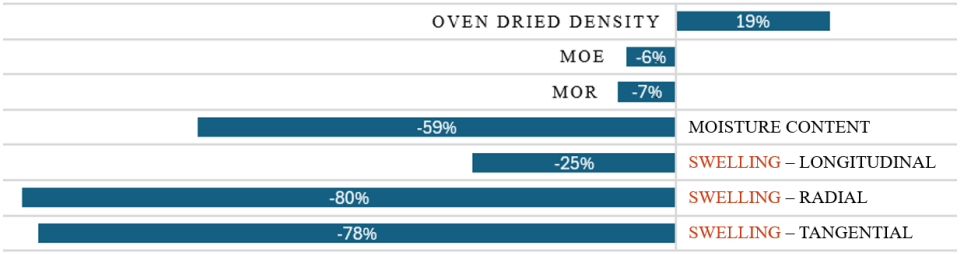

Figure 3.15: Relative change in properties post-acetylation (Jorissen et al., 2005, SHR, 2007; SHR, 2018).

Further research on acetylated Accoya® is mostly limited to structural pre-graded Radiata pine and to a thickness of 38 mm. However, F. Bongers and J. Alexander (2018) conducted a detailed investigation of the mechanical properties of (ungraded) acetylated Radiata pine ranging from 25 to 100 mm in thickness and widths from 100 to 250 mm at Karlsruhe University. Additionally, initial load duration tests were conducted. Based on this, in combination with quality control processes, a strength grade has been assigned to Accoya® timber with grading class A1 compared to values for the C22 class (EN 388) (table 3.7).

Table 3.7: C22 values compared with research results for Accoya® A1 (Bongers and Alexander, 2018).

Property	Symbols	Value for C22 (NEN-EN 338, 2024)	Test results
Bending strength [N/mm^2]	$f_{m,k}$	22	22.7
Tensile parallel [N/mm^2]	$f_{t,0,k}$	13	17.3
Tensile perpendicular [N/mm^2]	$f_{t,90,k}$	0.4	-
Compression parallel [N/mm^2]	$f_{c,0,k}$	20	40.2
Compression perpendicular [N/mm^2]	$f_{c,90,k}$	2.4	4.8
Shear strength [N/mm^2]	$f_{v,k}$	3.8	5.4
Average stiffness parallel [N/mm^2]	$E_{0,mean}$	10,000	9,920
Stiffness parallel [N/mm^2]	$E_{0,05}$	6,400	-
Average stiffness perpendicular [N/mm^2]	$E_{90,mean}$	320	-
Average shear strength [N/mm^2]	G_{mean}	630	-
Density [kg/m^3]	ρ_k	340	440
Average density [kg/m^3]	ρ_{mean}	410	526

The product that Accoya® has on the market is certified at C22. However, multiple studies have demonstrated that higher strength classifications are possible. For example, the research by Bongers, Alexander, et al., 2013 shows that with extra selection and meticulous grading, the material exceeds the mechanical properties specified for C24 in EN 338. For a bridge in Sneek, a higher material strength was also achieved by pre-selecting the planks used. However, this level of sorting is done to a lesser extent in the Accoya® factory.

Glued laminated Accoya®

For structural purposes, Accoya® timber is best utilized in the form of glued laminated timber. To optimize the available resource, it is advisable to position lamellas with higher strength classes as outer lamellas and lamellas with lower strength classes as inner lamellas. However, this makes the production process more difficult and is not always the norm. Several structural performance tests were conducted using Accoya® glued laminated timber. According to BS EN 14080 (9), characteristic material properties are provided for both homogeneous and combined glulam. It specifies that to meet the requirements of a GL28c (combined) beam, the central lamella should be of strength class C24 or higher, with the outer lamellas at a minimum of C30. Additionally, to fulfill the requirements of a GL32 (homogeneous) beam, the lamellas should be of strength class C35 or higher (Crawford et al., 2012). The bending stiffness appeared to be the most critical factor. A glulam member produced using Accoya® could feasibly be pre-selected using visual and acoustic sorting to produce a glulam product

that meets the equivalent requirements of GL24, GL28, and perhaps GL32.

However, in respect of the C22 certification for Accoya®, a GL22h glulam strength (figure 3.8) is normally achievable but not yet certified. There are standard tables presented in the NEN-EN 14080 that convert T-classes (tension strength classes of timber boards) to GL-classes, providing a minimum required finger joint strength for each GL-class. The strict requirements for strength graded structural timber regulated by the European Standard make certification difficult. As the mechanical properties of the wood change due to the treatment, the calculation methods specified in the Eurocode are no longer applicable to the material because they are only valid for non-modified wood (NEN, 2024).

Table 3.8: GL22h mechanical properties (NEN-EN 14080, 2013).

Bending strength	$f_{m,k}$	22 N/mm^2
Density-characteristic	ρ_k	380 kg/m^3
Density-mean	ρ_{mean}	400 kg/m^3
Modulus of elasticity //	$E_{0,mean}$	10000 N/mm^2
Modulus of elasticity 5%	$E_{0,0.05}$	8500 N/mm^2
Modulus of elasticity $\perp$	$E_{90,mean}$	300 N/mm^2
Tension strength //	$f_{t,0,k}$	15 N/mm^2
Tension strength $\perp$	$f_{t,90,k}$	0.5 N/mm^2
Compression strength //	$f_{c,0,k}$	19 N/mm^2
Compression strength $\perp$	$f_{c,90,k}$	2.5 N/mm^2
Shear strength	$f_{v,k}$	3.2 N/mm^2
Shear modulus	G_{mean}	650 N/mm^2

Through a detailed research process Blaß, Frese, and Kunkel, 2013 conducted a strength class of GL22c for glulam Accoya®. Initially, a sample of 632 boards was tested for dynamic Modulus of Elasticity (MOE_{dyn}). From these, 22 boards were used to determine the autocorrelation for tensile strength and stiffness prediction, and 101 boards were used to formulate regression equations based on 150 mm pieces. The remaining boards were used to construct Accoya® glulam beams for full-scale tests according to EN 408. Boards were sorted by MOE_{dyn}, with sub-samples selected to represent the overall batch accurately. The boards were distributed across the glulam beams' height based on their MOE_{dyn} values, ensuring that those in the tension and compression zones had higher MOE_{dyn} values. The final glulam beams were constructed with specific attention to finger joint quality and the spatial variability of knots. The testing showed that the glulam beams met the stiffness requirements for GL24c but fell short in bending strength, resulting in a final classification of GL22c. Currently, W. de Groot (TU Eindhoven) is working on a grant project for the certification of glulam Accoya.

Tillaart, 2021 conducted research on finger joints in glulam elements which are needed for elements longer than six meters. A reduction of 56% in tensile strength was found. However, these joints were not specifically designed for Accoya®, potentially leading to relatively low result values. The 1:12 ratio used for the finger joint is a standard ratio. It is likely that the type of adhesive used did not meet the necessary requirements, and that using a different adhesive could improve the strength of the finger joint.

Long-term experiences

In 2018, several (glulam) Accoya® projects were inspected by R. Klaassen, 2018. These projects consisted of houses, flats, and bridges built between 2007 and 2014. For some projects, heavy corrosion was observed in the metals due to extreme water loads and the use of non-corrosion resistant metals. In none of the projects studied were structural delamination or open corner connections found. This highlights the high potential for producing durable glued connections and well-performing laminated beams with acetylated wood. There were no clear signs of decay in evidence in any of the projects.

Figure 3.16: Krúsrak bridge in Sneek (Miebach, 2014).

Glulam Accoya® has been used in previous projects for heavier structural constructions in bridge construction and residential buildings. The most significant project involved two highway overpasses for the heaviest traffic class in Sneek in 2008, each 32 meters long and weighing 450 tons (figure 3.16). This was a world-first and opened up research into the possibilities for the use of Accoya® as heavy structural timber. One of these bridges showed cracks of up to 25mm during use stage. For these bridges, the requirements of the boards were derived from the NEN-EN 1194 in order to establish the target GL20h strength class (Tillaart, 2021).

Sustainability comparison

Vogtländer, 2010 conducted a life cycle assessment (LCA) for a bearing structure of a passenger bridge with a span of 16 meters and a width of 3 meters over a period of 1 year. For this bridge, Accoya® Radiata pine was compared with five other types of wood, concrete, and steel. In this assessment, the comparison also included Accoya® Scots pine, which has lower emissions due to its origin in Scandinavia instead of New Zealand. The research states that Accoya® Radiata pine shows moderate eco-costs compared to other materials like Azobé and Robinia. However, its eco-costs are higher than those of reinforced concrete and galvanized steel. The eco-costs for Accoya Radiata pine are also higher than those for Scots pine and beech due to the acetic anhydride used in the production process.

Lugt et al., 2014 conducted a cradle-to-grave analysis demonstrating that Accoya® wood generates significantly lower CO_2 emissions compared to non-renewable materials such as PVC, steel, and aluminum. The cradle-to-gate analysis investigates the environmental impacts of a product from the extraction of raw materials (”cradle”) to the point where the product leaves the factory (”gate”). Due to the combination of sustainable forestry practices, efficient production processes, and its extended lifespan, Accoya® is often CO_2-negative over its full life cycle. This is further enhanced by the potential to utilize biomass for energy production at the end of its lifecycle, contributing to avoided fossil fuel emissions. Notably, the use of locally sourced species such as Scots pine shows an even more favorable eco-profile, with a total emission of -25.0 kg CO_2eq per window frame.

Accoya® is produced from fast-growing, FSC-certified species such as Radiata pine, ensuring responsible forest management. The acetylation process, which involves modifying the wood at the molecular level using acetic anhydride, significantly enhances its durability and dimensional stability without employing harmful chemicals. Despite its high durability, Accoya® remains biodegradable. The acetylation process makes the wood less susceptible to biological decay by fungi and insects, slowing down its degradation rate compared to untreated wood. However, at the end of its life cycle, Accoya® can still decompose naturally without releasing toxic substances. Its slower degradation rate is a trade-off for its performance and longevity, aligning with sustainable practices by minimizing resource consumption over time.

3.3. Structural benefits Accoya®

Accoya® can perform significantly differently from unacetylated C22 timber caused by its minimal shrinking and swelling behaviour. Variations in the dimensions of timber can affect the fit and alignment of structural components, which can lead to gaps, misalignments, and uneven surfaces. Fluctuations in moisture content result in internal stresses within the timber, potentially causing warping or cracking. Additionally, repeated cycles of shrinking and swelling can cause fatigue over time, affecting the long-term durability and performance of the timber (Chiniforush et al., 2019).

Bongers, Marcroft, et al., 2014 conducted a comparison of the performance of Accoya® in service class 3 conditions and service class 1 conditions. Bending tests showed a 20% reduction in mean bending strength and the modulus of elasticity (MOE) in bending showed a increase of 10% when SC3 is compared to SC1. Tests on hanger joints showed that Accoya® performed better in SC3 conditions compared to SC1, with an increase in load capacity by 7%. This suggest that the standard k_{mod} factors used for solid timber in Eurocode 5 are not fully appropriate for Accoya®. Specifically, Accoya® demonstrates less degradation in structural properties under high moisture conditions. Given that the k_{def} factor is also highly dependent on moisture absorption in wood, this factor could also be more favorable for Accoya®. This provides advantageous opportunities to achieve the same strength and stiffness with less material in Accoya® compared to non-acetylated wood.

Together with the fact that Accoya® is made from sustainably sourced fast growing softwood and exhibits significantly less rot than non-acetylated wood, requiring less maintenance, it makes for a sustainable wood alternative.

3.4. Research gap

Current research and applications of Accoya® have primarily focused on non-structural uses, leaving limited data on its structural performance. Accoya® timber is rarely used in load-bearing applications, and while there are examples of wooden canopies and other structures in the Netherlands, Accoya® has not been utilized in these cases. Known for its minimal shrinking and swelling and high resistance to moisture, Accoya® possesses qualities critical for structural integrity. However, comprehensive studies evaluating its performance under structural loads are lacking. The behavior of moment-resisting connections in Accoya®, both with and without steel fasteners, remains under-researched. Experimental and numerical studies are needed to assess stiffness, strength, deflection, and internal stresses in Accoya® constructions and can thus contribute to the understanding of its altered behavior after acetylation.

Given its enhanced dimensional stability, Accoya® behaves differently from traditional timber and could enable alternative connection methods and structural designs. Moreover, the reduction factors commonly used to account for the effects of moisture absorption on mechanical properties may be more favorable for Accoya® than for non-acetylated wood, potentially supporting its broader use in structural applications.

4

Research method

This chapter details the methodological approach used to model rigid timber connections and the structural application of Accoya® in glued laminated timber constructions compared to non-acetylated timber. The research focuses on how the swell and shrinkage behavior of timber affects its structural performance. Based on the moment-resisting connections deemed necessary from the findings of the case study, two moment-resisting connections were selected for detailed analysis through Finite Element Method (FEM) modeling. These connections will be critically analysed to assess their performance in real-world applications. Through rigorous verification of the models, the aim is to create a model that approximates real-world behavior as closely as possible. However, the model will inherently remain an approximation of reality. For this reason, all aspects of the model that are realistically simulated will be explicitly identified, as will those aspects that are not accurately represented. Furthermore, the assumptions made during the modeling process will be clearly stated and substantiated. An overview of assumptions and limitations can be found in the discussion chapter.

Before a FEM model can be analysed, it is crucial that the input for the model is correctly verified. Material properties and factors within the model must all be accurately determined. By using simple models first to verify the effects of material properties and factors, it can be verified whether more complex models produce accurate results as well. Figure 4.1 illustrates the principle behind the methodology of this research.

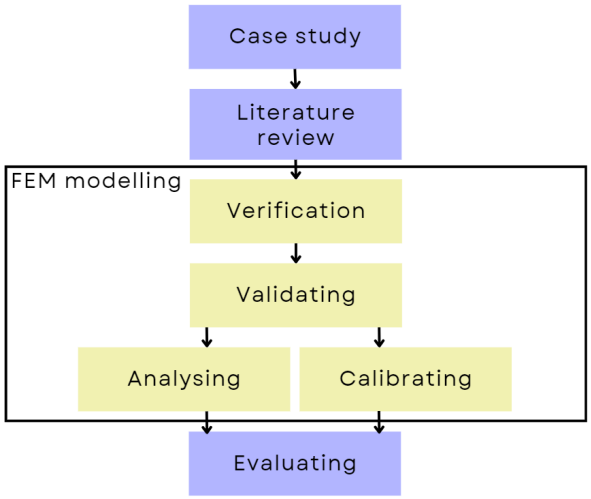

Figure 4.1: Research method flowchart.

To perform FEM analyses, specialized software is required. SCIA is used to analyze the general structure, which is a portal frame, while Abaqus is used for the detailed analysis of the connections. A license for Abaqus is provided by TU Delft through a remote computer, and a license for SCIA is provided by Arcadis.

The choice for modeling a portal frame with two cantilevered sections is based on the case study. In this portal frame, where moment-resistant connections are required, two types of connections are implemented. These two types of connections are modeled using Accoya® and Radiata pine to highlight the differences between them. Afterward, the difference in rotational stiffness can be implemented in the portal frame, allowing for the analysis of the resulting variations in force distribution within the frame. Figure 4.2 illustrates this principle. From this point onward, the unacetylated variant of Accoya® will be referred to as Radiata pine.

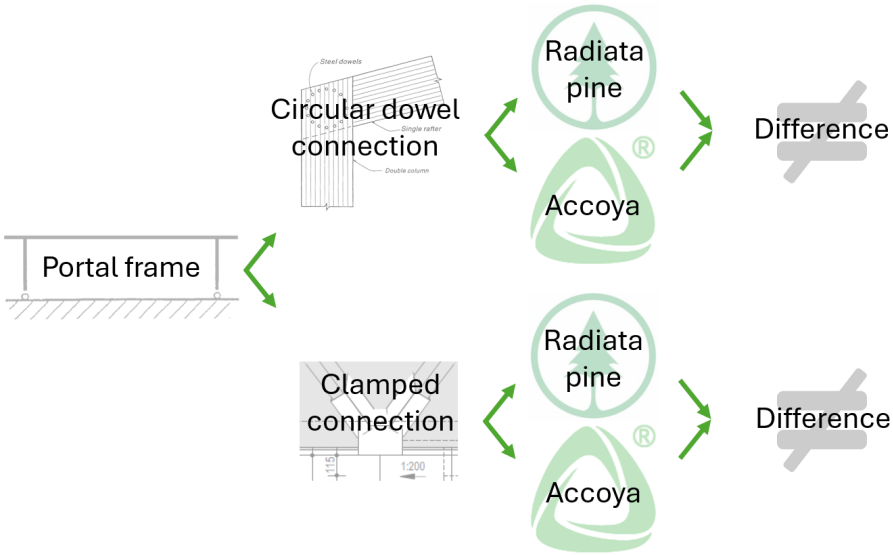

Figure 4.2: Modelling flowchart.

4.1. Introduction finite element method

The finite element method is a numerical approach used to solve problems governed by partial differential equations or those that can be expressed as the minimization of a functional. It works by dividing the domain of interest into a collection of smaller, finite elements. Continuous problems can be transformed into discretized finite element problems, where the unknowns are represented as nodal values. FEM modelling is especially advantageous for studying structures with complex geometries, varying material properties, and diverse load conditions (Nikishkov, 2001).

The application of FEM involves a systematic process that ensures accurate simulation and analysis of physical systems. Each step in this process is critical to setting up a model that can provide reliable and insightful results:

Discretization: The structure is divided into a mesh of smaller elements, with each element connected to its neighbors at nodes. This process breaks down a complex structure into manageable parts, making it easier to analyze.

Material Properties: Mechanical properties, such as Young's modulus, Poisson's ratio, and yield strength, are assigned to the elements. These properties define how each element will respond under different loads and conditions.

Boundary Conditions: External forces, constraints, and environmental effects (like temperature changes) are applied. These conditions replicate the real-world scenarios that the structure will face, ensuring the analysis reflects actual behavior.

Solution: The governing equations for each element are solved to provide a comprehensive picture of how the structure behaves under the given conditions. This step results in insights into stress distribution, deformation, and potential failure points. Real-world results must be used to verify whether the simulation provides an accurate approximation. This can only be done if actual data is available; otherwise, an assessment can be made regarding whether the simulation is likely to overestimate or underestimate the resultant loads or deflections.

The mathematical representation of this process is captured by the stiffness matrix, a key component in finite element analysis. This relationship is expressed as $\{F\} = [K]\{u\}$. The stiffness matrix relates the nodal displacements and rotations to the forces and moments at each node. Figure 4.3 illustrates this relationship for a typical beam element.

$$\begin{Bmatrix} V_1 \\ M_1 \\ V_2 \\ M_2 \end{Bmatrix} = \begin{bmatrix} k_{11} & k_{12} & k_{13} & k_{14} \\ k_{21} & k_{22} & k_{23} & k_{24} \\ k_{31} & k_{32} & k_{33} & k_{34} \\ k_{41} & k_{42} & k_{43} & k_{44} \end{bmatrix} \begin{Bmatrix} \Delta_1 \\ \theta_1 \\ \Delta_2 \\ \theta_2 \end{Bmatrix}$$

Figure 4.3: Beam element stiffness matrix.

Here, $\{F\}$ represents the vector of forces (V_1, M_1, V_2, M_2) acting on the beam element, which includes shear forces (V) and bending moments (M) at the two ends. The matrix $[K]$ is the stiffness matrix, containing coefficients (k_{ij}) that describe the relationship between the applied forces and moments and the corresponding displacements and rotations. Each element within the stiffness matrix $[K]$ is determined based on the material properties, geometric characteristics, and boundary conditions of the beam element. The vector $\{u\}$ denotes the displacements, which consist of translational displacements (Δ_1, Δ_2) and rotational displacements (θ_1, θ_2) at the beam's nodes (Němec et al., 2002).

This visual representation emphasizes the importance of understanding the stiffness properties of each element within the model, ensuring that the behavior of complex structures can be accurately simulated under real-world conditions.

4.2. Connection modelling

In this research, two types of connections are analysed for their structural performance. These connection types are particularly sensitive to the swelling behavior of wood, making them ideal for highlighting the influence of this phenomenon. By focusing on these connections, the study aims to provide a deeper understanding of how swelling impacts the mechanical integrity and overall behavior of timber structures, with particular attention to differences between acetylated and non-acetylated wood.

Before discussing the modeling methods for the two connections, the model parameters used in the analysis are highlighted, followed by the process of model verification. This verification ensures that the model's outputs are reliable before generating results. Refer to the discussion chapter, where the model assumptions and limitations are summarized in an overview.

4.2.1. Model input parameters

Abaqus does not have an option to select a unit system that the program consistently adheres to. All inputs and outputs are unitless, making it essential to choose and maintain a consistent unit system throughout the analysis. A unit system based on millimeters (mm) and Newtons (N) has been selected. As a result, quantities such as stress are expressed in N/mm² (or MPa), and density is given in ton/mm³.

Glulam Accoya® has not yet been recognized in the Eurocode, so a GL22h classification is selected based on current research and the ongoing certification process. To compare performance, the joints will also be modeled using unacetylated GL22h timber to identify the differences between the two materials. GL22h properties, along with the shrinkage and swelling values determined by SHR, 2007, will be applied. The only parameters that differ between Accoya® and unacetylated timber are the expansion factors, which account for the variation in swelling behavior between the two materials.

Table 4.1 presents the material properties used for both Accoya® and Radiata pine. The material behavior is modeled with orthotropic characteristics, reflecting the directional dependency of its mechanical properties. These properties reflect the characteristics of bonded laminated elements. The model in this study treats the material as a uniform entity, rather than simulating individual glued planks. This approach was chosen to avoid further complicating the model. This simplification will be considered when interpreting the numerical results. At the same time, it is assumed that the adhesive will not be the critical point of the material. Given the relatively low wood quality used, the wood itself is expected to be more critical than the adhesive.

Figure 4.4a shows the conceptual cross section of a glulam element that the model aims to replicate. Figure 4.4b presents a simplified representation illustrating how the material is actually modeled. In a 2D model, the material will exhibit properties in two directions within a plane, without considering individual lamellae, adhesive layers, or woodgrain patterns. For a 3D model, the material will be assigned distinct properties in three directions.

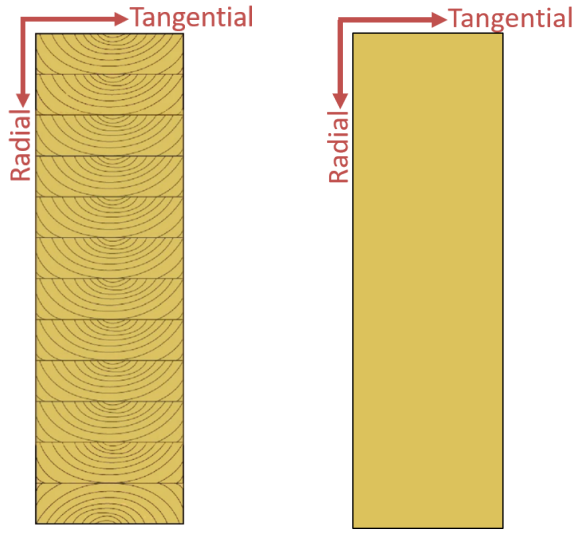

(a) Conceptual glulam cross section. **(b)** Simplified representation.

Figure 4.4: Glulam cross section with indicated directions.

Table 4.1: Material properties used for connection modelling based on GL22h properties.

Mass density	4×10^{-10}	tonne/mm^3
Modulus of elasticity $\perp$	300	N/mm^2
Modulus of elasticity //	10,000	N/mm^2
Poisson's ratio $\nu_{12/23}$	0.35	-
Poisson's ratio ν_{13}	0.05	-
Shear modulus $G_{12/23}$	650	N/mm^2
Shear modulus G_{13}	60	N/mm^2

To reduce the complexity, the model in this study will consider the material behavior of wood as linearly elastic. This results in the model continuing to behave linearly even when yield strengths are exceeded. This must be taken into account when interpreting the results. In reality, it is important to recognize that wood exhibits bilinear or even fully nonlinear behavior, especially under higher loads. Figure 4.5 illustrates the typical stress-strain relationship for wood parallel to the grain.

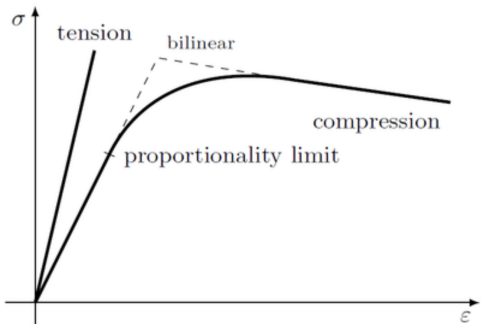

Figure 4.5: Stress-strain relationship for wood under tension and compression parallel to grain. Linearity in tension and nonlinearity in compression (Saad and Lengyel, 2022).

The modeling difference between Accoya® and non-acetylated wood is based solely on their swelling behavior. However, mechanical properties vary slightly before and after acetylation in reality. To isolate the effect of their differing dimensional stability, only this aspect was adjusted in the model. Additionally, strength and stiffness calculations are always based on a specific strength class, ensuring consistency in the evaluation of structural performance.

For the swelling behavior of the wood, the annual fluctuation in relative humidity is a major factor. In the Netherlands, daily average relative humidity typically ranges between 70% and 85%, which influences the corresponding wood moisture variation. Short-term humidity extremes are expected to have minimal impact on internal moisture content due to the delayed moisture absorption of wood. However, prolonged extremes can occur in conditions such as persistent condensation, placement in warm environments (e.g., behind glass), or poor ventilation, leading to more sustained effects on the wood's moisture content.

Taking these considerations into account, the swelling of the wood is based on the effects of exposure to relative humidity ranging from 65% to 95%. This range indicates a broad spectrum, suggesting that the wood is expected to be exposed to conditions ranging from 65% to 95% for an extended period, most likely on an annual basis. Consequently, it allows the wood to adjust its moisture content to corresponding balanced values over time, which influence the wood's swelling behavior. This swelling behavior represents the behavior that occurs during the first cycle of swelling within a year. In subsequent years, the swelling behavior is expected to decrease due to the hysteresis effect in moisture absorption and desorption. For this reason, the most plastic deformation is anticipated during the first year, making the initial annual cycle the most critical. Additionally, the relative humidity and moisture content at the time of installation are a crucial factor. For the models presented in this thesis, it is assumed that the moisture content corresponds to a relative humidity of 65% during installation. This represents a scenario where the wood, upon installation in the outdoor environment of the Netherlands, is at the lower end of its annual moisture cycle and will subsequently only exhibit swelling behavior and no shrinking behavior. From this point onward, the near-maximum possible swelling is expected to occur. This approach has been chosen to assess the potential risks associated with dimensional instability. However, in reality, this situation will not always arise. Table 4.2 shows the percentage swelling within the chosen range for both Accoya® and Radiata pine and is based on SHR research showed in appendix A. Since the swelling in the longitudinal direction is minimal, it is neglected in the model and set to zero. This simplification not only reflects the negligible impact in this direction but also simplifies the modeling process.

Table 4.2: Swelling for solid Radiata pine and Accoya® with a changing relative humidity from 65% to 95%.

Swelling direction	Radiata pine [%]	Accoya® [%]	Difference [%]
Tangential	3.73	0.81	-78,3
Radial	1.72	0.34	-80,2

The studies conducted by SHR on shrinkage and swelling behavior are based on individual planks. However, for the portal frame under investigation, including connections, glulam elements are used. For this reason, the expansion factors are reduced by 40%. These adjusted values are shown in table 4.3 and are the parameters used for modelling.

Table 4.3: Used swelling parameters for glulam Radiata pine and Accoya® with a changing relative humidity from 65% to 95%.

Swelling direction	Radiata pine [%]	Accoya® [%]	Difference [%]
Alpha11 (tangential)	2.238	0.486	-78,3
Alpha22 (radial)	1.032	0.204	-80,2
Alpha33 (longitudinal)	0.0	0.0	-

To induce swelling in the material, expansion factors that respond to changes in temperature were employed. In Abaqus, this was modeled by applying a temperature difference to the material using predefined fields. A difference of 10 degrees was introduced, and the expansion factors were divided by 10 to achieve the desired swelling effect using this method. In reality, temperature and, consequently, humidity play a significant role in the swelling behavior of wood. However, the primary objective of this method just is to achieve the correct swelling effect, regardless of the actual environmental conditions. The swelling has thus been modeled uniformly across the material. In reality, wood does not swell uniformly; moist edges are more likely to swell and shrink due to their closer proximity to fluctuating humidity levels. However, a uniform swelling of the material was chosen for the model. Following this swelling, stresses will develop based on the induced expansion.

For the interaction between surfaces, a distinction is made between two types: wood-to-wood contact and wood-to-steel contact. The interaction property parameters used are listed in table 4.4. The key difference between these two interaction properties is the variation in the friction coefficient. Wood-to-wood contact is rougher and experiences higher friction. Contact between surfaces with direct boundary conditions, such as a roller hinge, is considered frictionless. A verification model for surface interaction can be found in Appendix C.4.

Table 4.4: Interaction properties for wood-to-wood and steel-to-wood contacts

	Wood to wood	Steel to wood
Friction coefficient	0.4	0.3
Max. Elastic slip	0.005	0.005
Pressure-overclosure	Hard contact	Hard contact
Shear stress limit	No	No
Elastic slip stiffness	No	No

4.2.2. Primary verification

In the development and analysis of structural models, ensuring accuracy and reliability is critical. This requires comprehensive verification procedures to validate that the models behave as expected. In this study, three primary types of verification steps have been employed: Expansion tests, stress tests based on Hooke's Law, and validation of more complex models using verified simpler models. For these verification steps, different model parameters were used compared to those applied in the models that produce final results.

The expansion verification ensures that the material behavior aligns with expected swelling patterns in tangential and radial direction, critical for accurately modeling the dimensional changes in wood. Hooke's Law verification checks the linear elastic response of the material, confirming that the stress-strain relationship is consistent with theoretical expectations. Finally, the control models and extrapolation verification involves using simplified models to extrapolate results. Together, these verification steps form the basis of the model, demonstrating that the material behaves correctly under specified conditions.

- Expansion
- Hooke's law
- Control models / extrapolation

Expansion tests were conducted to verify whether the material expands as expected. The material was freely supported, allowing it to expand without any constraints. This verification was performed on a 2D material cross-section measuring 100 by 280 mm, in which a glulam element was hypothetically cut in longitudinal direction. The expansion was verified for both the tangential and radial directions, as shown in Appendix C.1: 2D Verification - "Tangential and Radial Swelling." Subsequently, the material was also tested as a 3D volume, with the results presented in Appendix C.3: 3D Verification - "Tangential and Radial Swelling." The numerical output of these tests was compared with analytical calculations derived from the formula below. Here, strain was calculated using a 10-degree temperature difference and the expansion factors determined for each direction.

$$u = L_0 \cdot \alpha \cdot \Delta T = L_0 \cdot \varepsilon$$

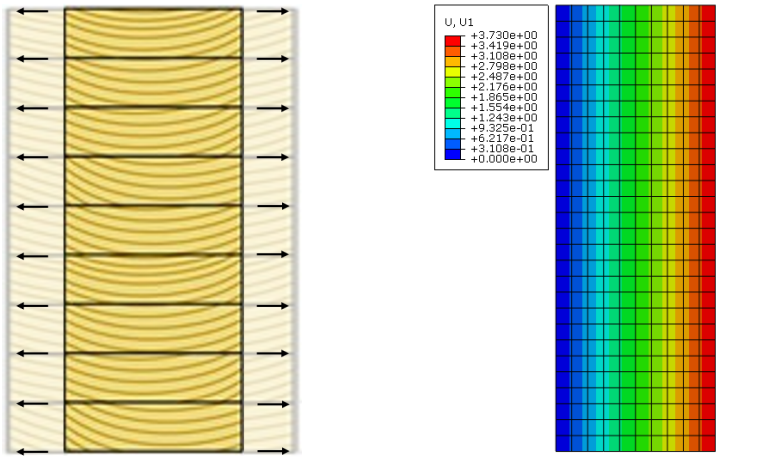

(a) Schematic tangential expansion. **(b)** Numerical tangential (U1) expansion (Abaqus).

Figure 4.6: Expansion modelling principle.

Hooke's law was used to verify tensile and compressive stresses by allowing the material to swell while restricting this swelling through boundary conditions. Appendix C.1: "Tangential Compressive Stress," demonstrates how a uniform compressive stress is generated in the tangential direction under these conditions. Additionally, Hooke's law was applied to verify stresses by imposing boundary conditions, forces, or displacements. The tests designed for verification involved applying forces solely perpendicular to each other, to ensure a clear distinction between the two directions on a surface.

$$\sigma = E \cdot \varepsilon = E \cdot \frac{\Delta L}{L_0}$$

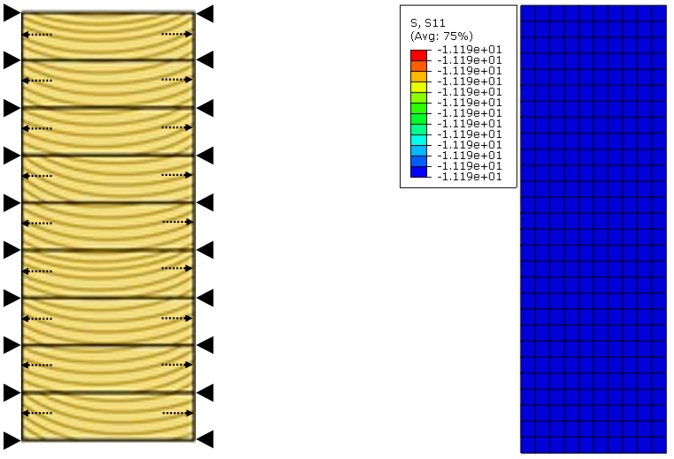

(a) Schematic tangential restricted expansion. **(b)** Numerical tangential (S11) stress (Abaqus).

Figure 4.7: Hooke's law principle.

Control models / extrapolation have been employed to validate models that are unsuitable for analytical control by using verified models as a reference. For instance, models in which stresses arise due to bending are particularly challenging to verify analytically. By leveraging control models, it is possible to ensure the accuracy of these complex models through comparison and extrapolation, thereby providing a more reliable validation approach for scenarios where direct analytical solutions are not feasible.

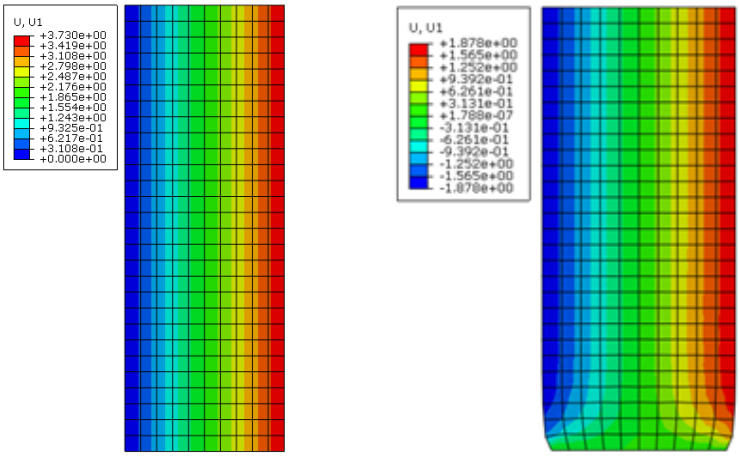

(a) Verified model (Abaqus). **(b)** To be validated model (Abaqus).

Figure 4.8: Control models / extrapolation example.

4.2.3. Clamped connection

The first of the two types of connections is the clamped connection. This connection was designed for the canopy of platform 5-6 at Nijmegen station. It clamps a wooden beam within a steel tube section. This tube is attached to a steel beam that runs along the length of the platform. The clamped connection serves to link both a 9-meter wooden roof structure, which covers the central part of the platform, to the main structure, as well two 2-meter cantilevered section. Connection details, along with design impressions, can be found in Appendix B. A moment-resistant connection is particularly important for the fixation of the two cantilevered sections. Various methods for achieving a moment-resistant connection for a timber cantilever are available, as described in chapter 3.1: "Rigid Timber Connections." In this case, wooden elements needed to be connected to the steel beam, and a steel tube was chosen to clamp the wooden elements.

Figure 4.9 shows a detail image of this connection and an impression of how it has been modeled. The original design includes curved wooden beams. However, the model does not incorporate these curved elements in order to avoid unnecessary complexity in the modeling process. The detail specifies that the element should be tapered near the hollow section. However, in the model, the wooden element is not tapered and has a length of 1000 mm.

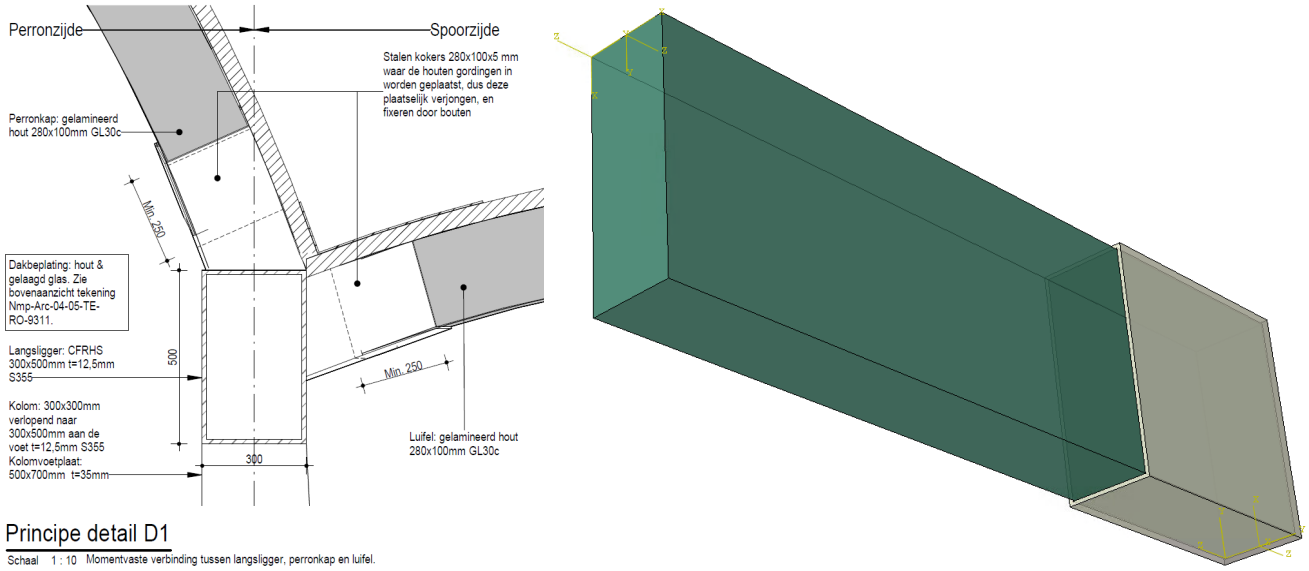

(a) Designed detail (Arcadis). **(b)** In green: wood element. In grey: steel tube (Abaqus).

Figure 4.9: Clamped connection.

The drawback of this connection is that its moment-resistance largely relies on the principle of the wood being tightly clamped within the tube. If it becomes even slightly loose, the connection could quickly loses a significant amount of moment resistance. Other types of connections might have been able to prevent this issue.

To secure this connection in place, dowels will be inserted, running tangentially through the connection. These dowels primarily serve to counteract forces acting outward from the steel tube and are directly connected to it. However, the purpose of the model is not to test the effect of these dowels on the connection. Instead, the aim is to investigate the behavior of the wood relative to the tube, determining the resulting stresses and evaluating the stiffness achievable for the two different materials. The dowels have been modeled as a line with boundary conditions based on the principle shown in Figure 4.10. This approach eliminates the need to create a hole in the wood's volume, and the dowel is treated as infinitely rigid. Considering that the forces transmitted by the dowel in reality are directed towards the steel tube, and the model does not focus on deformation or force absorption of the tube, this dowel modeling method is deemed sufficient. Appendix C.1: 'Single/double boundary condition dowel' presents the validation of this dowel modeling approach.

Figure 4.10: Boundary condition dowel principle.

The steel tube is modeled as a rigid surface that interacts with the wooden material through a defined interaction. Both the tube and the dowel are treated as infinitely rigid. In reality, a steel tube would exhibit deformation due to forces from the wood, which could result from wood swelling or load transfer from the structure. By assuming the tube to be infinitely rigid in the model, the focus remains on the behavior of the wood. This assumption is taken into account when interpreting the results.

The focus is on the swelling behavior of the wood. This material has been modeled as a homogeneous material to approximate the behavior of a laminated beam. Due to the curved wood structure in the tangential direction, the wood will not exhibit isotropic swelling. As shown in figure 4.11, the wood demonstrates distortions due to shrinkage and swelling anisotropy. The swelling of a laminated wooden element is less and less curved than that of a single plank because the layers in a laminated structure are bonded together, restricting the movement and deformation of individual layers. This bonding reduces the overall anisotropic expansion, leading to more uniform swelling across the element. The implementation of curved swelling in the model is detailed in Appendix C.2: 'Curved Swelling.'

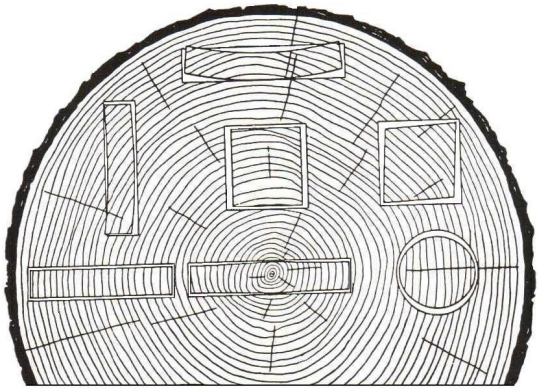

Figure 4.11: Distortions caused by shrinkage and swelling anisotropy (Niemz, Teischinger, and Sandberg, 2023).

The curved swelling will impact the force distribution in connections. After incorporating curved swelling (i.e. cupping) instead of perpendicular swelling into the model for a glulam cross-section, the total swelling in the tangential direction slightly decreases, while in the radial direction it increases. This effect is illustrated in figure C.22 in Appendix C.2. To demonstrate the effect of swelling on the internal force distribution, a simple dowel test was conducted. This test highlights the difference in internal force behavior when placing a dowel, as conducted in figure 4.10. Figure 4.12 illustrates the distribution of compressive stress for the 0° variant and the 9° variant. The 9° angle represents the maximum inclination of the fictitious wood fibers in the cross-section, indicating the extent of the curved swelling. This is explained in more detail in appendix C.2. It can be observed that the curved variant exhibits lower compressive stress throughout the dowel. This is because the curved variant expands less in width under the same change in relative humidity compared to the uncurved variant. This specific example is not fully representative of all expected stress differences between the curved and uncurved variants. However, it does provide an indication of the extent to which these variants differ in stress development.

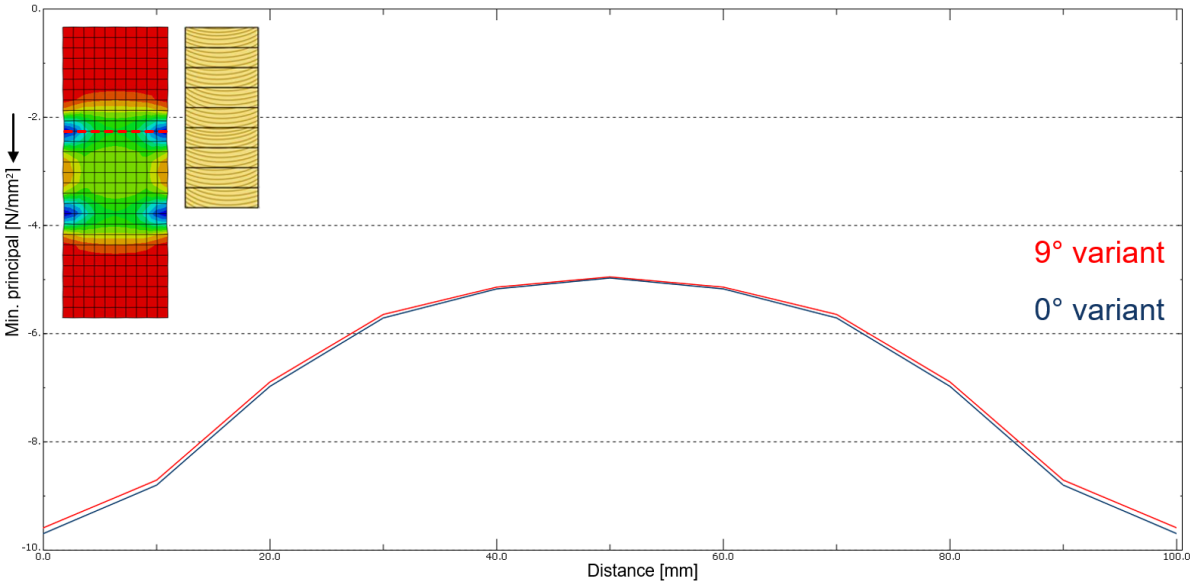

Figure 4.12: Compression stresses for uncurved (0°) and curved (9°) variant. Displayed stress located at the position of the dotted line shown at the upper left (Abaqus).

The maximum difference in compressive stress between the two variants found in these tests is less than 2%. The differences are mostly pronounced at critical points, in this case at the edges of the dowel. For further use of the models, both the 0° and 9° variants were applied. In reality, for a cross-section of 100 by 280 mm, the maximum curvature would not reach 9°; a value of 3° would be more appropriate. The choice of 9° degrees was made to better highlight the differences.

To test the effect of swelling in the steel tube with direct contact, experiments were conducted using Accoya® and Radiata pine, both at 0° and 9°. The tube was modeled as rigid, meaning it would not move, along with the boundary conditions. The wood swells by different amounts in the radial and tangential directions. These directions, when viewed in the longitudinal direction, are perpendicular to the tube.

The mesh for these connections is set to 20 mm. Keeping the mesh size moderate ensures that running the models does not take too long. Since the shape is relatively simple and rectangular, this mesh size is sufficient. However, sudden large value shifts between mesh elements were sometimes observed in the results. Because the mesh runs consistently through the material, material directions can be easily assigned to the mesh elements manually by repeating patterns. This approach simplifies the application of curved swelling for this detail. Figure 4.13b shows that the tube is modeled as a surface. In some other figures, the thickness of the tube is visible. However, this does not affect the model since it is considered rigid.

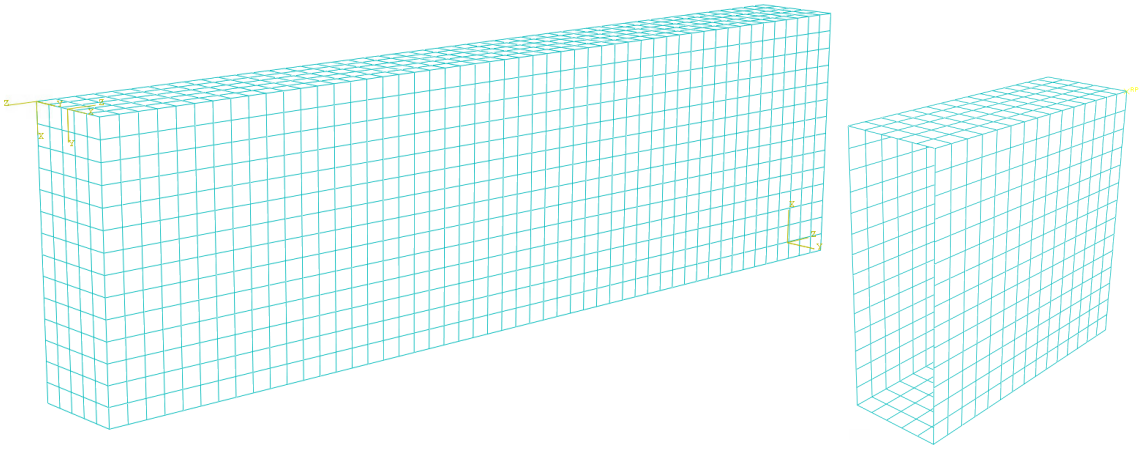

(a) Solid wooden element. **(b)** Tube.

Figure 4.13: Mesh size: 20 mm (Abaqus).

After determining the swelling behavior within the tube for the four material typologies (Accoya® and Radiata pine, both including curved and uncurved swelling), the potential for plastic deformation was assessed. When considering compressive stress, it is important to account for different yield strengths depending on whether the stress is aligned with or perpendicular to the grain. Perpendicular to the wood grain, the yield strengths for compressive stress is 2.5 N/mm², while in the longitudinal direction, it is 19 N/mm². Plastic behavior has not been incorporated into the model. Peak stresses in the model are examined carefully but are not the primary focus. The emphasis is on the overall pattern of stresses that are generated. After analyzing the internal wood stresses for the four material types, the necessary gap between the tube and the wood can be determined. This allows for an assessment of how much spacing is required, taking into account the wood's swelling behavior.

Another option would have been to investigate how the wood would fail if confined within a too-tight steel tube. Cracks could have been predicted, or parts of yielded areas could have been removed, after which new tests could be conducted with the model. However, this approach was not chosen in order to avoid further complicating the modeling process.

After testing two different tube dimensions for both Accoya® and Radiata pine, rotational stiffness tests were also conducted. A single dowel is implemented here to minimize force transfer and moment generation through these dowels. Only two variants were tested in total, both without considering swelling. Figure 4.14 illustrates the setup for the test. The model, which is 1000 mm in length, had a force applied to its surface where purple arrows are visible, simulating a shear stress across the cross-section. This method prevents the formation of local stresses at the point of application. Tests were conducted using various force magnitudes. The results are presented for a low shear force to ensure that the material remains within the linear elastic behavior range of the connection.

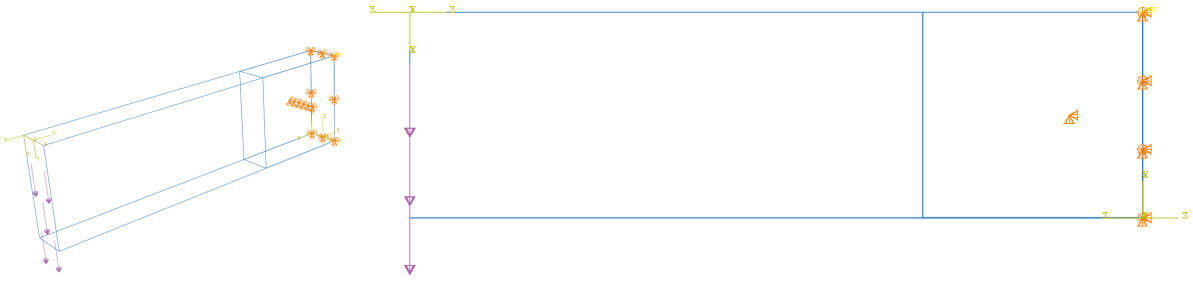

(a) Perspective. **(b)** Side view.

Figure 4.14: Applied force clamped connection (Abaqus).

4.2.4. Circular dowel connection

The second of the two types of connections is the circular dowel connection. This connection is a more standard moment-resistant type that joins wooden elements coming from different angles within a single plane. It was selected because of the critical impact that wood swelling has on its performance. Furthermore, the rotational stiffness of the connection can be analysed and compared using a relatively simple analytical approach. Figure 4.15b shows the connection modeled with four steel dowels. The elements here have the same cross-section as those in the clamped connection, measuring 100 by 280 mm, with a length of 1000 mm each.

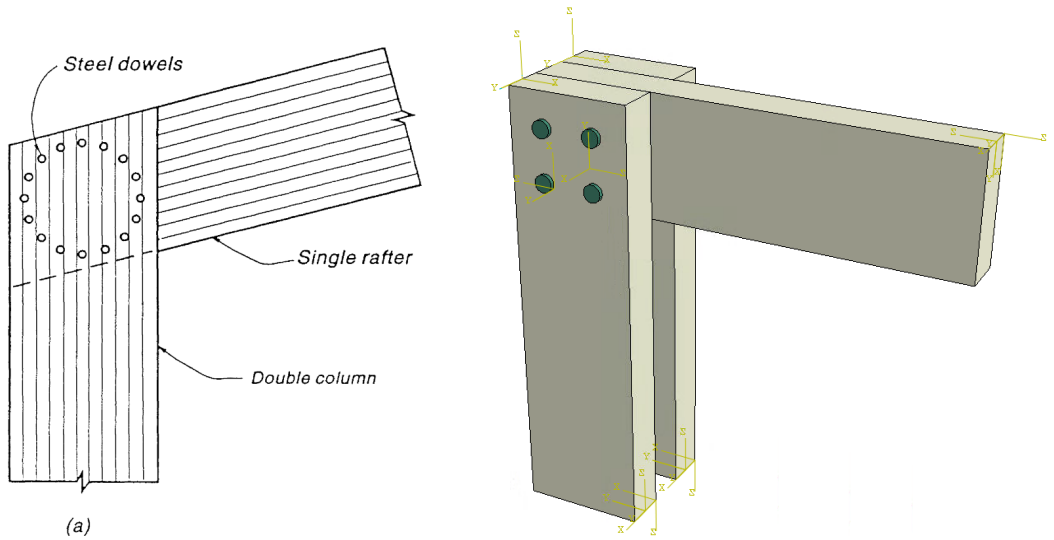

(a) Connection typology (Buchanan and Fairweather, 1993). **(b)** In grey: wood elements. In green: steel dowels (Abaqus).

Figure 4.15: Circular dowel connection.

Unlike the modeling of the clamped connection, the dowels in this setup are modeled as deformable elements with a volume. The dowels have to act as force-transmitting elements between the wooden components. If the dowels were instead modeled as boundary conditions, they would not be able to transfer forces to another element; instead, the forces would dissipate at the point where they attach to a boundary condition. A new material is created for the dowels, with a density and Young's modulus set to be 100 times higher than those of the wood. Holes with a diameter of 20 mm are made in the wood material to insert the dowels, and the mesh is adjusted accordingly to accommodate these changes. The mesh size is again set to 20 mm, but it is refined around the holes. The dowels also have a mesh size of 20 mm, which is consistent along their length. The shaft and head of the dowels were modeled separately and then connected using tie constraints.

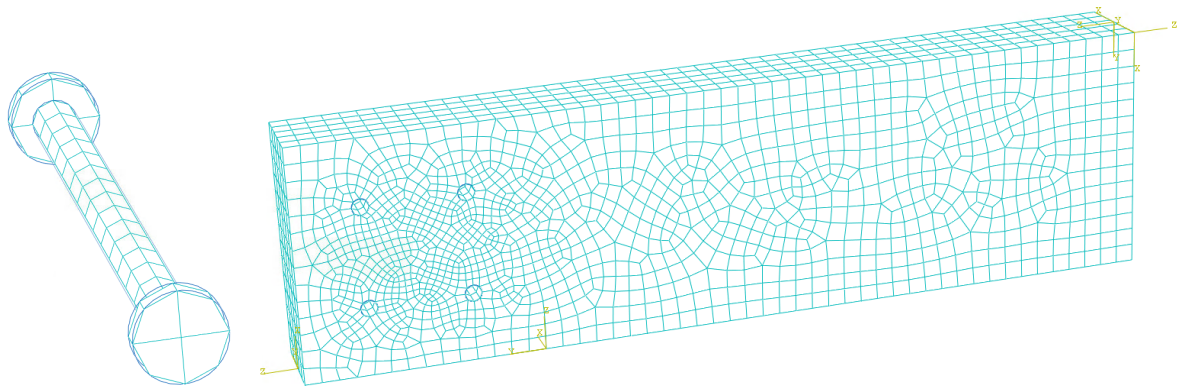

(a) Dowel. **(b)** Wooden element.

Figure 4.16: Mesh size: 20 mm (Abaqus).

As shown in Figure 4.16b, the mesh size no longer follows a repeating pattern, as it did with the clamped connection. This change makes it impractical to manually assign material orientations to each element. Consequently, the option to test the effect of curved swelling on this connection is no longer feasible. However, based on the test results shown in Figure 4.12, the impact of curved swelling is relatively small.

To mitigate the stress caused by wood swelling, slotted holes can be utilized. These slots allow limited movement, but only in the radial or longitudinal direction, helping to accommodate swelling in those directions. However, the wooden elements being connected are oriented at different angles to each other, which complicates this approach. Wood swells most significantly in the tangential direction, which is perpendicular to the grain and aligns with the direction of the dowel. Although the tangential direction remains consistent between the connected elements, the difference in their orientation means that the radial and longitudinal swelling directions do not align. This misalignment prevents the slotted holes from effectively accommodating the swelling, as they cannot offer the necessary freedom of movement across the elements. No slotted holes were used in the modeling of this connection.

Figure 4.17 illustrates how the wood expands in the Y direction, or horizontal direction. The vertical columns expand, and it is clearly visible that the expansion is constrained around the dowels. The horizontal rafter shows no expansion in this direction because no expansion is modeled in the longitudinal direction. The material around the dowels deforms. This deformation is amplified by the deformation scale factor, which particularly affects the one in the lower left corner, making it appear smaller.

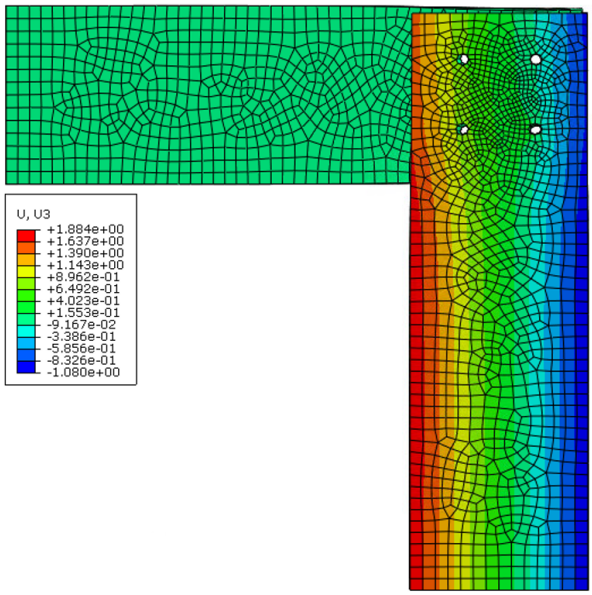

Figure 4.17: Y/U3 expansion. Deformation scale factor: 10 (Abaqus).

For this connection, the rotational stiffness was determined without accounting for material swelling. This was done both numerically and analytically, after which the results were compared. Figure 4.18 shows the dimension values used for the analytical calculation, with the dowel diameter measuring 20 mm. This analytical calculation uses the density of the wood, the dowel diameter, and the distance of the dowels from the center of rotation.

The current calculation for rotational stiffness does not account for the embedded strength of the dowel because it assumes that the wood around the dowel behaves elastically and does not undergo plastic deformation. This can lead to an overestimation of the joint stiffness. In reality, embedded strength affects how much the wood compresses around the dowel under load, causing slight movement in the joint. Additionally, the effects of creep, friction between the wooden elements, and the thickness of the elements were not considered in this calculation method. Creep is also not considered in the numerical model.

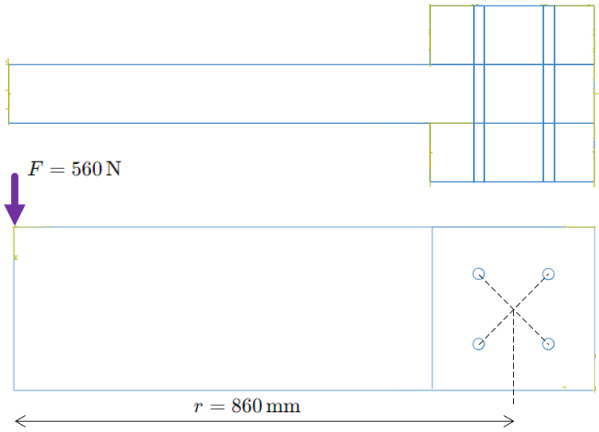

Figure 4.18: Top and side view.

$$K_{\text{ser}} = \tfrac{1}{23}\rho_{\text{mean}}^{1.5} d \qquad K_{\text{ser}} = \tfrac{1}{23} \cdot 400^{1.5} \cdot 20 \approx 6.96 \text{ kN/mm}$$

$$K_r = \textstyle\sum_{i=1}^{4} r_i^2 \cdot K_{\text{ser}} \qquad K_r = 4 \cdot 84.85^2 \cdot 6.96 \approx 2.004 \times 10^5 \text{ kNmm/rad}$$

$$K_{r,\text{totaal}} = 2 \cdot K_r \qquad K_{r,\text{totaal}} \approx \underline{4.007 \times 10^5 \text{ kNmm/rad}}$$

This analytical approach to the rotational stiffness of the connection is compared with the stiffness obtained from the model. For this purpose, a shear stress of 0,02 N/mm^2 was applied to the side surface which is a fictitious cross-section where purple lines are visible in figure 4.19a. This method prevents the formation of local stresses at the point of application. The total shear force (560 N) is obtained by multiplying this value by the cross-sectional area.

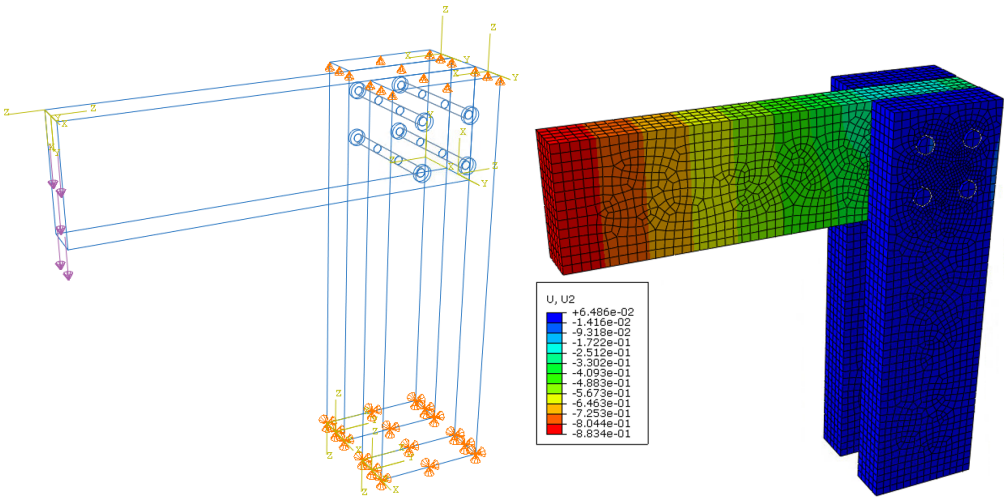

(a) setup for rotational stiffness test. **(b)** Vertical displacement. Deformation scale factor: 10.

Figure 4.19: Maximum deflection of the element is 0,8834 mm (Abaqus).

$$F = \tau \cdot A \qquad F = 0.02 \cdot 28,000 = 560 \text{ N}$$

$$\theta = \frac{u}{r} \qquad \theta = \frac{0.8834}{860} \approx 0.0010272 \text{ rad}$$

$$M = F \cdot r \qquad M = 560 \text{ N} \cdot 860 \text{ mm} = 481600 \text{ Nmm}$$

$$K_0 = \frac{M}{\theta} \qquad K_0 = \frac{481600 \text{ Nmm}}{0.0010272 \text{ rad}} \approx 4.688 \times 10^8 \text{ Nmm/rad}$$

$$K_0 \approx \underline{4.688 \times 10^5 \text{ kNmm/rad}}$$

Table 4.5 compares the results of the two approaches to rotational stiffness. The rotational stiffness from the model is found to be higher than the analytical result, showing a difference of 14,6%. One reason for the difference in outcomes could be that the force is not evenly distributed across the dowels. The model shows more deformation around the lower dowels compared to the upper ones. However, the analytical calculation assumes a central rotation center. If the rotation center shifts, the quadratic distance used in the formula automatically increases the rotational stiffness. Additionally, a comparison with experimental tests would provide the most accurate assessment. The 14,6% difference observed is relatively small and could vary with slight changes in the parameters.

Table 4.5: Comparison analytical and numerical rotational stifness.

Analytical	Numerical	Difference
$4,007 \times 10^5$ [kNmm/rad]	$4,688 \times 10^5$ [kNmm/rad]	14,6%

4.3. Portal frame modelling

As highlighted in chapter 2, 'Case study,' a standardized portal frame (figure 4.20) is used to analyze results found for the connections. In this portal frame, the rotational stiffness values found for the clamped connection and the circular dowel connection are tested using two different materials. The portal frame is modeled in SCIA as beams connected by nodes that join the beams. This is an efficient method to approximate the force distribution in a portal frame, utilizing line elements and connections. The nodes have the option to assign rigid, hinged, or semi-rigid properties to each side where an element is connected to a node.

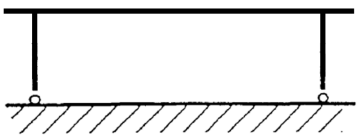

Figure 4.20: Standardized portal frame.

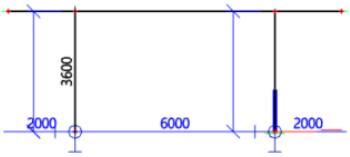

Figure 4.21: Modeled portal frame dimensions [mm] (SCIA).

In this model, two pinned connections are used at the base plate, and two rigid connections are applied between the columns and the beam. However, a stable frame like this can also be designed with rigid connections at the base and pinned connections at the tops of the columns, or with only rigid connections. In reality, designing a rigid or hinged connection is more complex than simply drawing or modeling it. A connection is almost never entirely hinged or fully rigid. Even a connection that is considered rigid still has an associated rotational stiffness and could be classified as semi-rigid. The clamped connection and circular dowel connection are also classified as rigid in this thesis. However, the rotational stiffness of these connections is assessed to determine the extent to which they are semi-rigid.

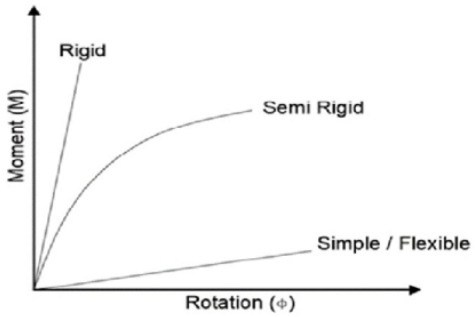

Figure 4.22: Relationship moment and rotation (Güray et al., 2023).

The determined rotational stiffness values will be incorporated into the portal frame model. These values will influence the overall force behavior of the structure and affect the moment distribution and displacements within the portal frame. To illustrate the effect of different design principles, figure 4.23 shows the moment distributions for three different configurations. The three types include either rigid or hinged connections. This model is loaded with a horizontal point load of 2 kN. Since the objective for the portal frame is to determine a method to ensure stability, the effect of different design principles was tested using a horizontal point load. Logically, a model should also be tested under a permanent vertically distributed load; however, this load will not critically impact the assessment of the portal frame's horizontal stability.

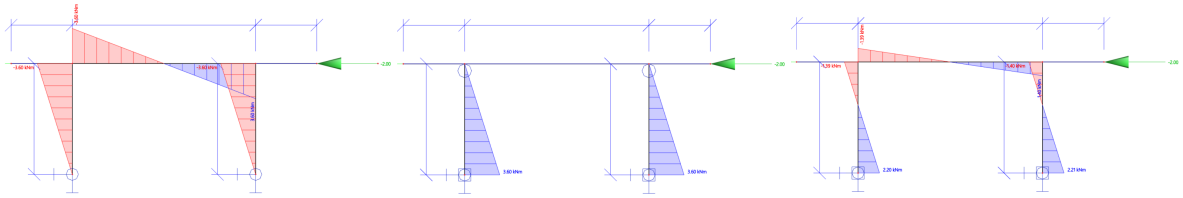

(a) Hinged base plate, rigid column-beam. **(b)** Rigid base plate, hinged column-beam. **(c)** Rigid base plate, rigid column-beam.

Figure 4.23: Moment distributions (SCIA).

For the configuration shown in figure 4.23a, the greatest moment formation occurs. In contrast, the configuration in figure 4.23b will result in the largest displacements. The most favorable moment distribution and smallest deformation are seen in the configuration from figure 4.23c. This configuration is also common in practice, though typically with partial rotational stiffness rather than fully rigid connections. When all connections are modeled with specific rotational stiffness rather than fully rigid, the moments are more evenly distributed across the structure, though displacements will increase. The effect of various connections with different rotational stiffnesses is tested in a configuration as shown in figure 4.24. In addition to evaluating the stiffness of the portal frame, the required strength of the connections and beams/columns is also assessed under varying rotational stiffness conditions.

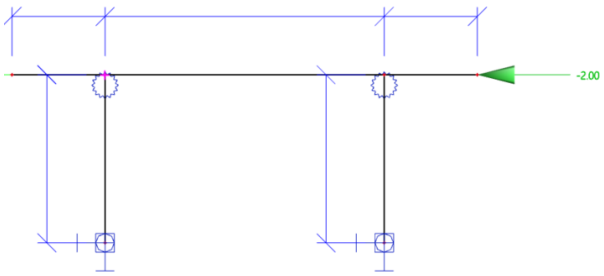

Figure 4.24: Configuration for investigating the effect of varying rotational stiffness with semi-rigid connections at the top and bottom of the columns (SCIA).

The values of the found rotational stiffnesses will be applied to all four connections to analyze the impact of each individual connection. Additionally, a combination of connections is constructed using either exclusively Accoya® or Radiata pine, in order to create a practical example. The effect of several setups can be illustrated through the resulting moment distributions and deflections. For this purpose, the properties of the modeled beam line elements are crucial as well. These elements are modeled with the characteristics of a 100 x 280 mm GL22h beam (figure 4.25) and is the cross-section dimension also used for connection modeling..

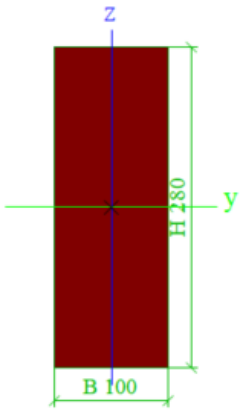

Figure 4.25: GL22h cross section (SCIA).

5

Results

This chapter provides a comparative analysis of the structural performance of Accoya® and Radiata pine (non-acetylated) timber in two types of connections: the clamped and circular dowel connections. The analysis focuses on how each timber type performs in terms of stiffness and susceptibility to failure. Found rotational stiffnesses were subsequently applied to a portal frame model to understand the impact of each timber type within a complete structural system.

5.1. Clamped connection

The results for the clamped connection consist of two components. First, the effect of swelling was tested for Accoya® and Radiata pine under identical conditions. The materials were compared using corresponding models. Based on these results, the necessary gap between the wood and the steel tube was determined to prevent material failure. Subsequently, these two models were compared in terms of rotational stiffness. In rotational stiffness tests, the material was not allowed to swell.

Swelling evaluation

The swelling of the materials were conducted in both the tangential and radial directions. These directions are perpendicular to the tube, leading to expected compressive stresses. No swelling occurs in the longitudinal direction, which aligns with the axis extending out of the tube.

In addition to differentiating between Radiata pine and Accoya®, this analysis also distinguishes between swelling with and without curvature (i.e. cupping). However, for most results, only the curved swelling variant (specifically the 9° variant) is presented, as the differences between curved and non-curved swelling are negligible compared to the differences between Accoya® and Radiata pine. For an explanation of curved swelling variants, see Appendix C.2.

Figure 5.1 shows the minimum principal stresses for four variants. Uniform color scales have been applied for these plots. The difference between the 0° and 9° variants is barely visually apparent here but can be deduced from the maximum values found. These maximum values are indicated in the title of each plot and are highlighted in table 5.1. This table compares the reduction in the observed stresses for the two materials with the reduction in swelling behavior in both directions. However, it is important to differentiate compressive stress in various directions from one another, as the properties of wood (and therefore the yield strengths) differ depending on whether the direction is perpendicular or parallel to the grain.

The table shows that the reduction in minimum principal stresses for both variants is 81.3% when Accoya® is modeled instead of Radiata pine. These values are identical because identical models were run, and the material was assigned only linear elastic properties. Thus, the material's response is consistent under varying stress conditions. The reduction in stress is slightly higher than the reduction in swelling behavior.

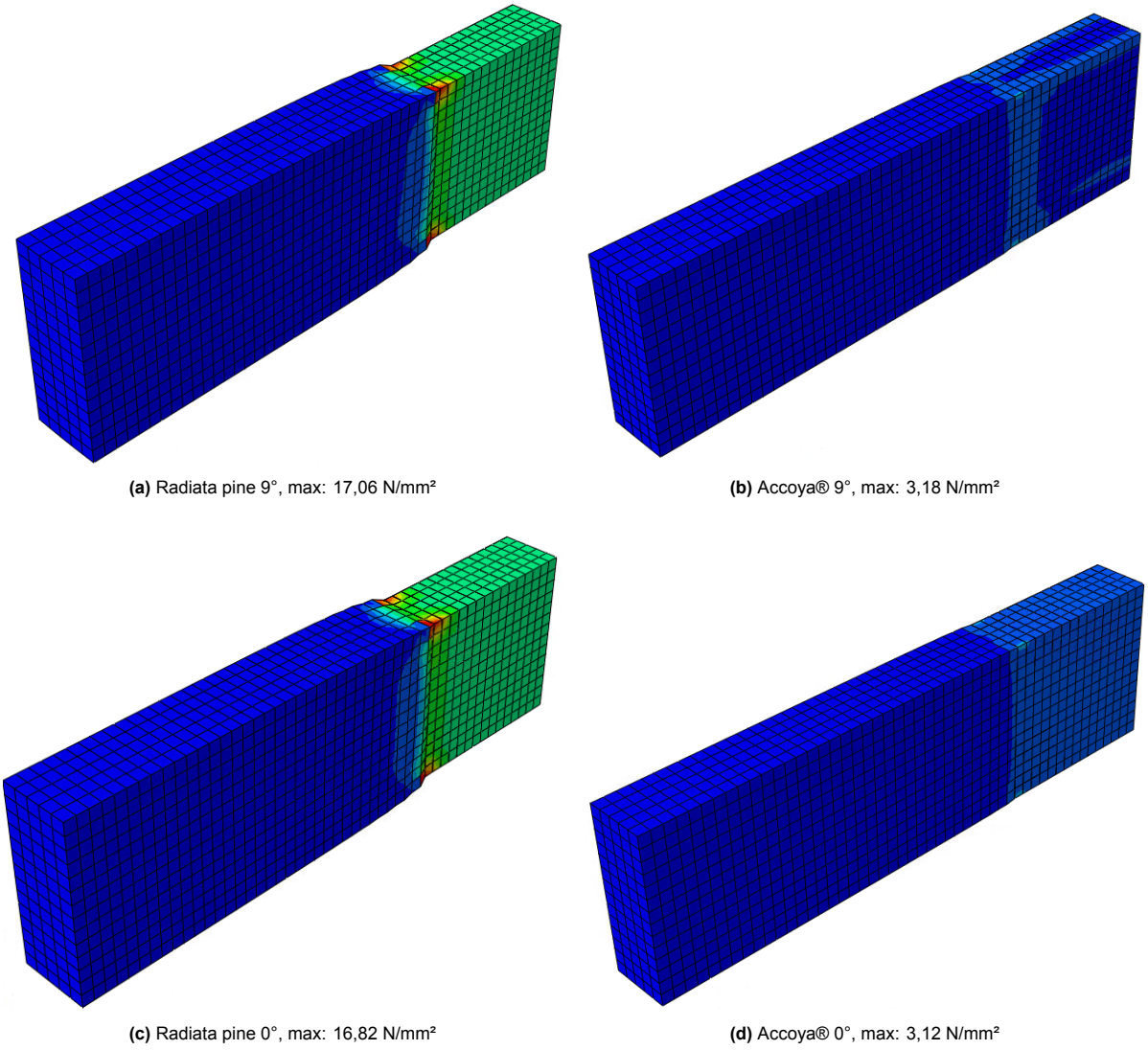

(a) Radiata pine 9°, max: 17,06 N/mm²

(b) Accoya® 9°, max: 3,18 N/mm²

(c) Radiata pine 0°, max: 16,82 N/mm²

(d) Accoya® 0°, max: 3,12 N/mm²

Figure 5.1: Min. principal stresses, deformation scale factor: 10 (Abaqus).

Table 5.1: Stress and swelling decrease.

	Radiata pine	Accoya®	Difference
Min. principal [N/mm^2]			
9° variant	17.06	3.18	-81.3%
0° variant	16.82	3.12	-81.3%
Swelling rates [%]			
Tangential	2.238	0.486	-80.2%
Radial	1.032	0.204	-78.3%

The maximum values for compressive stress are found in the corners of the material, where the tube terminates. In these corners, the stresses are significantly higher than those centrally located within the material or along the sides. This difference is clearly shown in figures 5.2 and 5.3, which plot the minimum principal stresses along the paths depicted in figure 5.4. Figure 5.2 shows that stresses in the corners more quickly reach a stress-free state after the end of the tube. This occurs because the corner of the material is not compressed by surrounding material. Along the the side face, however, mild compressive stress persists further beyond the tubes end. In both plots, an equilibrium in compressive stress within the tube is reached after the peak stress.

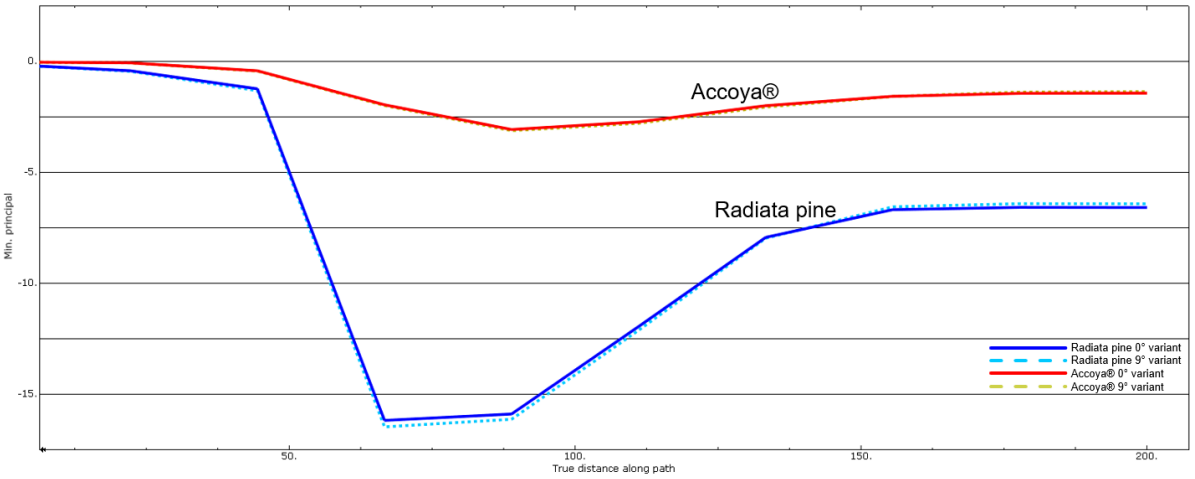

Figure 5.2: Min. principal stresses along corner path (1) (Abaqus).

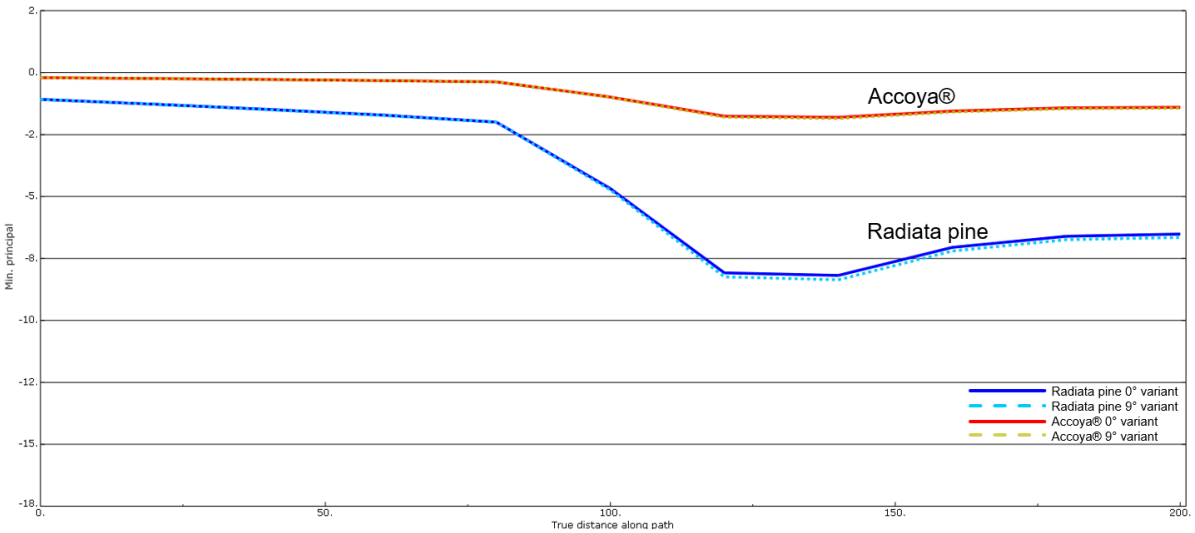

Figure 5.3: Min. principal stresses along side path (2) (Abaqus).

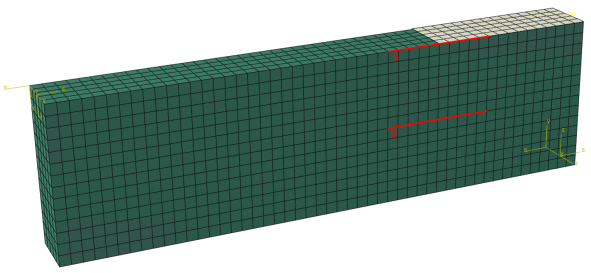

Figure 5.4: Paths followed for the graphs in figures 5.2 and 5.3.

To assess whether plastic deformation is expected, we consider in which directions yield strengths are exceeded. Figure 5.5 highlights the areas where the yield strength of 2.5 N/mm² is exceeded for the 9° variant. Figure 5.5b shows this occurs only in the corners for Accoya®. Since it is found that the yield strength is not reached perpendicular to the tube but only in the longitudinal direction (where the compressive yield strength is higher) and these are peak stresses, plastic deformation is not expected for Accoya® for the assumed degree of swelling. This deformation is expected only to contribute to

a favorable clamping fit within the tube. Figure 5.6a shows, with blue arrows, the contribution of the longitudinal compressive stress in the corners.

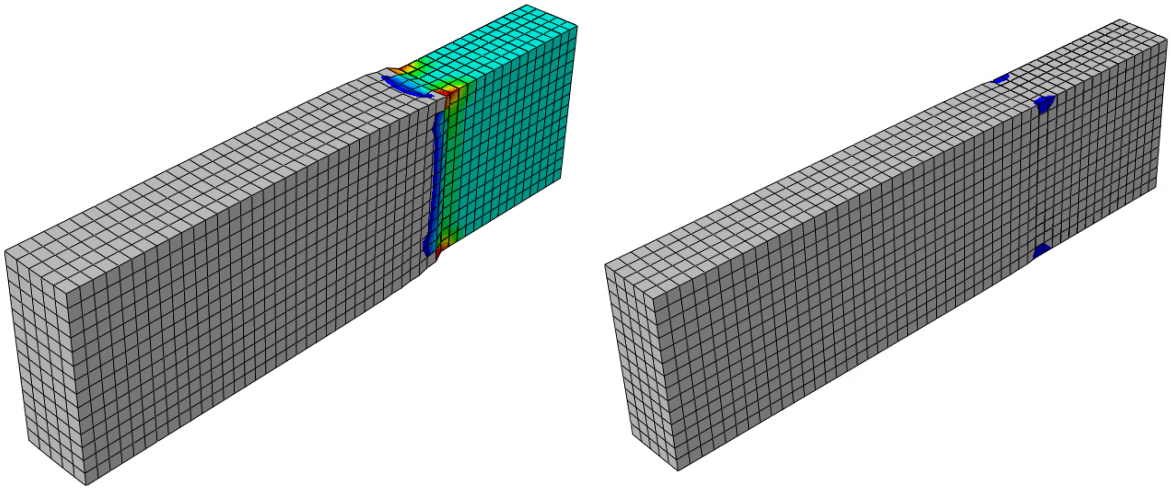

(a) Radiata pine 9°. **(b)** Accoya® 9°.

Figure 5.5: Compressive yielding areas (>2.5 N/mm²). Deformation scale factor: 10 (Abaqus).

Figures 5.6b and 5.6c display the critical areas for permanent damage. The same color scale is used across figure 5.5. Primarily, the compressive stress in the tangential direction exceeds the yield strength, with the entire material volume within the tube surpassing this threshold. Consequently, the wood faces a risk of permanent deformation from (mircro)cracking, or cellular deformation by chrushing. The maximum allowable shear stresses are slightly exceeded in the model; however, due to the minimal extent of this excess, it is not expected to lead to a failure mechanism. The maximum allowable tensile and bending stresses are not exceeded.

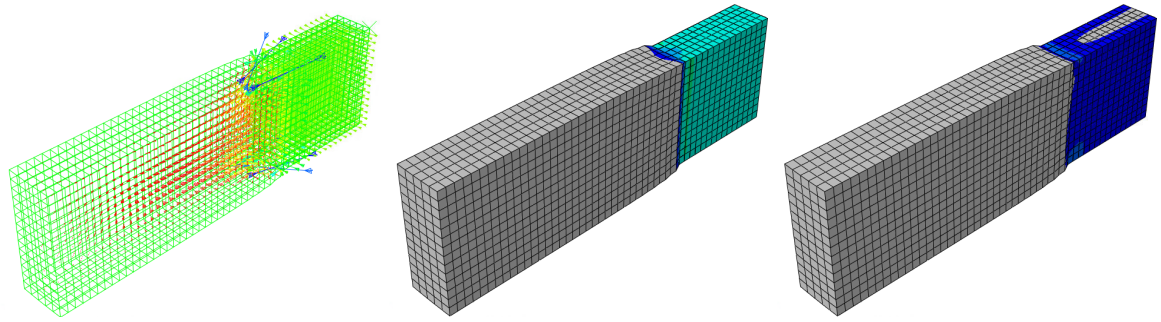

(a) Contribution of compression forces per direction. **(b)** Tangential compression yielded stresses, max: 8,04 N/mm². **(c)** Radial compression yielded stresses, max: 6,14 N/mm².

Figure 5.6: Radiata pine 9°. Deformation scale factor: 10 (Abaqus).

When compressive stresses applied perpendicular to the fibers ($\sigma_{c,90}$) exceed the yield strength, the tubular cell structure of the wood begins to buckle and collapse. The moisture content of the wood plays a role in determining how the wood will respond in situations where this exceedance occurs. Figure 5.7a shows how the wood fibers, which act like straws in a bundle, deform under compression. Initially, the cell walls may elastically bend, but as the yield strength is exceeded, plastic buckling can occur. Figure 5.7b provides a microscopic view of wood's cellular structure. Under high compressive stresses, these cells are crushed, as evidenced by the distortion and flattening of the originally hexagonal cell walls. This collapse is the primary mode of plastic deformation perpendicular to the fibers.

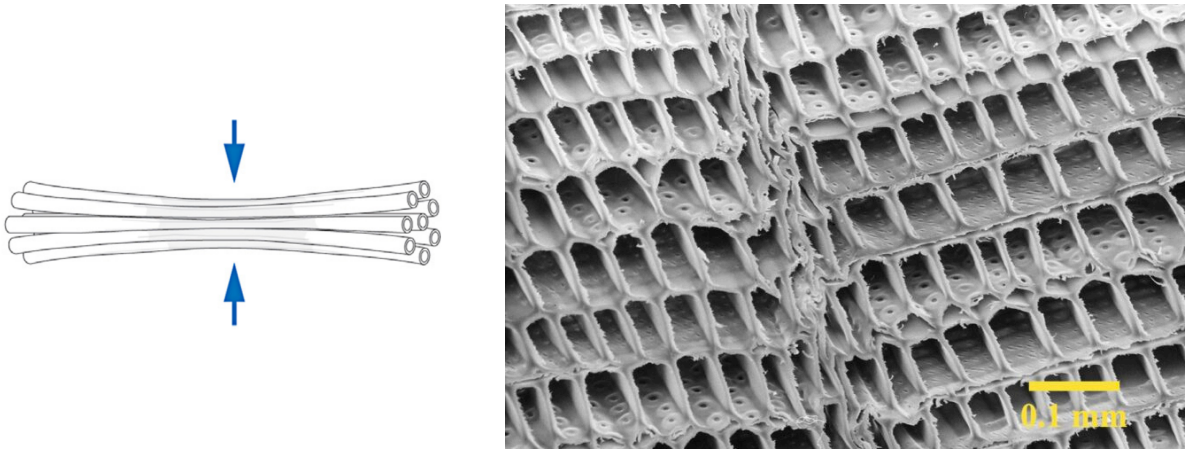

(a) Compression perpendicular to fiber: $\sigma_{c,90}$ (Malo, 2016). **(b)** A line of cells of Norway spruce collapsed under compression (Barlow, 2023).

Figure 5.7: Compression perpendicular to grain.

Figure 5.6a illustrates, with blue arrows, that the compressive peak stresses at the corners of the element are caused by stresses in the longitudinal direction of the element. Figure 5.8 displays the shear stresses in two planes along this longitudinal direction. These images show red and blue extremes, indicating opposite directions of shear stress. The shear yield strength of 3.2 N/mm² is slightly exceeded. However, this exceedance is negligible compared to the extent to which the compression yield strength is exceeded at the same locations. In a plastic model, a lower shear stress would be achieved due to the relaxation of stresses and the earlier redistribution of forces. This behavior contrasts with the current linear model, which allows compressive stresses to rise unrealistically high. A plastic model would account for material yielding and redistribution under load, reflecting a more realistic response of the system to stress concentrations.

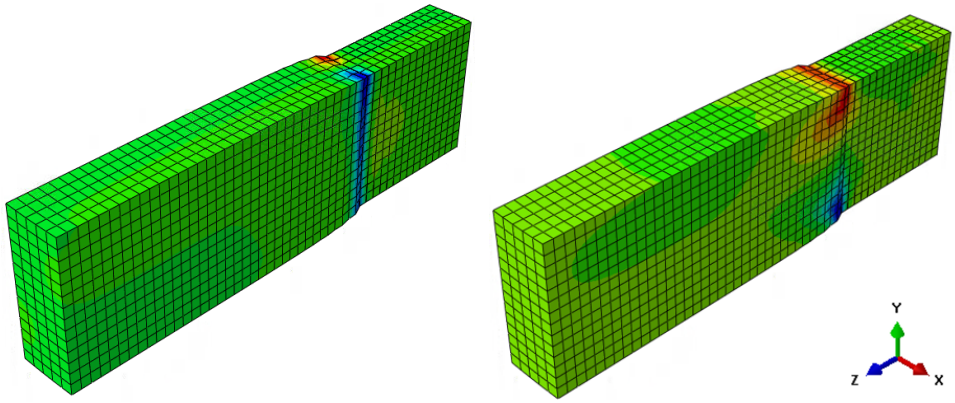

(a) YZ-plane, max: 4,15 N/mm². **(b)** XZ-plane, max: 4,04 N/mm².

Figure 5.8: Shear stresses. Deformation scale factor: 10 (Abaqus).

Rotational stiffness comparison

Based on the swelling evaluation, where tests were conducted with a tube directly adjoining the material without a gap, it can be assessed which materials are suitable for a direct-fitting tube or whether a gap should be designed. Since no plastic deformation is expected for Accoya® for this detail, it can be designed with a direct-fitting tube. For Radiata pine, however, the yield compression value is exceeded in both directions perpendicular to the fiber and tube across nearly the entire volume within the tube, with a maximum exceedance (8,04 N/mm²) of up to three times the yield strength (2,5 N/mm²).

With a 1 mm gap around the material, an additional 2 mm of space is provided in each direction within the tube. Theoretically, the loss of compressive stress in a linear stress calculation in the tangential direction can be determined as follows.

$$\sigma = E \cdot \frac{\Delta L}{L_0} = E \cdot \varepsilon = 300 \cdot \frac{2}{100} = 6\ N/mm^2$$

Given that the compression yield strenght in the tangential direction is exceeded by 5.54 N/mm² (figure 5.6b) according to the model, this gap is a reasonable choice for the Radiata pine variant. With this allowance, no areas of the material are expected to undergo plastic deformation, allowing the material to secure itself within the tube upon swelling without causing damage.

According to regulations for geometric manufacturing tolerances of steel profiles (NEN-EN 1090-2, 2018), a deviation of 0.2% to 1.0% is permitted. The 1 mm clearance currently assigned to the section represents an adjustment of 0.7% and 2.0% for how the wood fits radially and tangentially within the tube, for a profile measuring 100 by 280 mm. These tolerances must be considered when designing similar connections.

The rotational stiffness of the detail will directly change with adjustments to the gap size. Rotational stiffness was tested without material swelling for a tube directly adjoining the wood and for a tube with a 1 mm gap. The vertical displacement for these two variants is shown in figures 5.9 and 5.10.

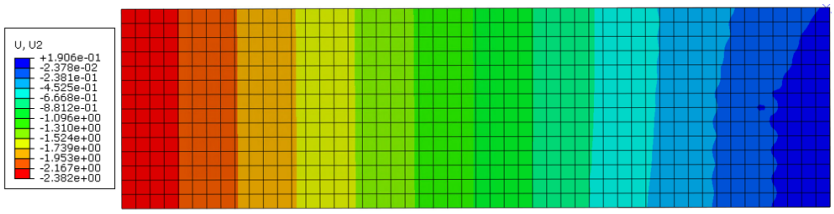

Figure 5.9: 0 mm gap variant, vertical displacement (Abaqus).

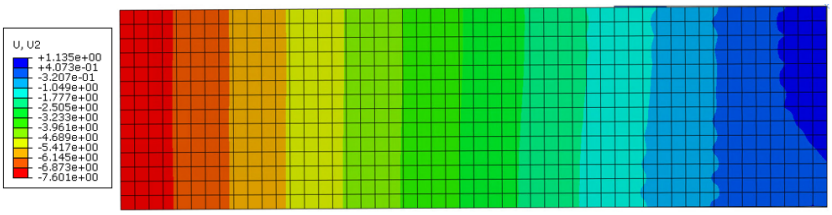

Figure 5.10: 1 mm gap variant, vertical displacement (Abaqus).

Based on the applied force (560 N) and the resulting vertical displacement, the rotational stiffness for the two variants can be determined. There is a direct linear relationship between this vertical displacement and the rotational stiffness. The variant with a 1 mm gap is therefore loose within the tube. Thus, before applying the force, a displacement of 4.5 mm was introduced at the end surface of the model. Given that the lever arm from the inserted dowel to the end of the section is 200 mm, the free displacement of the connection 900 mm from the dowel will be 4.5 mm. This is the point at which the wooden element contacts the tube.

	0 mm gap variant: (Accoya®)	1mm gap variant: (Radiata pine)
$F = \tau \cdot A$	$F = 0.02 \cdot 28,000 = 560$ N	$F = 0.02 \cdot 28,000 = 560$ N
$\theta = \frac{u}{r}$	$\theta = \frac{2,382}{900} \approx 0,0026467$ rad	$\theta = \frac{7,601}{900} \approx 0,0084457$ rad
$M = F \cdot r$	$M = 560$ N $\cdot\ 900$ mm $= 504000$ Nmm	$M = 560$ N $\cdot\ 900$ mm $= 504000$ Nmm
$K_0 = \frac{M}{\theta}$	$K_0 = \frac{504000 \text{ Nmm}}{0,0026467 \text{ rad}} \approx 1.904 \times 10^8$ Nmm/rad	$K_0 = \frac{504000 \text{ Nmm}}{0,0084457 \text{ rad}} \approx 5,968 \times 10^7$ Nmm/rad
	$K_0 \approx \underline{1.904 \times 10^5 \text{ kNmm/rad}}$	$K_0 \approx \underline{5,968 \times 10^4 \text{ kNmm/rad}}$
		Without 4,5 mm free displacment:
		$K_0 \approx \underline{1,463 \times 10^5 \text{ kNmm/rad}}$

There is no standard analytical method available for this type of connection to verify the numerical rotational stiffness values found, as is possible with the circular dowel connection. The rotational stiffness values obtained here are more than twice as low compared to the circular dowel connection. However, the results of this model focus not on the differences between connection types but rather on the differences between materials for identical connections. The rotational stiffness for the 1mm gap variant is reported both with and without free movement in the tube.

Under a load that consistently acts on the connection from the same angle, the second mentioned rotational stiffness will apply. However, if the force approaches from the opposite side, causing the rotational stiffness to rely on the tube, a shift may occur. In practice, this can be prevented by incorporating more than one dowel.

5.2. Circular dowel connection

The results for the circular dowel connection consist of two components. First, the effect of swelling was tested for Accoya® and Radiata pine under identical conditions. The materials were compared using corresponding models. Based on these results, necessary adjustments have been made in the model to prevent material failure, and a certain degree of material failure has been pre-modeled. Subsequently, these two models were compared in terms of rotational stiffness. In rotational stiffness tests, the material was not allowed to swell.

Swelling evaluation

The swelling of the materials were conducted in both the tangential and radial directions. Since this connection includes three wooden elements, one of which is rotated 90 degrees relative to the other two, only the tangential direction remains consistent across all three wooden elements. Figure 5.11 shows the (Y) deformation of the rotated elements relative to each other. In tangential direction (horizontal direction in figure 5.11), the dowels pass through the connection, and the wood exhibits the greatest expansion per unit distance.

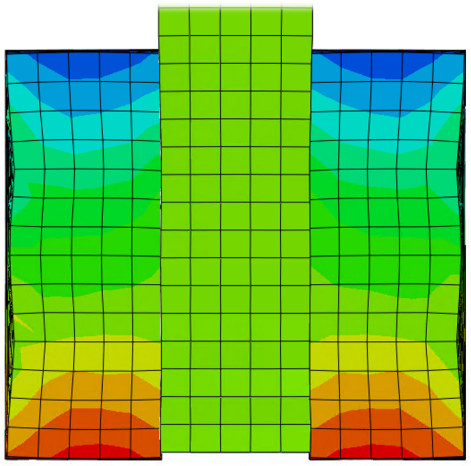

Figure 5.11: Top view horizontal (Y) displacement, deformation scale factor: 5 (Abaqus).

Figures 5.12 and 5.13 show the minimum principal stresses for Accoya® and Radiata pine with identical color scales. The dowels are not visible in these results. The results do not include curved swelling due to the complex mesh distribution of the wooden elements, as explained in the methodology chapter. The highest compressive stresses occur near the ends of the dowels, as well as along the dowel in the central element, where it is pressed into the wood due to the swelling of the two rotated outer elements.

Here, it is again important to recognize the significance of verifying the direction in which the stresses occur as the properties of wood (and therefore the yield strengths) differ depending on whether the direction is perpendicular or parallel to the grain. Additionally, high peak stresses are present. In reality, these will not manifest due to plastic deformation or fracturing of the wood. Through plastic deformation of the material, the internal stress distribution will be reallocated. The material would not sustain such high stress levels as suggested by the model.

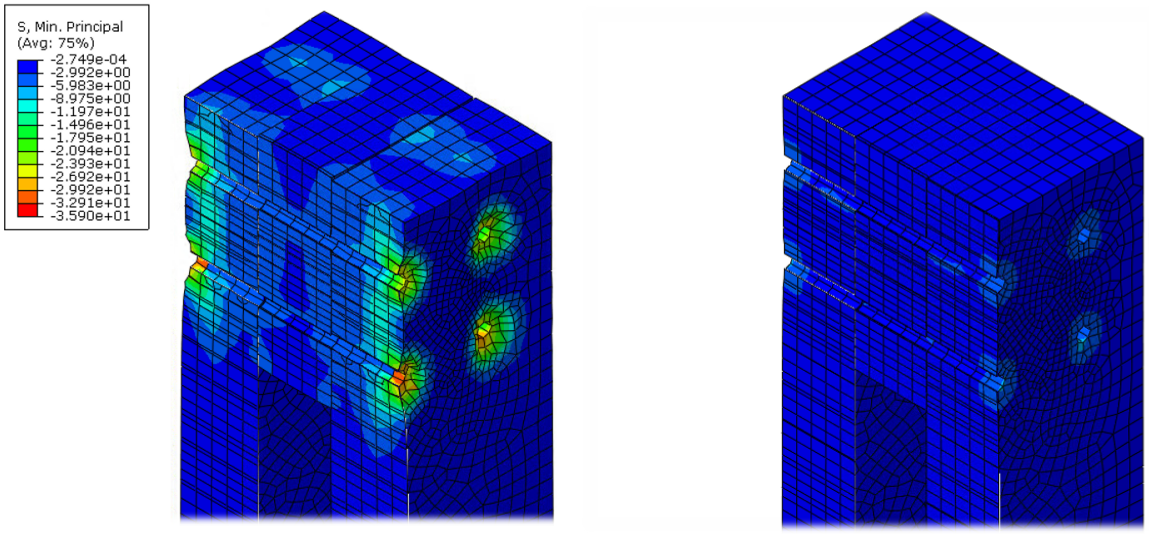

(a) Radiata pine. **(b)** Accoya.

Figure 5.12: Vertical cut, min. principal stresses, deformation scale factor: 5 (Abaqus).

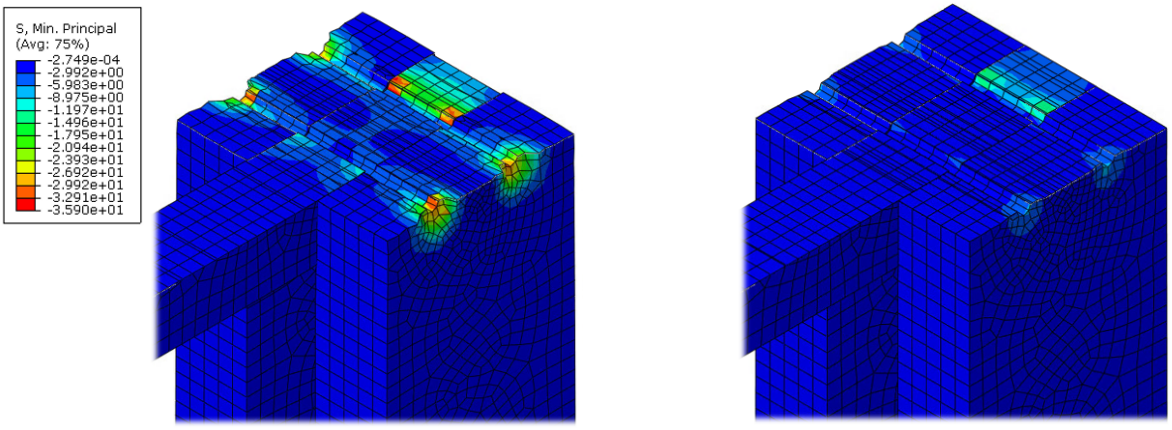

(a) Radiata pine. **(b)** Accoya.

Figure 5.13: Horizontal cut, min. principal stresses, deformation scale factor: 5 (Abaqus).

Figure 5.14 highlights the areas where the compression yield strength is exceeded, identifying regions where stresses may be critical for plastic deformation. In the Radiata pine model, this threshold is surpassed in nearly all regions where the dowels are positioned, with stresses reaching up to 11 times the compression yield strength. In contrast, for Accoya, this value is only slightly exceeded, with peak stresses reaching up to twice the compression yield strength in the tangential direction.

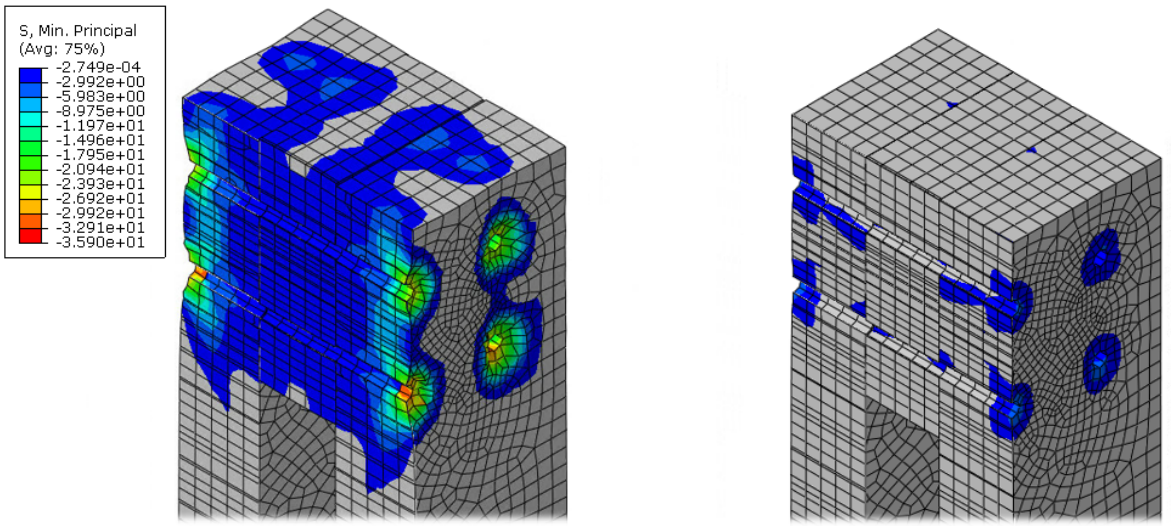

(a) Radiata pine. **(b)** Accoya.

Figure 5.14: Compressive yielding areas (>2.5 N/mm²). Deformation scale factor: 5 (Abaqus).

Figure 5.15 shows the compressive yielding areas per direction. The Y- and Z-directions are not labeled based on the grain direction, as the elements are rotated relative to each other. The cross-sections were selected to highlight the most critical locations for each direction. The central element shows a large highlighted area for the Z-direction (S33) compression stresses (figure 5.15c). However, it should be noted that this stress occurs along the length of this element, which aligns with its longitudinal (grain) direction, in which the wood is significantly stronger. However, the yield strength parallel to the grain (19 N/mm²) is slightly exceeded here.

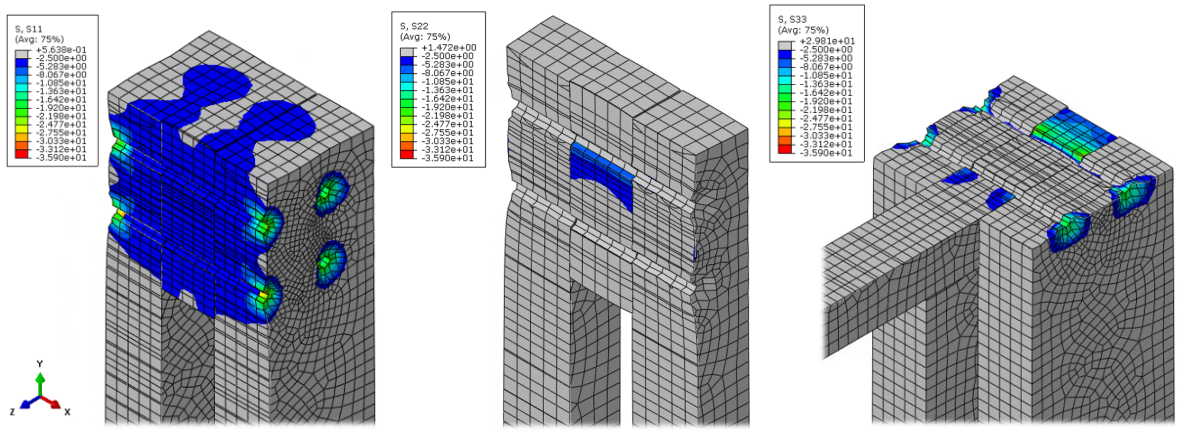

(a) Tangential (X) direction. **(b)** Y-direction. **(c)** Z-direction.

Figure 5.15: Radiata pine compressive yielding areas (>2.5 N/mm²). Deformation scale factor: 5 (Abaqus).

In addition to compressive stresses, which are critical in this example, tensile stresses were also identified in some locations where the tensile yield strength is exceeded. Figure 5.16 shows a cross-section of the outer element. These tensile stresses are less significantly exceeded compared to the compressive stresses and are therefore expected to play a lesser role. When a portion of the material yields under compression, it is anticipated that the tensile stresses will also redistribute and diminish.

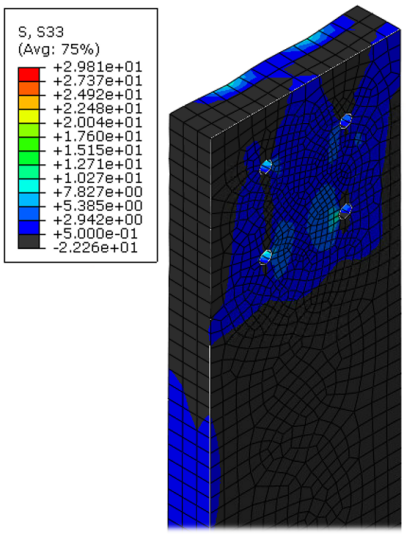

Figure 5.16: Yielded tangential tensile forces outer element (>0.5 N/mm²), deformation scale factor: 5 (Abaqus).

For this particular modeled connection, four dowels are used to avoid extra complexity in the model and to better capture and analyze the effect of individual dowels. In connections designed to withstand high shear forces or moments, typically more than four dowels are applied in a circular arrangement. With a greater number of dowels, the forces can be distributed across more dowels, reducing the load on each individual dowel. This also applies to the stresses arising from radial swelling between dowels.

Rotational stiffness comparison

Based on the swelling evaluation, the suitability of the connection type in its current form was assessed. Given that the stresses found for the Accoya® variant do not significantly exceed yield strenghts, the model used for the swelling evaluation was used to test the rotational stiffness, this time excluding swelling. For the Radiata pine model, two adjustments are made. First, the dowel lengths are extended to provide the material with additional space in the tangential direction. In practice, similar measures

could involve adding flexible adhesive in the additional space or using more flexible dowels. Second, the embedment of the dowel hole is pre-modeled at the most critical location where swelling-induced stresses are expected to cause ductile deformation.

Predicting (brittle) cracks in the material is challenging to model accurately. To estimate potential cracking, many additional assumptions would need to be made, and the connection could deform to the extent that it loses its full stiffness. Therefore, the two adjustments described were chosen to observe potential differences in rotational stiffness without overcomplicating the model.

The model indicates high peak stresses caused by dowel compression, but a more significant concern is the general exceedance of compression yield strengths. By extending the dowels by 6 mm, a theoretical reduction in compressive stress in the tangential direction is anticipated, based on a the following linear stress calculation.

$$\sigma = E \cdot \frac{\Delta L}{L_0} = E \cdot \varepsilon = 300 \cdot \frac{6}{300} = 6 \; N/mm^2$$

By extending the dowels, the wooden elements will exert less pressure against each other due to the gap that may form between the elements (figure 5.17), reducing the contribution of shear resistance between these elements. Additionally, an extra moment effect will occur on the dowels. Both factors will lead to a decrease in rotational stiffness.

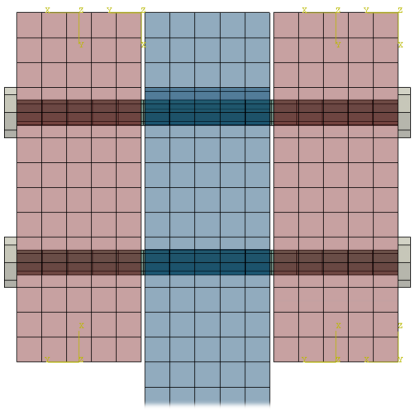

Figure 5.17: Adjusted connection with a 3mm gap between the elements, top view (Abaqus).

In addition to extending the dowels, the dowel hole in the central element has been pre-modeled as embedded due to ductile failure at the most critical location. This type of failure typically arises from external forces in practice; however, internal forces from swelling can also contribute to its occurrence. Figures 5.15b and 5.15c illustrate the cause and rationale for the pre-modeled failure of this dowel hole. Both figure 5.17 and 5.18 show the location of the pre-modeled embedded hole.

Figure 5.18: Embedded dowel hole in the central element due to ductile failure (Abaqus).

The rotational stiffness has already been tested in the methodology chapter using the original model. This is now also conducted with the adjusted model, which represents the Radiata pine variant. Figure 5.19 show the results of both tests.

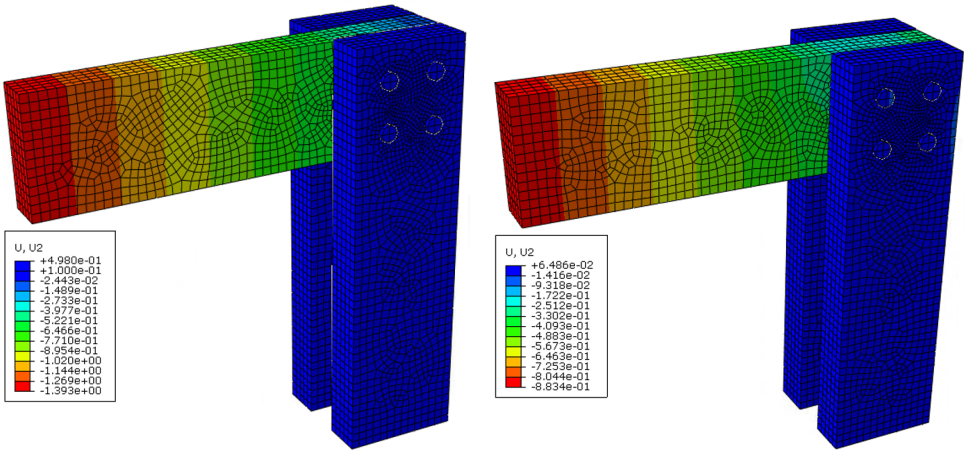

(a) Radiata pine variant, max. 1,393 mm. **(b)** Accoya® variant, max. 0,8834 mm.

Figure 5.19: Vertical displacements, deformation scale factor: 10 (Abaqus).

The rotational stiffness values, calculated based on the applied force (560 N) and vertical displacement of the two variants, are determined as outlined below. There is a direct linear relationship between this vertical displacement and the rotational stiffness.

	Radiata pine variant:	Accoya® Variant:
$F = \tau \cdot A$	$F = 0.02 \cdot 28,000 = 560$ N	$F = 0.02 \cdot 28,000 = 560$ N
$\theta = \frac{u}{r}$	$\theta = \frac{1{,}393}{860} \approx 0,0016198$ rad	$\theta = \frac{0{,}8834}{860} \approx 0,0010272$ rad
$M = F \cdot r$	$M = 560$ N $\cdot\, 860$ mm $= 481600$ Nmm	$M = 560$ N $\cdot\, 860$ mm $= 481600$ Nmm
$K_0 = \frac{M}{\theta}$	$K_0 = \frac{481600 \text{ Nmm}}{0{,}0016198 \text{ rad}} \approx 2,973 \times 10^8$ Nmm/rad	$K_0 = \frac{481600 \text{ Nmm}}{0{,}0010272 \text{ rad}} \approx 4,688 \times 10^8$ Nmm/rad
	$K_0 \approx \underline{2,973 \times 10^5}$ kNmm/rad	$K_0 \approx \underline{4,688 \times 10^5}$ kNmm/rad

The results for rotational stiffness for the two connections—clamped and circualr dowel—provide a broad approximation rather than precise predictions of real-world performance. Due to model simplifications, these findings offer a general understanding of how Accoya® and Radiata pine might behave in each connection type, but they should not be regarded as exact representations. The analysis highlights general trends in stiffness and stress distribution for each timber type, giving an overall sense of their structural behavior rather than detailed, accurate data. The results are better suited for interpretation as relative differences between the two materials.

5.3. Portal frame implementation

In this section, the rotational stiffness values derived from the connection models are implemented into the portal frame model to evaluate their impact on overall structural behavior. The specific portal frame configuration used for this analysis, as outlined in the methodology chapter, allows a comparison of how Accoya® and Radiata pine could influence frame stability, internal force distribution, and displacement under load. This implementation provides insights into the practical implications of material choice on frame performance. The model used includes four semi-rigid connections at the top and bottom of the

columns. First, the rotational stiffness varies but is applied consistently across all four connections in each analysis. Second, a combined configuration of the two connection types is tested, utilizing either Accoya® properties or Radiata pine properties. All with a horizontal point load of 2 kN on the model. This analysis focuses not on the absolute values of moment and displacement but on the differences between these values.

Since the semi-rigid connections approximate moment-fixed connections and are expected to behave similarly, the portal frame with moment-fixed connections is shown first for comparison in figure 5.20.

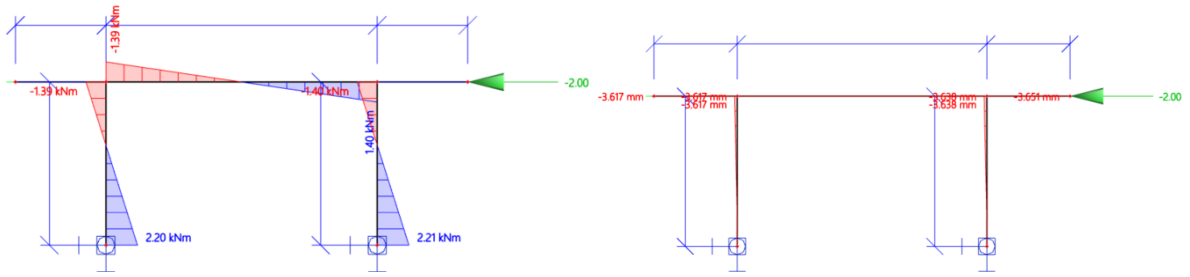

(a) Moment distributions, max: 2,21 kNm. **(b)** Displacements, max: 3,6 mm.

Figure 5.20: Rigid base plate, rigid column-beam (SCIA).

Table 5.2 and figure 5.21 show the values found for the rotational stiffness of the two connection types, using two different materials. The distinction between 'clamped connection (1)' and 'clamped connection (2)' lies in whether or not the free rotation allowed in the 1mm variant is included. This is explained in chapter 5, Results: Clamped Connection; Rotational Stiffness Comparison.

Table 5.2: Rotational stiffness values.

	Radiata pine [kNmm/rad] $\times 10^5$	Accoya® [kNmm/rad] $\times 10^5$	Absolute difference
Clamped connection (1)	0,5968	1,904	· 3,19
Clamped connection (2)	1,463	1,904	· 1,30
Circular dowel connection	2,973	4,688	· 1,58

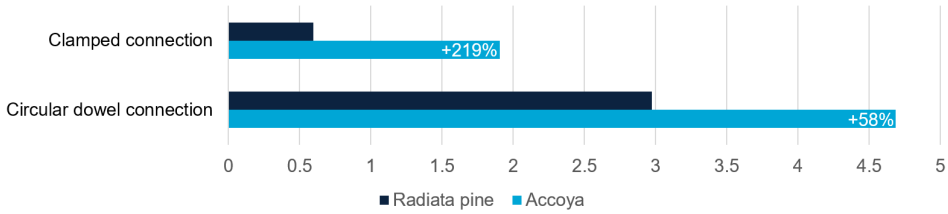

Figure 5.21: Rotational stiffness values [kNmm/rad $\times 10^5$].

Identical connection properties

First, identical rotational stiffnesses are assigned to all four connections. These rotational stiffness values are implemented in the portal frame model in figures 5.22 and 5.24. For the clamped connection, the values from 'clamped connection (1)' are used.

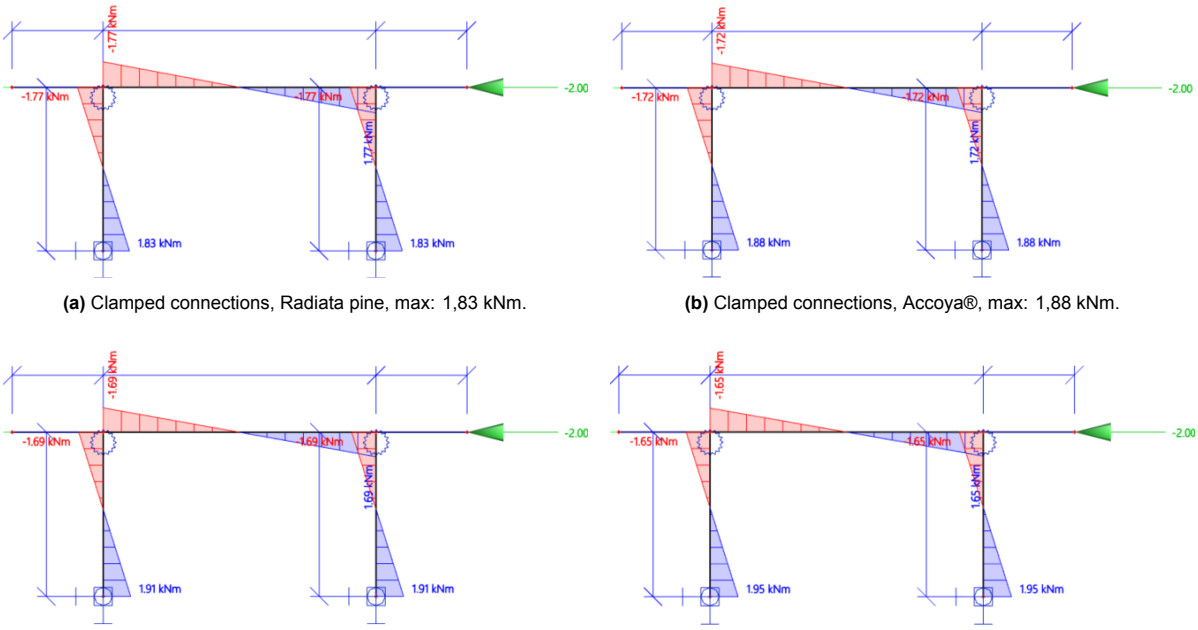

(a) Clamped connections, Radiata pine, max: 1,83 kNm.

(b) Clamped connections, Accoya®, max: 1,88 kNm.

(c) Circular dowel connections, Radiata pine, max: 1,91 kNm.

(d) Circular dowel connections, Accoya®, max: 1,95 kNm.

Figure 5.22: Moment distributions (SCIA).

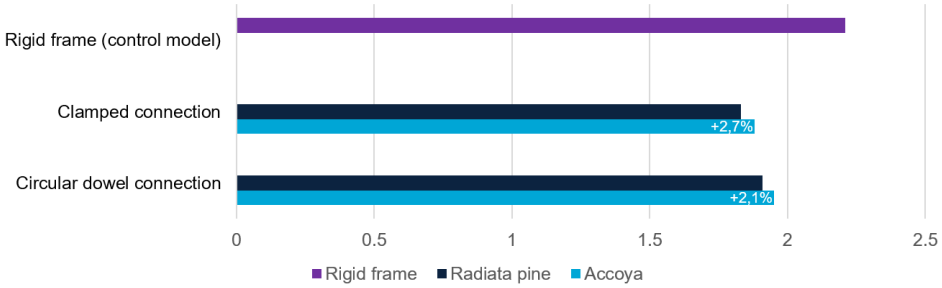

Figure 5.23: Max. moment [kNm].

The observed trend is that as rotational stiffness decreases, the moment distribution becomes more spread across the portal frame. Greater rotational stiffness leads to higher moments, as stiffer frames more directly absorb and transfer the applied moments. Figures 5.24 and 5.25 show the corresponding horizontal displacements, illustrating that as rotational stiffness decreases, displacements increase.

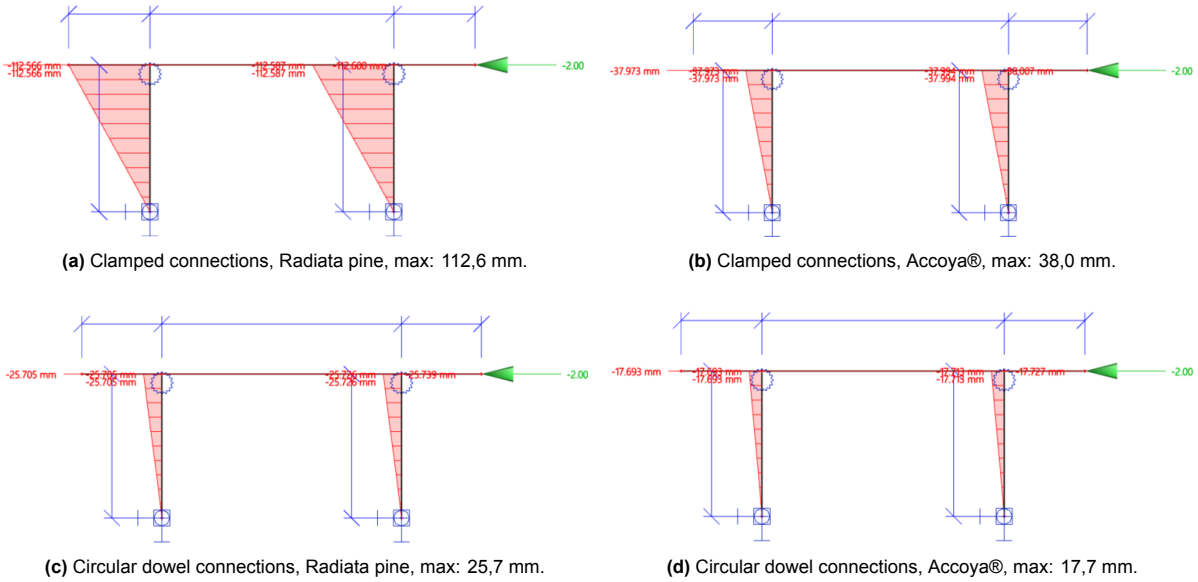

(a) Clamped connections, Radiata pine, max: 112,6 mm.

(b) Clamped connections, Accoya®, max: 38,0 mm.

(c) Circular dowel connections, Radiata pine, max: 25,7 mm.

(d) Circular dowel connections, Accoya®, max: 17,7 mm.

Figure 5.24: Horizontal displacements (SCIA).

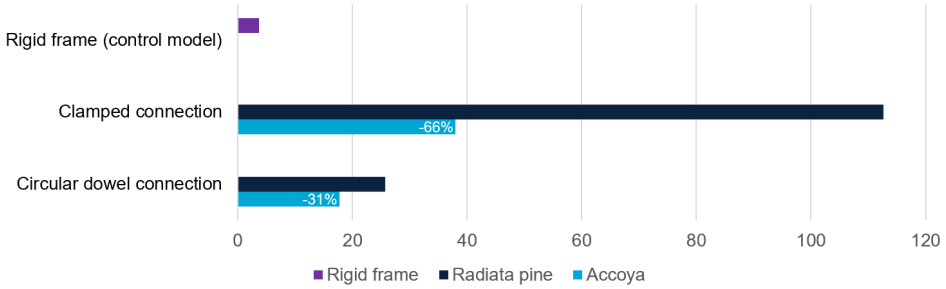

Figure 5.25: Max. horizontal displacements [mm].

These portal frames illustrate the effect of varying rotational stiffness within a portal frame. Here, the cantilevers are modeled as continuous beams running through the entire beam. In reality, as seen in the design of the Nijmegen station platform 5-6, these cantilevers can be designed as separate elements individually connected at the node. In such cases, the rotational stiffness at the node connecting to the cantilever directly influences its deflection. Stiff connections are therefore of utmost importance in minimizing deflection in cantilevers.

Combined connection properties

Second, for a more practical example and an additional comparison between the two materials, a combined connection configuration is implemented. The clamped connection is applied at the base joint, while the circular dowel connection is positioned at the top of the column, based on their logical and appropriate suitability for these locations. For this example, a more comprehensive stability analysis and strength analysis are conducted.

Table 5.3: Combined connections comparison.

	Radiata pine	Accoya®	Relative difference
Max. moment [kNm]	2,83	2,27	-20%
Max. horizontal displacement [mm]	45,5	25,8	-43%

With this combination of connections, the greatest moment effect and the largest horizontal displacement are observed when using Radiata pine rotational stiffness values. The maximum moment naturally occurs at the top of the column, where the rotational stiffness is higher (figure 5.26).

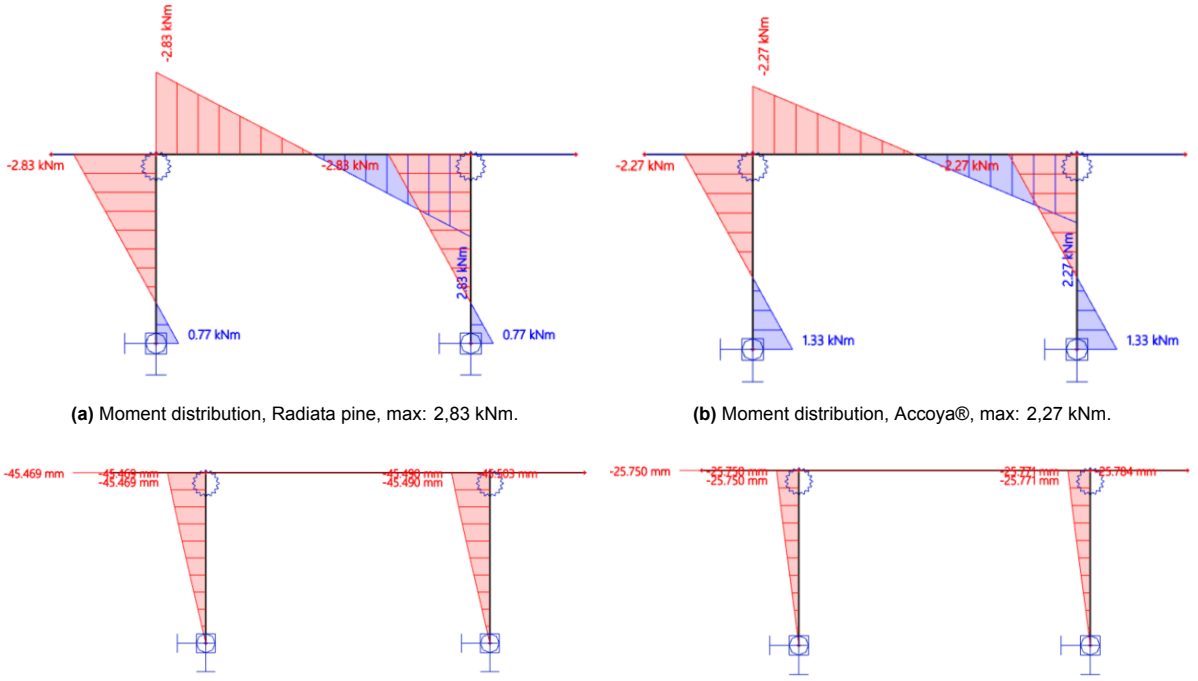

(a) Moment distribution, Radiata pine, max: 2,83 kNm.

(b) Moment distribution, Accoya®, max: 2,27 kNm.

(c) Horizontal displacement, Radiata pine, 45,5 mmm.

(d) Horizontal displacement, Accoya®, max: 25,8 mm.

Figure 5.26: Combined connections comparison (SCIA).

The frame properties are based on a GL22h strength class with dimensions of 100 x 280 mm. This represents a relatively narrow construction but with rotational stiffness appropriate for these dimensions. A horizontal point load of 2 kN has been applied. It is important to note that the focus here is on the relative differences in stiffness observed, and not on these specific dimensions or load magnitudes. Nevertheless, the deviations are briefly compared to the standards according to NEN-EN 1990 A.1.4.3. For an industrial building with a single story, the maximum allowable horizontal displacement is 1/150 of the height (3600 mm / 150 = 24 mm). For other single-story buildings, this limit is 1/300 of the height (3600 mm / 300 = 12 mm). Both limits are exceeded, but the more favorable limit is surpassed by only 7.5% when using Accoya® properties.

A strength analysis is performed by checking the portal frame for bending strength. For this verification calculation, the primary emphasis is placed on assessing the strength of the columns and beams. The connections are excluded from consideration here, as they have already been subjected to a comprehensive and detailed analysis. The shared parameters used are listed below in a single column. The bending strength for GL22h [22 N/mm²] has been applied and the partial factor for glulam [1.3] has been applied.

$$I = \frac{b \cdot h^3}{12} = \frac{100 \cdot 280^3}{12} \approx 1.83 \times 10^8 \,\text{mm}^4$$

$$\sigma_{\text{design}} = \frac{f_{m,k}}{\gamma_m} = \frac{22}{1.3} \approx 16.92 \,\text{MPa}$$

For both materials, a bending strength unity check has been performed below. There is a linear relationship between the unity check and the maximum moment formation for both materials. The unity check demonstrates that the structure, in its current configuration, comfortably meets the requirements.

	Radiata pine Variant:	Accoya® Variant:
M_{max}	$M_{\text{max}} = 2.83\,\text{kNm}$	$M_{\text{max}} = 2.27\,\text{kNm}$
$\sigma_{\text{bending}} = \frac{M \cdot c}{I}$	$\sigma_{\text{bending}} = \frac{2.83 \cdot 10^6 \cdot 140}{1.83 \cdot 10^8} \approx 2.17\,\text{MPa}$	$\sigma_{\text{bending}} = \frac{2.27 \cdot 10^6 \cdot 140}{1.83 \cdot 10^8} \approx 1.74\,\text{MPa}$
$\text{U.C.} = \frac{\sigma_{\text{bending}}}{\sigma_{\text{design}}}$	$\text{U.C.} = \frac{2.17}{16.92} \approx 0.1283$	$\text{U.C.} = \frac{1.74}{16.92} \approx 0.1028$

In the current model, it becomes evident that when this construction is tested for stability and strength, stiffness is clearly the critical factor. Stiffness has been evaluated based on the NEN standards, which the structure fails to satisfy, whereas the strength requirements are more than adequately satisfied. This indicates that, for this specific construction, particular attention must be given to the moment-resistant connections, ensuring they maintain a sufficiently high rotational stiffness.

6

Discussion

In this discussion, the focus is on summarizing all the assumptions and limitations of the findings of this study, followed by a literatur reflection. Many of these aspects have already been addressed in the results chapter and, predominantly, in the research method chapter.

Modeling assumptions and limitations

Perhaps the most significant limitation of the model used is its inability to simulate anything beyond linear elastic material behavior. As long as internal forces remain within all yield strengths, the anisotropic model can reasonably predict material behavior. If yield strengths are exceeded in the model, it can no longer generate a realistic material response due to the perpetuation of infinite linear material behavior. The inability to simulate plastic behavior also affects the interaction between different stress types. For instance, in the models, shear yield strengths are occasionally exceeded, which would not be expected if compressive stress were not to continue infinitely in a linear manner. When a material undergoes plastic deformation, stresses are more evenly distributed, and relaxation occurs. For this reason, a distinction has been made between models used for swelling analysis and those used for rotational stiffness analysis. Combining models, and thereby linear responses that should have been plastic, will not produce realistic outputs. To distinguish the rotational stiffness of Accoya® and Radiata pine, a manual adjustment was applied to the Radiata pine models. While a more accurate approach would involve directly modeling the plastic behavior, this was not implemented due to its complexity. Instead, a simpler method was chosen, as manually predicting plastic behavior in a separate preliminary step would result in an even greater deviation from reality. This manual prediction was intentionally kept imprecise, as it was already based on significant assumptions.

In developing the model for this study, several simplifications were necessary, though they introduce limitations that must be carefully considered when interpreting the results. One notable simplification is the assumption of uniform moisture absorption across the Accoya® and Radiata pine modeled materials. In reality, moisture does not diffuse uniformly; instead, it enters most rapidly along the grain direction due to the anisotropic structure of wood. This directional behavior affects swelling, which varies depending on moisture entry points and can cause localized dimensional changes throughout the structure. The material, however, was allowed to undergo curved swelling (i.e., cupping) in the model, which can be a factor in delayed moisture absorption. In reality, wood may undergo stress relaxation following (curved) swelling, gradually reducing the internal stresses that initially arise due to moisture absorption. This relaxation can mitigate the buildup of internal stresses in natural wood over time, an effect that is not accounted for in the static model applied in this study. This relaxation is caused by the viscoelastic property of wood, which is more pronounced at higher moisture contents.

For the model used in this study, it is assumed that the wood is designed and installed under a relative humidity of 65%, subsequently swelling to a relative moisture content of 95% after construction. Assuming relatively dry conditions during construction and prolonged exposure of the wood joints to condensation during the first annual humidity cycle, this represents a realistic but not inherently obvious scenario. This cycle is intended to simulate the potential risks of moisture fluctuations and dimen-

sional instability. To allow the wood to fully equilibrate to a moisture content corresponding to a relative humidity of 95%, it must be exposed to such conditions for a prolonged period. Considering that condensation primarily occurs at night and typically evaporates during the day, the likelihood of sustained high humidity conditions is low unless ventilation is inadequate. Achieving a balanced moisture content corresponding to a specific relative humidity can take over a year. However, it should be noted that the research data from SHR are not based on such extended periods. These values are based on fully oven-dried wood to ensure a baseline moisture content of 0%, which was subsequently conditioned to a specific relative humidity for a period until 'equilibrium was reached based on stablized wieght and dimension measurements' (SHR, 2007, 2018). It is crucial to understand that the first annual cycle is replicated in the models, as this cycle is the most critical for plastic deformation due to the hysteresis effect and the wood undergoes its full range of moisture uptake and release for the first time.

The model input parameters are discrete and produce precise outcomes. Results do not require detailed interpretation. Material properties are based on the GL22h strength class and values provided by SHR. The dimensions in the model are discretely defined and play a significant role in internal force interactions. Even small changes in dimensions have a substantial impact on these forces. The clamped connection is highly dependent on precise dimensions and quickly loses stiffness when dimensions deviate. According to regulations for geometric manufacturing tolerances of steel profiles (NEN-EN 1090-2, 2018), a deviation of 0.2% to 1.0% is permitted. The 1 mm clearance assigned to the section represents an adjustment of 0.7% and 2.0% for how the wood fits radially and tangentially within the tube, for a profile measuring 100 by 280 mm. Dimensional tolerances of the wooden component also play a role. These tolerances are not included in the model, which therefore provides specific but limited insights. The primary goal of the model is to simulate the material, with differences observed in identical scenarios solely due to variations in swelling parameters.

In reality, wood grains and thus the direction of wood properties will not be perfectly perpendicular as the model implies. Fiber inclination or grain deviation can significantly influence the mechanical behavior of the wood. When fibers are not aligned with the main load direction, the tensile and compressive strengths of the wood may decrease. Non-straight grain patterns increase the likelihood of cracking and splitting, as stress can accumulate along the curved fiber structures. Curved grains can also generate shear stresses that are more challenging to predict with a standard orthotropic model. Since the properties no longer align precisely with the orthogonal axes, stress transformations arise that would not normally occur in a wood model with straight grains. However, the model has incorporated the curvature of the tangential axis if curved swelling (i.e., cupping) is included but does not account for further variations in the position and direction of the wood grain. This cupping effect was incorporated and tested in the model at various magnitudes. For the results, a cupping variant with a larger cupping effect than typically observed was utilized. This approach was chosen to amplify even minor effects of cupping and to identify its potential consequences. Additionally, the model assumes uniform material properties throughout the material, without accounting for the effects of individual laminates and adhesive layers. However, due to the relatively low strength class of the material used, adhesive failure is not expected, as the material itself is relatively weak and likely to govern failure behavior.

The model treats model parameters, except from expansion factors, equally for Accoya® and Radiata pine, though this is an approximation. The molecular structure of Accoya® has been fundamentally altered through acetylation, which affects its mechanical response, strength retention, and resistance to stiffness loss over time. These changes could mean that Accoya® retains its structural properties longer than unmodified timber, but this remains under-researched. Therefore, while maintaining similar parameters simplifies the model, it likely does not fully reflect the differential performance of Accoya® versus unmodified timber.

In practice, wood under sustained loads undergoes creep deformation over time, gradually reducing its stiffness and affecting its long-term structural performance. Accoya®, being chemically modified, might exhibit distinct creep behavior compared to unmodified timber, as its altered molecular structure reduces susceptibility to moisture and creep-related deformation. However, accurately capturing this in a time-dependent model would require more advanced simulations beyond the scope of this study.

Fatigue, also excluded from this model, is another important real-world factor, particularly in outdoor applications where cyclic moisture fluctuations lead to repeated swelling and shrinkage. This cyclical stress can gradually degrade wood, particularly unmodified types like Radiata pine, whereas Accoya®

may perform differently due to its reduced moisture absorption and higher dimensional stability. This phenomenon was not tested using the static model.

Steel components in the model were treated as either significantly stiffer or infinitely stiff, simplifying the interactions between wood and steel. In reality, however, steel parts would exhibit some degree of flexibility, potentially reducing stress concentrations at the wood-steel interface. This added flexibility could lessen the stresses imparted on the wood, an effect not captured in the current model.

Literature reflection

Comparable research has been conducted on moisture-induced deformations and their influence on the structural performance of timber structures using FEM modeling. For instance, models have been developed to predict crack formation. However, none of these studies specifically focus on highlighting the differences in dimensional stability between various wood species or materials. Accoya®, in particular, has not yet been modeled in this context.

This study's findings tend to align with those of Bongers, Marcroft, et al., 2014, who observed that Accoya® maintains its structural integrity under high-moisture conditions more effectively than unmodified timber. The increase in load capacity and minimal bending strength reduction in service class 3 (SC3) conditions suggest that Accoya®'s performance remains more stable even in these conditions. This supports the notion that the k_{mod} and k_{def} factors in Eurocode 5 may be less applicable to Accoya® and could be optimized to reflect its resilience to moisture-induced degradation. Adjusting these values might enable more efficient designs using less material.

The thesis has focused on Accoya® to stay within the timeframe of a single study. It is important, however, to remain aware of other wood modification techniques that demonstrate similar performance. For example, Densified Veneer Wood, made from compressed veneer layers, also exhibits high dimensional stability and good strength, though it is significantly heavier and more expensive. Additionally, furfurylated and thermally modified wood are alternatives, though they offer lower dimensional stability than Accoya®.

Additionally, the issue of wood swelling has been amplified in this thesis by specifically targeting connections where swelling would have the greatest impact on performance. The influence found in these cases is therefore not representative of the general swelling issue. From a design engineering perspective, such situations are typically avoided. However, a more dimensionally stable wood variant like Accoya® offers new possibilities for design, enabling connections and applications that would otherwise be limited by swelling concerns.

From a practical standpoint, the modeling approach used here was efficient, enabling analysis within the project's timeframe. However, while this approach offers preliminary insights, experimental testing would yield a more comprehensive understanding of Accoya®'s performance, especially regarding time-dependent factors like creep and fatigue. Direct experiments would provide stronger evidence to challenge or support potential modifications to Eurocode parameters for Accoya® and further confirm its structural advantages in real-world applications. However, with a numerical model, internal stress distributions can be more easily analysed, and a wide range of configurations and parameters can be tested using a single model without the need for extensive material and time resources. It remains essential to compare numerical models with real-world experiments.

7

Conclusion

In this conclusion, the research questions are revisited to clearly summarize the findings of this study. The main question, *"How does Accoya® timber compare to non-acetylated timber in terms of structural performance?"* is central to this discussion. First, the sub-questions are addressed, followed by a comprehensive answer to the main question.

The first sub-question; *"What are the characteristic properties of Accoya® and glulam Accoya®, and how is this certified?"* can be answered based on the literature review. Accoya® has been approved by the German Institute for Building Technology (DIBt) for general structural use in load-bearing constructions. This approval qualifies Accoya® in the A1 grade as strength class C22 according to the European strength classification system EN 338. However, after acetylation, Accoya® has a slightly lower modulus of elasticity than standard wood of the same class, yet it maintains comparable strength properties. Additionally, research indicates that the mechanical properties of Accoya® can approach certain standards of the GL classification, specifically the GL22h classification for laminated wood, although full certification for this has not yet been completed. Accoya® offers exceptional resistance to moisture due to its acetylation process, with shrinkage and swelling reduced by approximately 80% under Dutch climate conditions compared to untreated Radiata pine. This makes Accoya® particularly suitable for use in wet or humid environments and reduces the risk of deformation and degradation due to moisture.

The second sub-question; *"How do rigid clamped and circular dowel connections perform in Accoya® compared to unmodified Radiata pine?"* is addressed using FEM models. The models indicate notable performance distinctions compared to unmodified Radiata pine. The connections were selected based on their susceptibility to swelling-induced stresses. The amount of swelling reduction observed for Accoya® compared to unmodified Radiata pine is -80,2% in the radial direction and -78,3% in the tangential direction under the selected conditions, resulting in a comparable reduction in compressive stresses. For the clamped connection, a total reduction in peak stresses of 81.3% was found, and for the circular dowel connection, a reduction of 51.5%. More importantly, for the two modeled connections, the Accoya® variants show minimal exceedance of yield strengths after a realistic amount of swelling, based on annual fluctuations in relative humidity in the Netherlands. However, the unmodified Radiata pine variant shows exceedances that could lead to plastic deformation of the material, even without considering factors such as creep, fatigue, and external loading.

The results were then used to assess how the connection should be modified to prevent plastic deformation due to swelling, or to investigate how the connection might undergo ductile failure, which was subsequently pre-modeled. In this way, an attempt was made to identify differences in rotational stiffness between the two materials. Accoya® connections exhibit higher rotational stiffness than Radiata pine, indicating improved load-bearing capacity and reduced deformation under similar loads. Accoya's greater rotational stiffness in clamped and circular dowel connections is estimated at 219% and 58% respectively compared to Radiata pine, underscoring its structural advantage due to reduced swelling and enhanced dimensional stability. This clearly indicates that the clamped connection is significantly

more sensitive to the unstable dimensional properties of wood, exhibiting a disproportionately greater impact relative to the actual difference in swelling reduction. The rotational stiffness was evaluated based on the contribution of the steel tube; however, in reality, adding more than one dowel would result in a higher rotational stiffness.

The third sub-question; *"What role does the enhanced dimensional stability of Accoya® timber play in mitigating the effects of rotational stiffness variability in portal frame structures?"* is adressed to asses the effect of dimensional instability on changes in rotational stiffness and analyse these effects using a portal frame model. This specific test shows that the maximum deflection when using Accoya® decreases by 31% to 66%. It is important to recognize that further extrapolated models involve additional assumptions, and results cannot be implemented precisely. The focus is more on demonstrating a difference and its practical impact rather than achieving exact values.

The fourth sub-question; *"How can Accoya® be utilized more advantageously in terms of strength and stiffness calculations considering adjustments to the k_{def} and k_{mod} factors compared to non-acetylated timber?"* cannot be directly answered based on this research. The intention is to lay a foundation to support potential adjustments to the factors. Under moist conditions, Accoya® retains its strength and stiffness much better than non-acetylated wood, suggesting that the standard k_{mod}-values from Eurocode 5 may underestimate Accoya®. Existing literature has shown that Accoya® experiences less degradation in structural properties under SC3 conditions than regular wood, with a reduction in bending strength of only 20%, while the modulus of elasticity even shows a slight increase. Although this thesis aimed to investigate the stiffness of connections, it does not provide results on (time-dependent) creep behavior, to which the k_{def} factor applies. However, based on this research, it can be stated that a higher degree of stiffness is expected, which would likely reinforce stiffness even in time-dependent scenarios. This thesis supports the adjustment of k_{mod} and k_{def}-values but does not provide exact guidelines or specific value changes. Further experiments and detailed data analysis would be necessary to substantiate these adjustments precisely.

Based on the results of this thesis, it can be concluded that Accoya® wood, due to its acetylation process, offers distinct advantages over non-acetylated wood such as Radiata pine in structural applications. Accoya® is well-suited for applications where moisture variations and mechanical stability play a crucial role, such as in outdoor structures and load-bearing connections. Compared to unmodified wood, Accoya® can reduce the need for steel in certain applications, contributing to lower material usage and reduced CO_2 emissions. Beyond replacing steel, Accoya® enables lighter constructions, reducing material consumption and easing structural loads. Thus, Accoya® can play a valuable role in making the construction industry more sustainable and enabling the development of environmentally friendly structures.

Future research

Future research should focus on experimental testing to gain a more comprehensive understanding of Accoya®'s long-term performance, particularly regarding time-dependent properties such as creep, fatigue and viscoelasticity. This study's use of static models with simplified assumptions about moisture absorption and material interactions could be complemented by dynamic simulations and practical tests that reflect real environmental conditions. The current model demonstrates its capability by accounting for all the factors considered within a static linear elastic application. It can be utilized to test various types of connections, with dimensions or properties easily adjustable to suit different scenarios.

Additionally, an experimental analysis of the k_{mod} and k_{def} factors specifically for Accoya® would be valuable, potentially informing revisions to Eurocode standards to better align with the unique properties of modified wood. Finally, investigating how Accoya®'s altered molecular structure impacts long-term structural performance, including potential reductions in strength over time, could provide critical data to further support its use in structural applications.

References

1090-2, NEN-EN (2018). *Stichting Koninklijk Nederlands Normalisatie Instituut*. URL: https://www.nen.nl.

14080, NEN-EN (2013). *Stichting Koninklijk Nederlands Normalisatie Instituut*. URL: https://www.nen.nl.

338, NEN-EN (2024). *Stichting Koninklijk Nederlands Normalisatie Instituut*. URL: https://www.nen.nl.

384, NEN-EN (2013). *Stichting Koninklijk Nederlands Normalisatie Instituut*. URL: https://www.nen.nl.

Accoya (2024). *Accoya.com*. URL: https://www.accoya.com.

Antonsson, S. et al. (2009). "Comparison of the physical properties of hardwood and softwood pulps". In: *Nordic Pulp Paper Research Journal* 24.4, pp. 409–414.

Arcadis (2022). "Detail tekening kap p5-6 PHS Nijmegen". In: *Nmp-Arc-04-05-TE-RO-9313*.

Armstrong, L.D. and G. Christensen (1961). "Influence of Moisture Changes on Deformation of Wood Under Stress". In: *Nature* 191, pp. 869–870.

Augustino, D.S. and B.A. Antwi-Afari (2018). "Parameterized Modelling of Global Structural Behaviour of Modular Based Two Storey Timber Structure". In: *Linnaeus University*.

Barlow, C. (2023). "Micrographs of wood structure". In: *Euphonics*.

Bautechniek, Deutsches Institut für (2022). "Allgemeine bauaufsichtliche Zulassung Accoya Schnittholz und Accoya Color Grey". In.

Blaß, H.J., M. Frese, and H. Kunkel (2013). "Brettschichtholz aus acetylierter Radiata Kiefer". In: *Scientific Publishing* 25.

Blaß, H.J. and C. Sandhaas (2017). *Timber Engineering, Principles for Design*. Karlsruher Institut für Technologie (KIT).

Bongers, F. and J. Alexander (2018). "Strength classification of acetylated radiata pine". In.

Bongers, F., J. Alexander, et al. (2013). "Structural design with Accoya wood". In: *International Wood Products Journal* 4.3, pp. 172–176.

Bongers, F., J. Marcroft, et al. (2014). "Structural performance of Accoya® wood under service class 3 conditions". In: *World Conference on Timber Engineering*.

Bongers, F. and S.J. Uphill (2019). "The potential of wood acetylation". In: *International Scientific Conference on Hardwood Processing*, pp. 49–59.

Buchanan, A.H. and R.H. Fairweather (1993). "Seismic design of glulam structures". In: *Bulletin of the New Zealand Society for Earthquake Engineering* 26.4, pp. 415–436.

Chiniforush, A.A. et al. (2019). "Long-term behaviour of steel-timber composite (STC) shear connections". In: *Engineering Structures* 196.

Colling, F. and R.H. Falk (1993). “Investigation of laminating effects in glued-laminated timber”. In: *International council for building research studies and documentation*.

— (1995). “Laminating Effects in Glued-Laminated Timber Beams”. In: *Journal of Structural Engineering* 121.12.

Crawford, D. et al. (2012). “Assessment of structural performance of Accoya® wood for GluLam fabrication”. In: *World Conference on Timber Engineering*.

Dinwoodie, J.M. (2000). *Timber: Its Nature and Behaviour.* Taylor Francis.

e.V., Studiengemeinschaft Holzleimbau (2012). *Glulam-Bulletin*. Wuppertal, Elfriede-Stremmel-Straße 69.

Fridley, K.J., L.A. Soltis, and D.R. Rammer (1992). “Duration of Load Effect for Wood Connections”. In: *Journal of Structural Engineering* 118.11, pp. 3148–3161.

Güray, E. et al. (2023). “Structural analysis of a chair side frame connected with semi-rigid joints by slope-deflection method”. In: *TUBITAK*.

Hartley, I. and M.F. Hamza (2001). “Wood: Moisture Content, Hygroscopicity, and Sorption”. In: *Encyclopedia of Materials: Science and Technology*, pp. 9668–9673.

Hill, C.A.S. (2006). “Wood Modification: Chemical, Thermal and Other Processes.” In: *John Wiley and Sons*.

John, A. (2023). “Home cooling, humidity”. In: *Energy Conservation and Environmental Protection*.

Jorissen, A. et al. (2005). “The influence of acetylation of Radiata pine in structural sizes on its strength properties”. In: *European Conference on Wood Modification*.

KNMI, (Koninklijk Nederlands Meteorologisch Instituut) (2024). *Vochtigheid*. URL: `https://www.knmi.nl/kennis-en-datacentrum/uitleg/vochtigheid`.

Lahtela, V. and T. Karki (2015). “Determination and comparison of some selected properties of modified wood”. In: *Wood research* 60, pp. 763–772.

Lanata, F. (2015). “Monitoring the long-term behaviour of timber structures”. In: *Journal of Civil Structural Health Monitoring* 5, pp. 167–182.

Lankveld, C. et al. (2014). “Accoya® wood flooring and decking in extreme environments”. In: *European Conference on Wood Modification*.

Leijten, A.J.M. (1988). “Timber connections with metal fasteners.” In: *Journal of Wood Science*.

Lugt, P. van der et al. (2014). “The Potential Role of Wood Acetylation in Climate Change Mitigation”. In: *European Conference on Wood Modification*.

Malo, K.A. (2016). “Innovative Bridge Design Handbook”. In: *Construction, Rehabilitation and Maintenance*, pp. 273–297.

Meteovista (2024). *Vochtigheidgrafieken voor Nederland*. URL: `https://www.weerplaza.nl/nederland/nederland/14400/klimaat/vochtigheid/?utm_source=chatgpt.com`.

Miebach, F. (2014). “Sneek bridges show potential of timber”. In: *Structural Engineer*.

Němec, I. et al. (2002). “Concepts and Applications of Finite Element Analysis”. In: *Journal of Applied Mathematics and Physics* 4.4.

NEN (2024). *Stichting Koninklijk Nederlands Normalisatie Instituut*. URL: `https://www.nen.nl`.

Niemz, P., A. Teischinger, and D. Sandberg (2023). *Springer Handbook of Wood Science and Technology*. Switzerland: Springer.

Nikishkov, G.P. (2001). “Introduction to the Finite Element Method”. In: *UCLA*.

Prorail (2012). “Ontwerpvoorschrift perron- en sporenkappen”. In: *AM infrasystemen*.

— (2024). *Nijmegen, restauratie en renovatie perronkappen*. URL: `https://www.prorail.nl/projecten/maatregelen-nijmegen-perronkap`.

R. Klaassen B. Tjeerdsma, R. Hillebrink (2018). “Monitoring the performance of Accoya in different applications”. In: *European Conference on Wood Modification*.

Ramage, M.H. et al. (2017). “The wood from the trees: The use of timber in construction”. In: *Renewable and Sustainable Energy Reviews* 68.1, pp. 333–359.

Rebouças, A.S. et al. (2021). “Ductile Moment-Resisting Timber Connections: A Review”. In: *Buildings* 12.2.

Ross, R. (2021). “Wood handbook: Wood as an engineering material”. In: *U.S. Department of Agriculture, Forest Service*.

Saad, K. and A. Lengyel (2022). “Strengthening Timber Structural Members with CFRP and GFRP: A State-of-the-Art Review.” In: *Polymers* 14.12.

Sargent, R. (2019). “Evaluating dimensional stability in solid wood: a review of current practice”. In: *Journal od Wood Science*.

SHR (2007). “Dimensional stability of Accoya wood under different moisture conditions”. In: *Stichting Hout Research*.

— (2018). “Longitudinal swelling and shrinking of Accoya and Radiata pine”. In: *Stichting Hout Research*.

Sotayo, A., S. Green, and G. Turvey (2016). “Experimental and Finite Element (FE) modelling of timber fencing for benchmarking novel composite fencing”. In: *Composite Structures* 158.1, pp. 44–45.

Tian, P. et al. (2024). “Prediction Distribution Model of Moisture Content in Laminated Wood Components”. In: *Polymers*.

Tillaart, E.M. van den (2021). “Preliminary Model of Glued Laminated Accoya® Wood Based on the Board’s Tensile Properties with the Dynamic Modulus of Elasticity as Sorting Parameter”. In.

Vogtländer, J.G. (2010). “Life Cycle Assessment of Accoya® Wood and its applications”. In.

Weibull, W. (1939). “A statistical theory of strength of materials”. In: *Royal Swedish Institute for Engineering Research*.

Yurrita, M. and J.M. Cabrero (2021). “On the need of distinguishing ductile and brittle failure modes in timber connections with dowel-type fasteners”. In: *Engineering Structures* 242.11.

Zaliha, A.S. and Y.A. Kadir K.B. Awang (2018). “Mortise and tenon failures in school furniture”. In: *FRIM*.

A

SHR Accoya and Radiata pine tables

swelling *(longitudinal)*					
	from	35% RH	65% RH	90 % RH	water saturated
	to	0 % RH	35 % RH	65 % RH	90 % RH
		[mm/m][1)]	**[mm/m][1)]**	**[mm/m][1)]**	**[mm/m][1)]**
individual	**Accoya**	0,13	0,15	0,27	0,17
	Radiata	1,15	0,26	0,36	0,34
cumulative	from	35% RH	65% RH	90 % RH	water saturated
	to	0 % RH	0 % RH	0 % RH	0 % RH
		[mm/m][1)]	**[mm/m][1)]**	**[mm/m][1)]**	**[mm/m][1)]**
	Accoya	0,13	0,28	0,55	0,72
	Radiata	1,15	1,41	1,77	2,11
shrinking *(longitudinal)*					
	from	0 % RH	0 % RH	0 % RH	0 % RH
	to	35% RH	65% RH	90 % RH	water saturated
		[mm/m][1)]	**[mm/m][1)]**	**[mm/m][1)]**	**[mm/m][1)]**
	Accoya	-0,26	-0,54	-0,69	-0,92
	Radiata	-1,09	-1,65	-2,16	-2,26
moisture content					
		35% RH	65% RH	90 % RH	water saturated
		[%][1)]	**[%][1)]**	**[%][1)]**	**[%][1)]**
	Accoya	1,5%	3,0%	5,1%	114,1%
	Radiata	5,5%	11,2%	17,9%	161,9%

Figure A.1: Longitudinal swelling and shrinking of Accoya® and Radiata pine. All numbers represent the median values of 10 individual samples (Stichting Hout Research, 2018).

Species	Batch		Oven dry	Relative Humidity adsorption → 25%	35%	50%	65%	80%	95%	Water saturated
Accoya™ wood	LG118	rad. swell. [%]	0	0.10	0.11	0.16	0.28	0.34	0.60	0.67
(New Zealand)		*stdev*	*0*	*0.03*	*0.03*	*0.03*	*0.05*	*0.05*	*0.12*	*0.12*
	LG122	rad. swell. [%]	0	0.09	0.13	0.16	0.29	0.35	0.65	0.73
		stdev	*0*	*0.02*	*0.02*	*0.02*	*0.03*	*0.04*	*0.11*	*0.13*
	LG123	rad. swell. [%]	0	0.10	0.13	0.15	0.27	0.32	0.61	0.68
		stdev	*0*	*0.02*	*0.03*	*0.03*	*0.05*	*0.05*	*0.11*	*0.13*
	average	rad. swell. [%]	**0**	**0.10**	**0.12**	**0.16**	**0.28**	**0.34**	**0.62**	**0.69**
		stdev	**0**	**0.02**	**0.03**	**0.03**	**0.04**	**0.05**	**0.11**	**0.13**
Accoya™ wood	LG135	rad. swell. [%]	0	0.11	0.13	0.17	0.29	0.35	0.66	0.74
(Chile)		*stdev*	*0*	*0.04*	*0.05*	*0.06*	*0.09*	*0.10*	*0.22*	*0.25*
Radiata Pine	Ref-LG122	rad. swell. [%]	0	0.55	0.67	0.86	1.23	1.50	2.95	3.40
(New Zealand)		*stdev*	0	*0.09*	*0.11*	*0.14*	*0.19*	*0.23*	*0.54*	*0.63*

Species	Batch		Oven dry	Relative Humidity adsorption → 25%	35%	50%	65%	80%	95%	Water saturated
Accoya™ wood	LG118	tang. swell. [%]	0	0.12	0.17	0.27	0.45	0.58	1.26	1.46
(New Zealand)		*stdev*	*0*	*0.03*	*0.04*	*0.05*	*0.07*	*0.10*	*0.26*	*0.31*
	LG122	tang. swell. [%]	0	0.12	0.18	0.28	0.47	0.60	1.30	1.51
		stdev	*0*	*0.03*	*0.03*	*0.04*	*0.07*	*0.08*	*0.20*	*0.24*
	LG123	tang. swell. [%]	0	0.12	0.17	0.26	0.44	0.56	1.23	1.43
		stdev	*0*	*0.03*	*0.04*	*0.04*	*0.06*	*0.07*	*0.15*	*0.17*
	average	tang. swell. [%]	**0**	**0.12**	**0.17**	**0.27**	**0.45**	**0.58**	**1.26**	**1.47**
		stdev	**0**	**0.03**	**0.04**	**0.04**	**0.06**	**0.08**	**0.20**	**0.24**
Accoya™ wood	LG135	tang. swell. [%]	0	0.14	0.16	0.25	0.42	0.52	1.12	1.30
(Chile)		*stdev*	*0*	*0.06*	*0.08*	*0.11*	*0.17*	*0.21*	*0.45*	*0.56*
Radiata Pine	Ref-LG122	tang. swell. [%]	0	0.91	1.12	1.50	2.19	2.73	5.92	7.89
(New Zealand)		*stdev*	0	*0.12*	*0.12*	*0.13*	*0.15*	*0.17*	*0.42*	*0.76*

Figure A.2: Radial and tangential swelling of Accoya® and Radiata pine. The green row shows the average values of 3 batches of each 15 samples. The Radiata Pine row shows the average values of 1 batch of 10 samples. (Stichting Hout Research, 2007).

Species	Batch		Oven dry	← desorption Relative Humidity 25%	35%	50%	65%	80%	95%	Water saturated
Accoya™ wood	LG118	rad. shrink. [%]	0.64	0.57	0.50	0.39	0.36	0.24	0.09	0
(New Zealand)		*stdev*	*0.12*	*0.10*	*0.09*	*0.07*	*0.06*	*0.05*	*0.03*	*0*
	LG122	rad. shrink. [%]	0.73	0.65	0.56	0.47	0.42	0.30	0.12	0
		stdev	*0.18*	*0.13*	*0.15*	*0.10*	*0.10*	*0.08*	*0.06*	*0*
	LG123	rad. shrink. [%]	0.67	0.59	0.53	0.41	0.37	0.27	0.11	0
		stdev	*0.13*	*0.11*	*0.10*	*0.10*	*0.08*	*0.07*	*0.05*	*0*
	average	rad. shrink. [%]	**0.68**	**0.60**	**0.53**	**0.42**	**0.38**	**0.27**	**0.11**	**0**
		stdev	**0.14**	**0.12**	**0.11**	**0.09**	**0.08**	**0.07**	**0.05**	**0**
Accoya™ wood	LG135	rad. shrink. [%]	0.73	0.62	0.55	0.43	0.39	0.28	0.09	0
(Chile)		*stdev*	*0.26*	*0.22*	*0.20*	*0.16*	*0.13*	*0.10*	*0.05*	*0*
Radiata Pine	Ref-LG122	rad. shrink. [%]	3.33	2.48	2.22	1.80	1.50	1.20	0.36	0
(New Zealand)		*stdev*	0.66	*0.54*	*0.50*	*0.43*	*0.39*	*0.31*	*0.11*	*0*

Species	Batch		Oven dry	← desorption Relative Humidity 25%	35%	50%	65%	80%	95%	Water saturated
Accoya™ wood	LG118	tang. shrink. [%]	1.49	1.27	1.15	0.93	0.78	0.58	0.19	0
(New Zealand)		*stdev*	*0.34*	*0.28*	*0.25*	*0.22*	*0.18*	*0.15*	*0.07*	*0*
	LG122	tang. shrink. [%]	1.53	1.31	1.19	0.97	0.81	0.61	0.20	0
		stdev	*0.25*	*0.21*	*0.19*	*0.16*	*0.15*	*0.10*	*0.04*	*0*
	LG123	tang. shrink. [%]	1.45	1.24	1.12	0.91	0.77	0.57	0.18	0
		stdev	*0.18*	*0.15*	*0.14*	*0.12*	*0.10*	*0.08*	*0.04*	*0*
	average	tang. shrink. [%]	**1.49**	**1.27**	**1.15**	**0.94**	**0.79**	**0.58**	**0.19**	**0**
		stdev	**0.26**	**0.22**	**0.20**	**0.16**	**0.14**	**0.11**	**0.05**	**0**
Accoya™ wood	LG135	tang. shrink. [%]	1.32	1.13	1.03	0.83	0.69	0.53	0.18	0
(Chile)		*stdev*	*0.55*	*0.47*	*0.43*	*0.35*	*0.29*	*0.23*	*0.09*	*0*
Radiata Pine	Ref-LG122	tang. shrink. [%]	7.17	5.75	5.30	4.56	3.96	3.38	1.46	0
(New Zealand)		*stdev*	0.76	*0.71*	*0.71*	*0.68*	*0.65*	*0.62*	*0.36*	*0*

Figure A.3: Radial and tangential shrinking of Accoya® and Radiata pine. The green row shows the average values of 3 batches of each 15 samples. The Radiata Pine row shows the average values of 1 batch of 10 samples. (Stichting Hout Research, 2007).

B

Nijmegen station platform 5-6 canopy

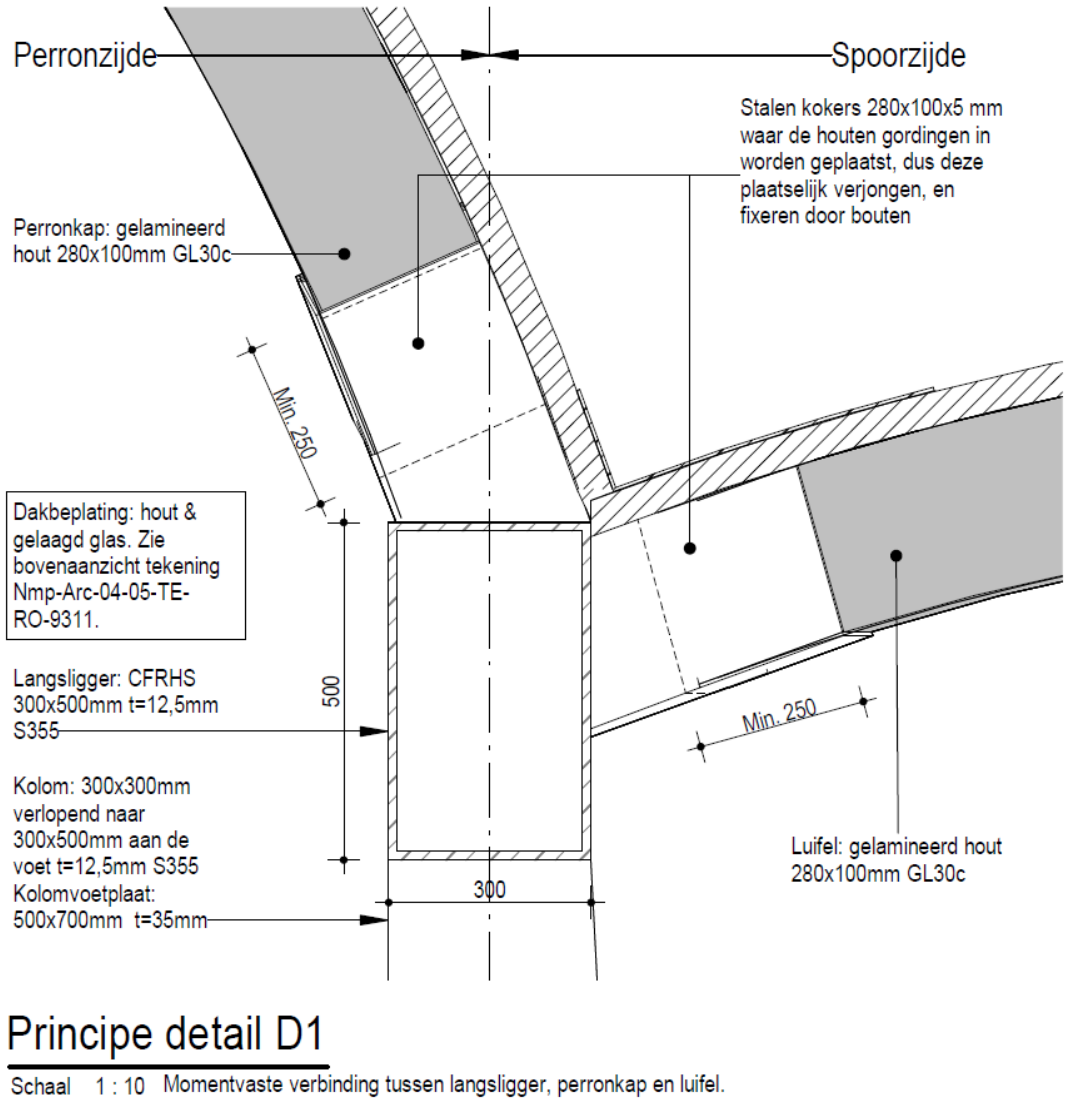

Figure B.1: Detail D1 (Arcadis, 2022).

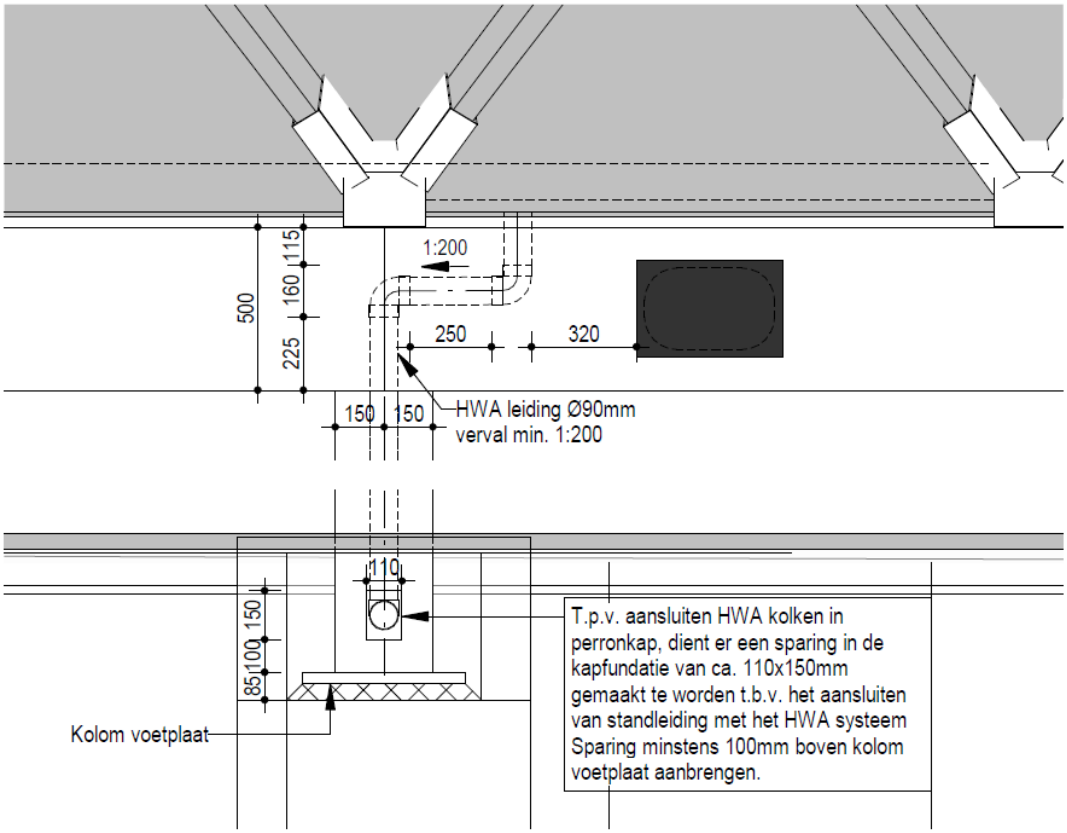

Principedetail D7

Schaal 1 : 20

Aansluiting HWA-leiding door langsligger en kolom, en dimensies van de sparing in kolom t.b.v. het aansluiten van HWA-leiding op HWA-systeem

Figure B.2: Detail D7 (Arcadis, 2022).

Figure B.3: Render impression (Prorail, 2024).

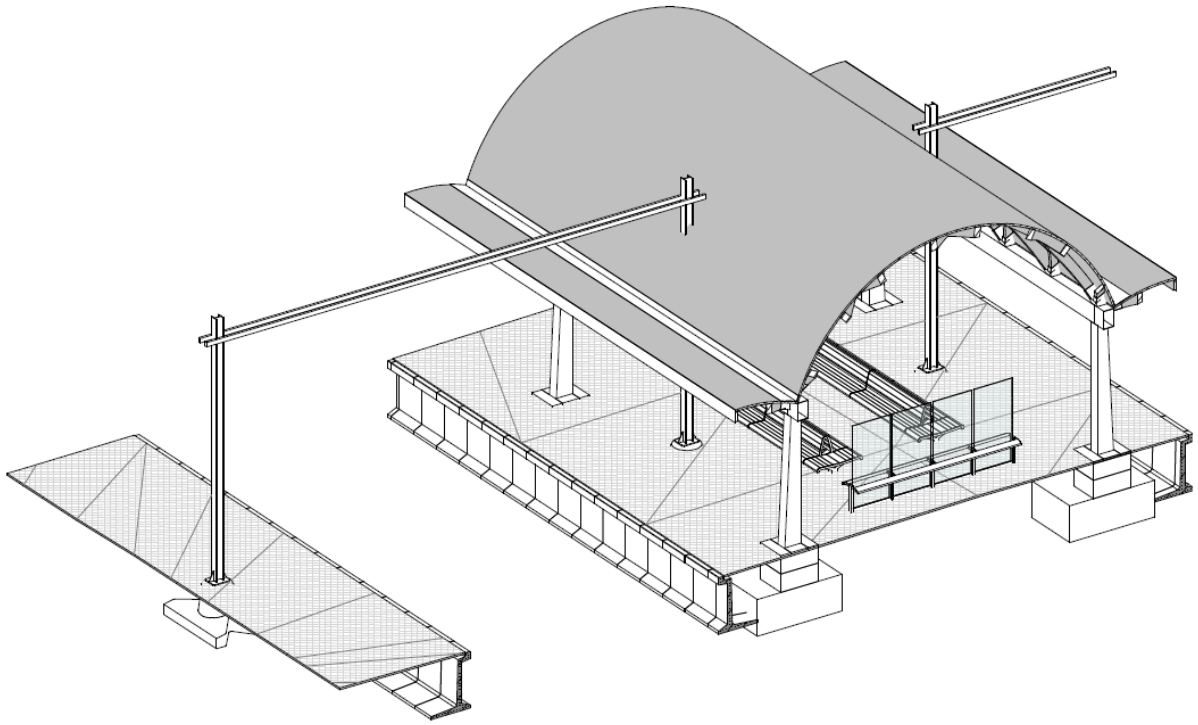

Figure B.4: 3D view (Arcadis, 2022).

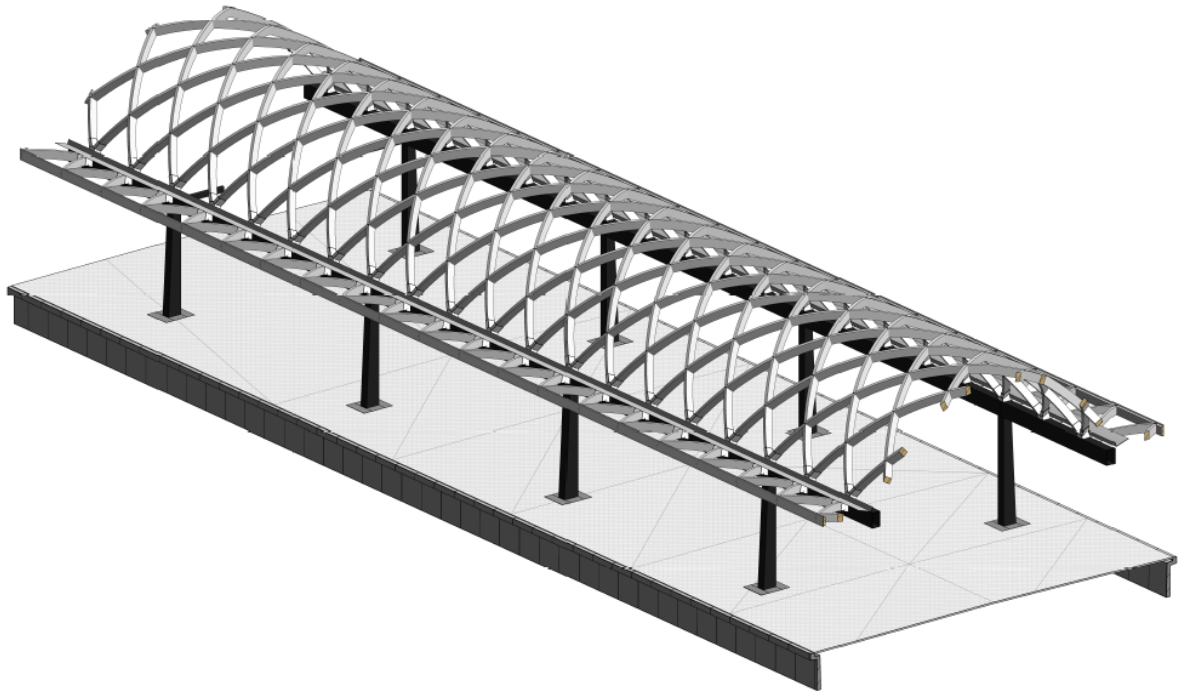

Figure B.5: Structural frame (Arcadis, 2022).

C

FEM model verification

Table C.1 shows the model parameters used for the verification models in this appendix. The expansion factors differ from those of the analysis models.

Table C.1: GL22h verification model parameters.

Density-mean	ρ_k	4e10^{-10}	ton/mm^3
Modulus of elasticity //	$E_{0,mean}$	300	N/mm^2
Modulus of elasticity -|	$E_{90,mean}$	10.000	N/mm^2
Poisson's ratio	$v_{12/23}$	0,35	-
Poisson's ratio	v_{13}	0,05	-
Shear modulus	$G_{12/23}$	650	N/mm^2
Shear modulus	G_{13}	60	N/mm^2
Expansion (tangential)	*alpha11*	3,73	%
Expansion (radial)	*alpha22*	1,72	%
Expansion (longitudinal)	*alpha33*	0	%

C.1. 2D verification

For the verification process, a 2D cross-section of 280x100 mm was chosen as the starting point. This cross-section is based on the dimensions of the detail in Nijmegen platform 5-6 canopy (Appendix B). Figure C.1 provides a schematic representation of this glulam cross-section. The right cross-section in this image shows a simplified section without lamellae and woodgrain details. This approach makes the material easier to describe, as it is modeled solely as a 2D plane with varying properties in two directions. Further in this appendix, a situation sketch, numerical output, analytical calculations or control models for comparisons are presented for each validation check.

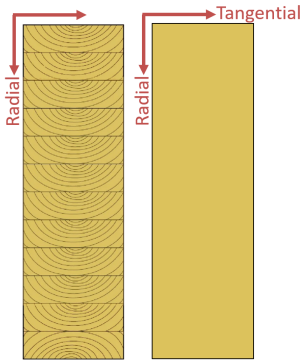

Figure C.1: Schematic representation 100x280 mm glulam cross section.

Tangential and radial swelling

Model for verification of free swelling in tangential and radial direction. Each box in figure C.2 represents an element from the mesh. A mesh size of 10 [mm] has been applied. Boundary conditions are highlighted in orange. The expansion is generated by a thermal expansion coefficient and a temperature change of 10°C to simulate the swelling of the wood.

Table C.2 compares the analytical calculation with the numerical output. The expansion is analytically calculated based on the length of the element, expansion coefficients and change in temperature.

$$u = L_0 \cdot \alpha \cdot \Delta T = L_0 \cdot \varepsilon$$

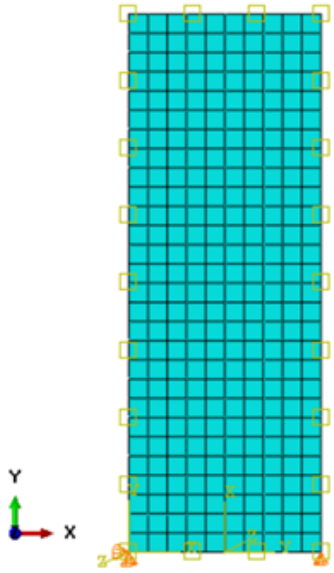

Figure C.2: Situation sketch (Abaqus).

Table C.2: Analytical and numerical comparison verification.

		Analytical calculation	Numerical output	Difference
Tangential expansion (X)	[mm]	100*3,73% = 3,730	3,730	0,0
Radial expansion (Y)	[mm]	280*1,72% = 4,816	4,816	0,0
Max. Principal	[N/mm^2]	0,0	0,0	0,0
Min. Principal	[N/mm^2]	0,0	0,0	0,0

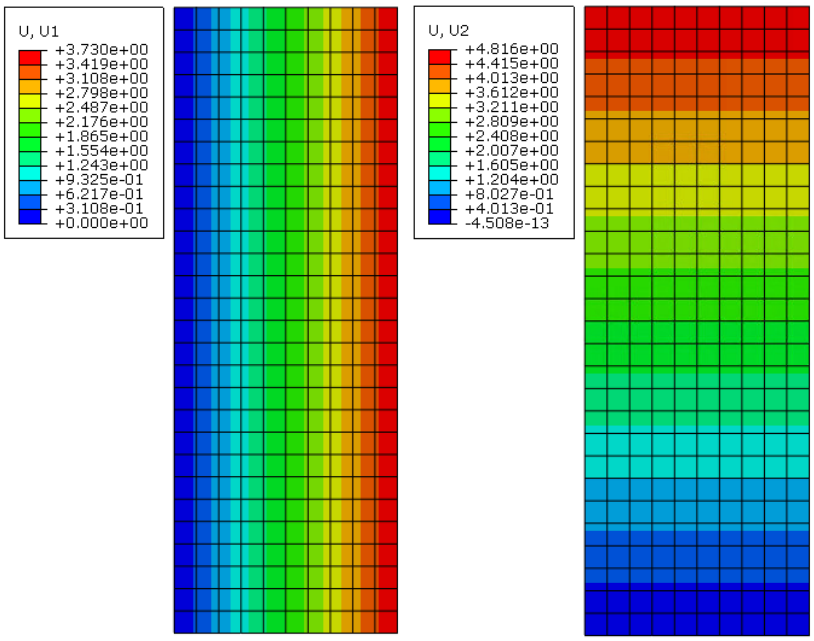

(a) Tangential expansion. **(b)** Radial expansion.

Figure C.3: Numerical output, deformation scale factor: 5,798 (Abaqus).

Tangential compressive stress

Model for verifying compressive stress in the tangential direction, created by rollers placed on the left and right sides of the model, and by allowing the model to swell.

Table C.3 compares the analytical calculation with the numerical output. The compressive stress is analytically calculated using Hooke's Law.

$$u = L_0 \cdot \alpha \cdot \Delta T = L_0 \cdot \varepsilon$$

$$\sigma = E \cdot \varepsilon = E \cdot \frac{\Delta L}{L_0}$$

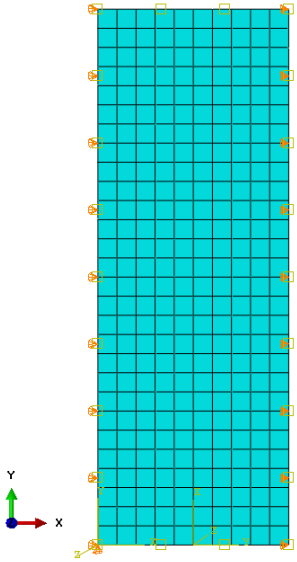

Figure C.4: Situation sketch (Abaqus).

Table C.3: Analytical and numerical comparison verification.

		Analytical calculation	Numerical output	Difference
Tangential expansion (X)	[mm]	100*0% = 0,0	0,0	0,0
Radial expansion (Y)	[mm]	280*1,72% = 4,816	4,828	0,012
Max. Principal (X)	[N/mm^2]	0,0	0,0	0,0
Max. Principal (Y)	[N/mm^2]	0,0	0,0	0,0
Min. Principal (X)	[N/mm^2]	300*(3,73/100) = 11,19	11,19	0,0
Min. Principal (Y)	[N/mm^2]	300*0 = 0,0	0,0	0,0

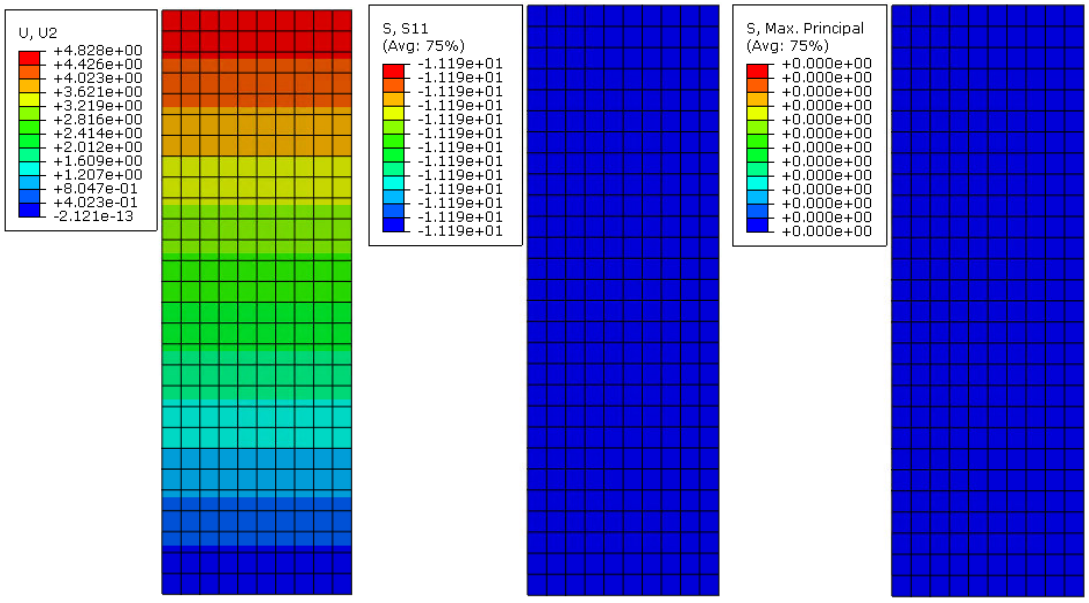

(a) Radial expansion. **(b)** Tangential stresses (S11). **(c)** Min. principal stresses.

Figure C.5: Numerical output, deformation scale factor: 5,798 (Abaqus).

Radial compressive stress

Model for verifying compressive stress in the radial direction, created by rollers placed on the top and bottom, and by allowing the model to swell.

Table C.4 compares the analytical calculation with the numerical output.

$$u = L_0 \cdot \alpha \cdot \Delta T = L_0 \cdot \varepsilon$$

$$\sigma = E \cdot \varepsilon = E \cdot \frac{\Delta L}{L_0}$$

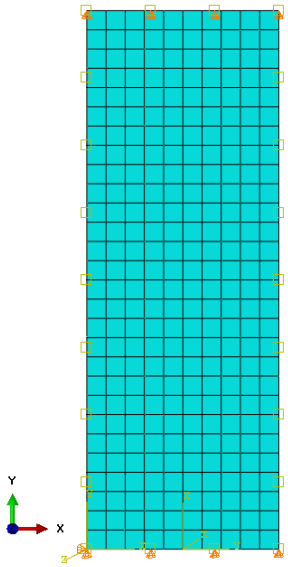

Figure C.6: Situation sketch (Abaqus).

Table C.4: Analytical and numerical comparison verification.

		Analytical calculation	Numerical output	Difference
Tangential expansion (X)	[mm]	100*3,730% = 3,730	3,730	0,0
Radial expansion (Y)	[mm]	280*0% = 0	$\pm 6e^{-14}$	0,0
Max. Principal (X)	[N/mm^2]	0,0	0,0	0,0
Max. Principal (Y)	[N/mm^2]	0,0	0,0	0,0
Min. Principal (X)	[N/mm^2]	300*0 = 0,0	0,0	0,0
Min. Principal (Y)	[N/mm^2]	300*(4,816/280) = 5,16	5,16	0,0

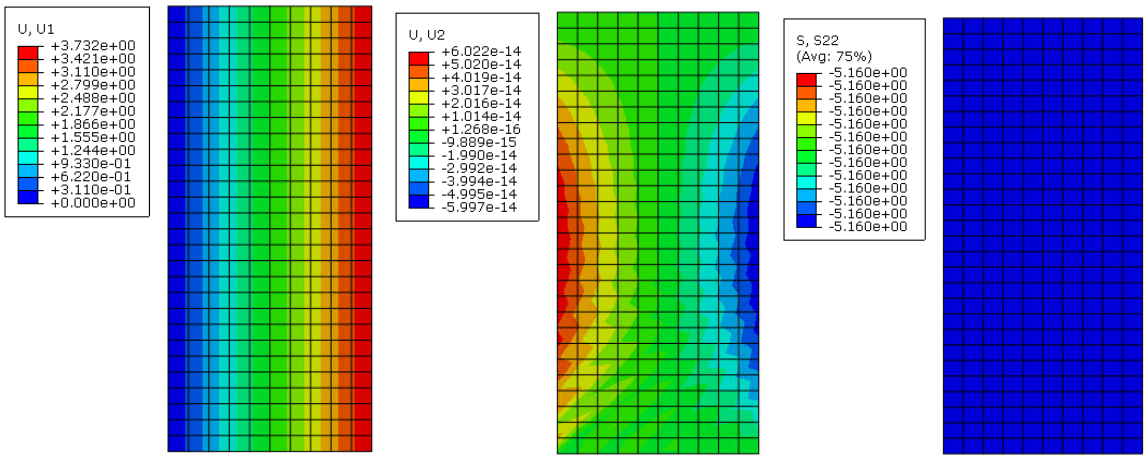

(a) Tangential expansion. **(b)** Radial expansion, values below e^{-14}. **(c)** Radial stresses (S22).

Figure C.7: Numerical output, deformation scale factor: 5,798 (Abaqus).

Radial compressive stress 2

Model for verifying compressive stress in the radial direction, created by a uniform downward force on top [15,87 N/mm] and rollers placed at the bottom, and by allowing the model to swell. The same test results were found for a uniform downward displacement of 10,0 mm.

$$F = \frac{E \cdot A \cdot u}{L_0} \quad \Rightarrow \quad q = \frac{F}{L_0}$$

$$\frac{300 \cdot 100 \cdot (10,0 + 4,816)}{280} = 1587,4 \quad \Rightarrow \quad \frac{1587,4}{100} = 15,87\,\text{N/mm}$$

Table C.5 compares the analytical calculation with the numerical output.

$$u = L_0 \cdot \alpha \cdot \Delta T = L_0 \cdot \varepsilon$$

$$\sigma = E \cdot \varepsilon = E \cdot \frac{\Delta L}{L_0}$$

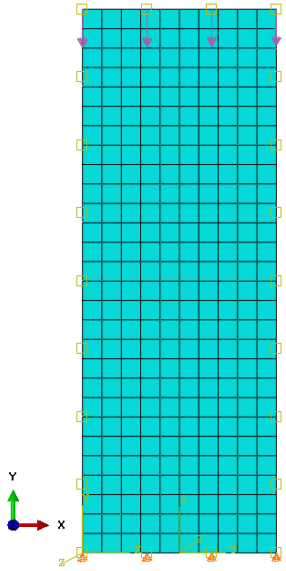

Figure C.8: Situation sketch (Abaqus).

Table C.5: Analytical and numerical comparison verification.

		Analytical calculation	Numerical output	Difference
Tangential expansion (X)	[mm]	100*3,730% = 3,730	3,736	0,006
Radial expansion (Y)	[mm]	-10,0	-9,996	-0,004
Max. Principal (X)	[N/mm^2]	0,0	0,0	0,0
Max. Principal (Y)	[N/mm^2]	0,0	0,0	0,0
Min. Principal (X)	[N/mm^2]	300*0 = 0,0	0,0	0,0
Min. Principal (Y)	[N/mm^2]	300*((15,87*280)/300)/280 = 15,87	15,87	0,0

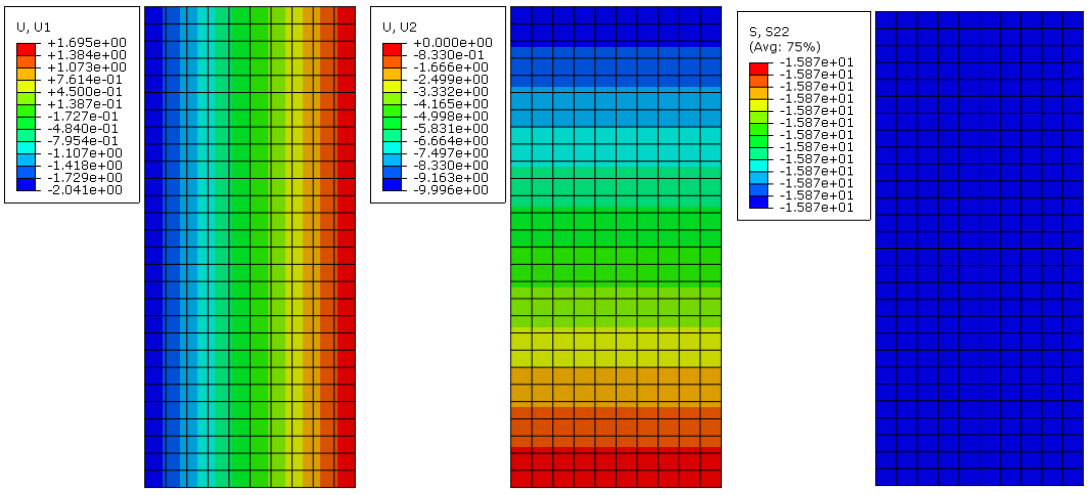

(a) Tangential expansion. **(b)** Radial expansion. **(c)** Radial stresses (S22).

Figure C.9: Numerical output, deformation scale factor: 2,8 (Abaqus).

Radial tensile stress

Model for verifying tensile stress in the radial direction, created by a uniform upward displacement on top [10 mm] and rollers placed at the bottom, and by allowing the model to swell.

Table C.6 compares the analytical calculation with the numerical output.

$$u = L_0 \cdot \alpha \cdot \Delta T = L_0 \cdot \varepsilon$$

$$\sigma = E \cdot \varepsilon = E \cdot \frac{\Delta L}{L_0}$$

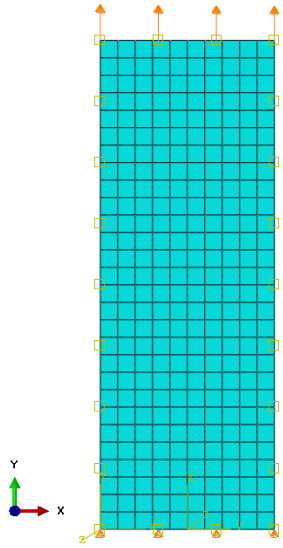

Figure C.10: Situation sketch (Abaqus).

Table C.6: Analytical and numerical comparison verification.

		Analytical calculation	Numerical output	Difference
Tangential expansion (X)	[mm]	100*3,730% = 3,730	3,728	-0,002
Radial expansion (Y)	[mm]	10,0	10,0	0,0
Max. Principal (X)	[N/mm^2]	300*0 = 0	0,0	0,0
Max. Principal (Y)	[N/mm^2]	300*((4,816-10)/280) = 5,554	5,554	0,0
Min. Principal (X)	[N/mm^2]	0,0	0,0	0,0
Min. Principal (Y)	[N/mm^2]	0,0	0,0	0,0

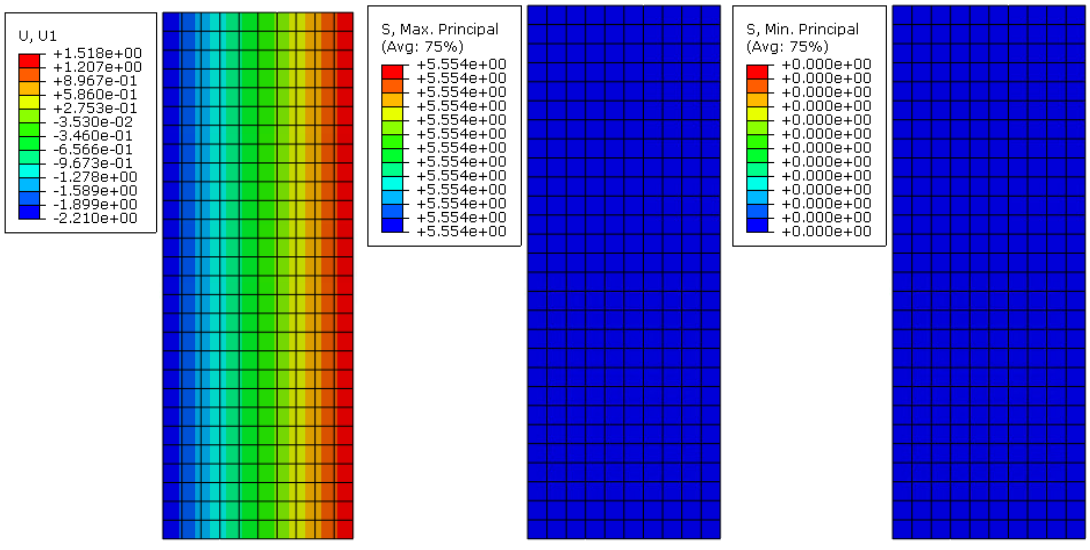

(a) Tangential expansion. **(b)** Max. principal stresses. **(c)** Min. principal stresses.

Figure C.11: Numerical output, deformation scale factor: 5,798 (Abaqus).

Restricted bottom edge

Model to create increased stress by restricting displacement with free rotation along the bottom edge. In addition, a uniform downward displacement of 10 mm is applied to the top edge.

No analytical calculations were performed for this model. Table C.7 compares the numerical output of this model with the *Radial compressive stress 2* test.

The control model did not exhibit any tensile stresses, whereas this model does. Compressive stress has developed in the tangential direction, and the overall stress levels have increased. This can be explained by the curved deformation at the bottom and the interaction of stresses in two directions.

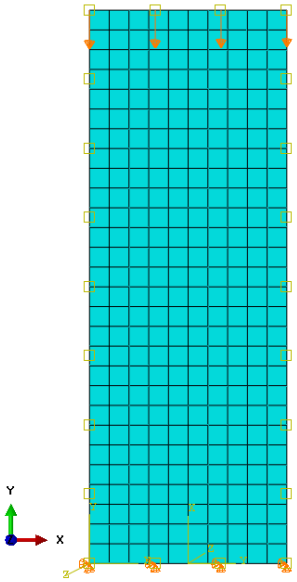

Figure C.12: Situation sketch (Abaqus).

Table C.7: Control model comparison verification.

		Control model: *2D radial compressive stress 2*	Numerical output	Difference
Tangential expansion (X)	[mm]	3,730	3,756	0,026
Radial expansion (Y)	[mm]	-10,0	-10,0	0,0
S11 - tension (X)	[N/mm^2]	0,0	0,3161	0,3161
S22 - tension (Y)	[N/mm^2]	0,0	0,0	0,0
S11 - compression (X)	[N/mm^2]	0,0	8,903	8,903
S22 - compression (Y)	[N/mm^2]	15,87	20,47	4,60
Max. Principal	[N/mm^2]	0,0	0,3302	0,3302
Min. Principal	[N/mm^2]	15,87	21,51	5,64

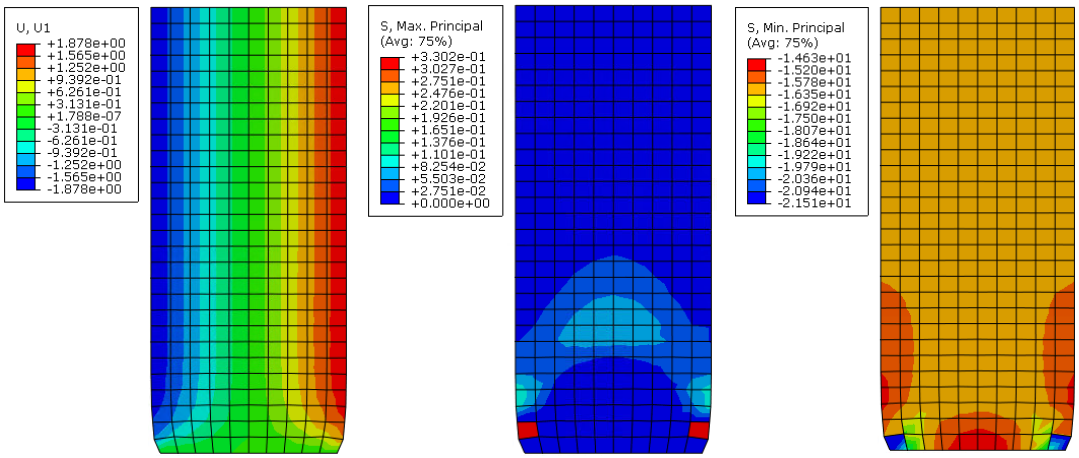

(a) Tangential expansion. **(b)** Max. principal stresses. **(c)** Min. principal stresses.

Figure C.13: Numerical output, deformation scale factor: 2,8 (Abaqus).

Single boundary condition dowel

Model for validating stresses caused by the application of a single boundary condition dowel. The principle of a dowel is modeled here as a volumeless element with a shaft that is free to move in the tangential direction, and a head with a width of 10 mm.

The analytical calculation conducted here for compression serves only as a reference, not as a verification. This calculation does not account for the distributed stresses that occurs between the heads of the dowels. Table C.8 compares the analytical calculation with the numerical output.

$$u = L_0 \cdot \alpha \cdot \Delta T = L_0 \cdot \varepsilon$$

$$\sigma = E \cdot \varepsilon = E \cdot \frac{\Delta L}{L_0}$$

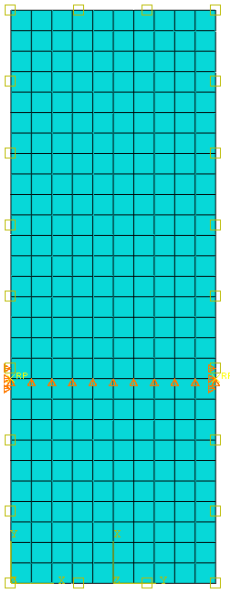

Figure C.14: Situation sketch (Abaqus).

Table C.8: Analytical and numerical comparison verification.

		Analytical calculation	Numerical output	Difference
Tangential expansion (X)	[mm]	100*2,238% = 2,238	x	x
Radial expansion (Y)	[mm]	280*1,032% = 2,899	x	x
S11 - compression (X)	[N/mm^2]	300*(2,238/100) = 6,714	x	x
S22 - compression (Y)	[N/mm^2]	-	x	-

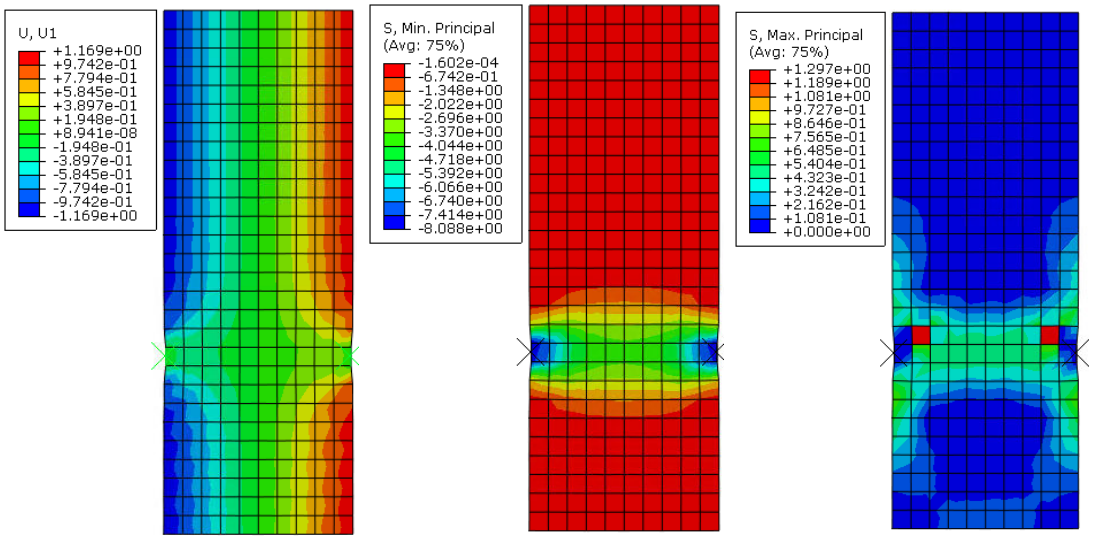

(a) Tangential expansion. **(b)** Min. principal stresses. **(c)** Max. principal stresses.

Figure C.15: Numerical output, deformation scale factor: 2,8 (Abaqus).

Double boundary condition dowel

Model for validating stresses caused by the application of two boundary condition dowels. The principle of a dowel is modeled here as a volumeless element with a shaft that is free to move in the tangential direction, and a head with a width of 20 mm.

The analytical calculation conducted here for compression serves only as a reference, not as a verification. This calculation does not account for the distributed stresses that occurs between the heads of the dowels. Table C.9 compares the analytical calculation with the numerical output.

$$u = L_0 \cdot \alpha \cdot \Delta T = L_0 \cdot \varepsilon$$

$$\sigma = E \cdot \varepsilon = E \cdot \frac{\Delta L}{L_0}$$

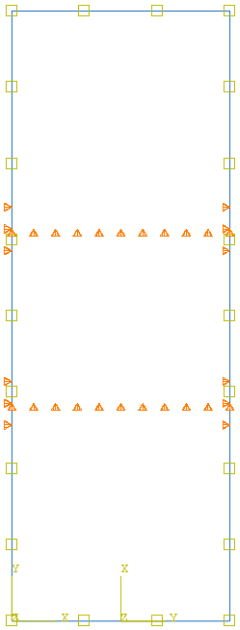

Figure C.16: Situation sketch (Abaqus).

Table C.9: Analytical and numerical comparison verification.

		Analytical calculation	Numerical output	Difference
Tangential expansion (X)	[mm]	100*2,238% = 2,238	2,438	0,200
Radial expansion (Y)	[mm]	(280-80)*1,032% = 2,064	2,270	0,206
S11 - compression (X)	[N/mm^2]	300*(2,238/100) = 6,714	9,633	2,919
S22 - compression (Y)	[N/mm^2]	300*(80*0,01032/80) = 3,096	5,682	2,586

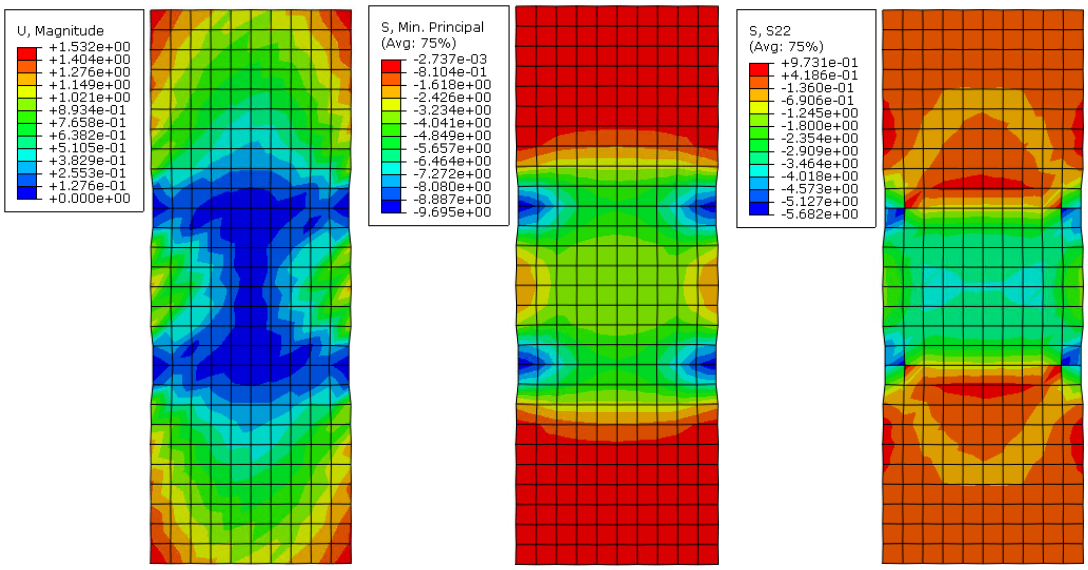

(a) Magnitude expansion. **(b)** Min. principal stresses. **(c)** Radial stresses.

Figure C.17: Numerical output, deformation scale factor: 2,8 (Abaqus).

C.2. Curved swelling

Three methods were used to simulate the swelling of the material in a curved manner to simulate cupping on a backsawn board. Each method is briefly outlined here, along with an explanation for why it was either selected or rejected.

Analytical fields for swelling were developed to model the swelling behavior of the material per element using a formula describing the swelling field over the axes. This approach could realistically simulate the swelling of wood. However, the problem with this method is that the material orientations do not move with the deformation. As the material swells, it experiences rotations, while the material orientations with their properties remain fixed to the original perpendicular coordinate system. Since the goal is to align the direction of the material properties with the annual rings of the wood to better reflect its true behavior during swelling, this method was proved unsuitable.

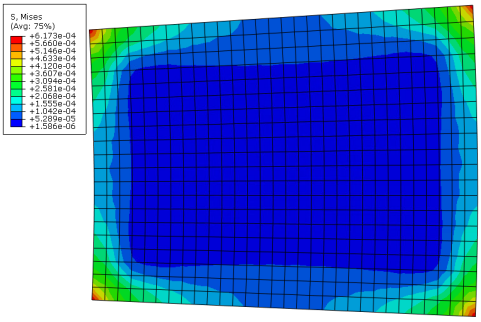

Figure C.18: Swelling induced by analytical field X+Y (Abaqus).

Cylindrical material orientations with a rotational centre were developed to guide the swelling direction and material properties in a curved manner through the material. Several different rotational centers were tested. The closer the rotational center was placed to the material, the greater the variation in curvature from one side of the material to the other. Since increased stresses concentrated near the rotational center, and realistic swelling behavior in a glulam element could not be achieved, this method was proved unsuitable.

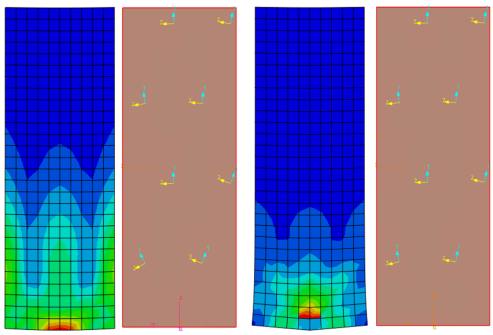

(a) Rotational centre placed 140 mm under bottom edge.

(b) Rotational centre placed on bottom edge.

Figure C.19: Cylindrical material orientation applied to a 280x100 mm part (Abaqus).

Uniform curved material orientations were applied to create consistent curvature throughout the material. In figure C.20, the material rotation is applied up to an angle of 15 degrees on both the left and right sides. The yellow and blue lines are projected onto all elements, indicating the local material orientation. The red line indicates the neutral axis, where the material orientation is 0 degrees. In the horizontal direction, 10 elements are arranged in a row, with each row receiving the same curvature in material orientation. Consequently, in this configuration, each vertical column of elements shares the same material orientation.

This method results in more uniform behavior across the cross-section compared to the two previously discussed methods. It provides a better approximation of the swelling behavior and material orientation of a glulam element. Since a glulam element is composed of multiple layers (which, in this cross-section, would be vertically stacked), the material exhibits more uniform swelling. Due to the cooperation between the laminates, the concept of a rotational centre no longer applies. Therefore, this method is considered the most suitable for accurately representing the swelling behavior of glulam elements.

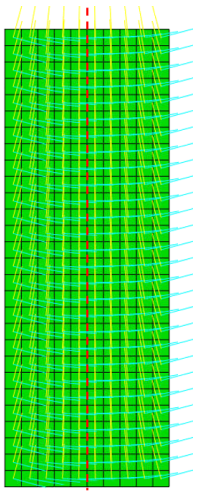

Figure C.20: Uniform curved material orientation with a red dashed neutral axis (Abaqus).

Uniform curved material orientation method

Figure C.21 shows in yellow the three variants in which the uniform curved material orientation method was applied. The bottom yellow line symbolizes the swelling behavior along two perpendicular axes and will be referred to as the 0° variant. The three curved lines above it represent the material orientation curvature applied to the material, with the maximum curvature angle at the sides of the part specified in degrees for this type of cross-section. The material orientations can be seen for each element in figure C.23.

The table in figure C.10 and graph in figure C.22 present the numerical output of these four variants. The values in this table and graph represent the maximum values found for each variant. Figures C.25 to C.28 respectively show the tangential expansion, radial expansion, max. principal stresses, and min. principal stresses. Each figure shares a consistent color scale.

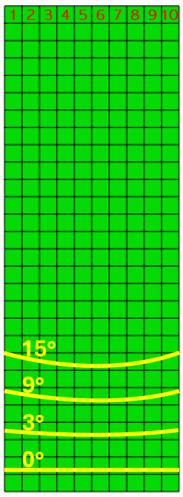

Figure C.21: Four variants used with their maximum angle of rotation for uniform curved material orientation.

Table C.10: Numerical results for three uniform curved material orientation variants and the uncurved variant.

		Perpendicular axes	3° variant	9° variant	15° variant
Tangential expansion (X)	[mm]	3,730	3,728	3,708	3,672
Radial expansion (Y)	[mm]	4,816	4,825	4,891	5,014
S11 - tension (X)	[N/mm^2]	0,0	0,001081	0,009736	0,02655
S22 - tension (Y)	[N/mm^2]	0,0	5,554	0,04032	0,1066
S11 - compression (X)	[N/mm^2]	0,0	0,005057	0,04445	0,1176
S22 - compression (Y)	[N/mm^2]	0,0	0,01114	0,09275	0,2238
Max. Principal	[N/mm^2]	0,0	0,004604	0,04032	0,1066
Min. Principal	[N/mm^2]	0,0	0,01117	0,09510	0,2399

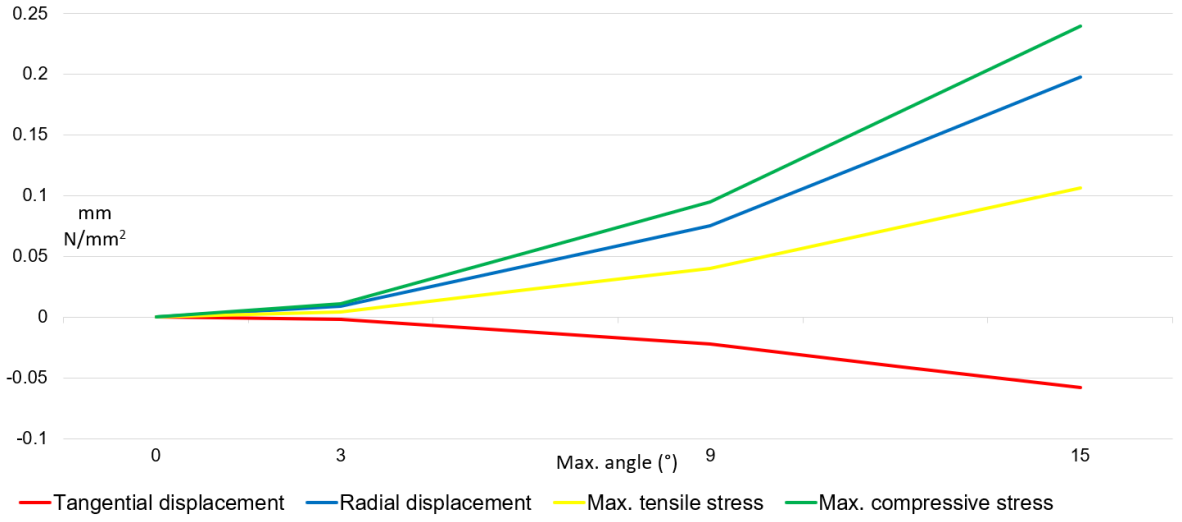

Figure C.22: Difference in displacement and stresses with the perpendicular variant as baseline measurement.

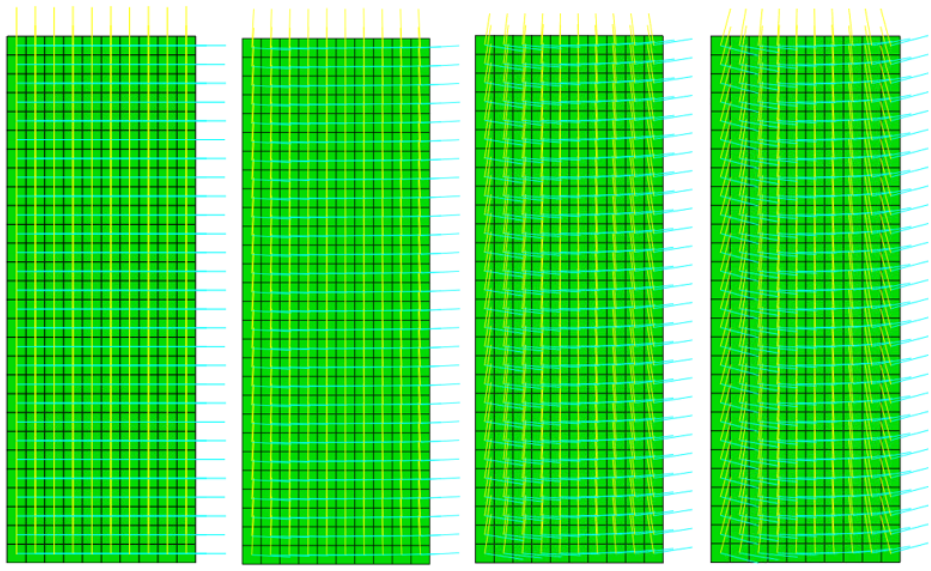

Figure C.23: Material orientations per element projected on undeformed parts (Abaqus).

Figure C.24 shows the arrays with angular displacements assigned to each row of elements for each variant. These arrays contain 10 values presented in the order of the red numbers as indicated in figure C.21 and follow the curvature of a circle.

[0°, 0°, 0°, 0°, 0°, 0°, 0°, 0°, 0°, 0°]	[−3°, −1.70°, −1.12°, −0.65°, -0.21°, 0.21°, 0.65°, 1.12°, 1.70°, 3°]	[−9°, −5.11°, −3.37°, −1.95°, -0.64°, 0.64°, 1.95°, 3.37°, 5.11°, 9°]	[−15°, −8.51°, −5.62°, −3.25°, -1.06°, 1.06°, 3.25°, 5.62°, 8.51°, 15°]

Figure C.24: Curvature arrays for the four variants.

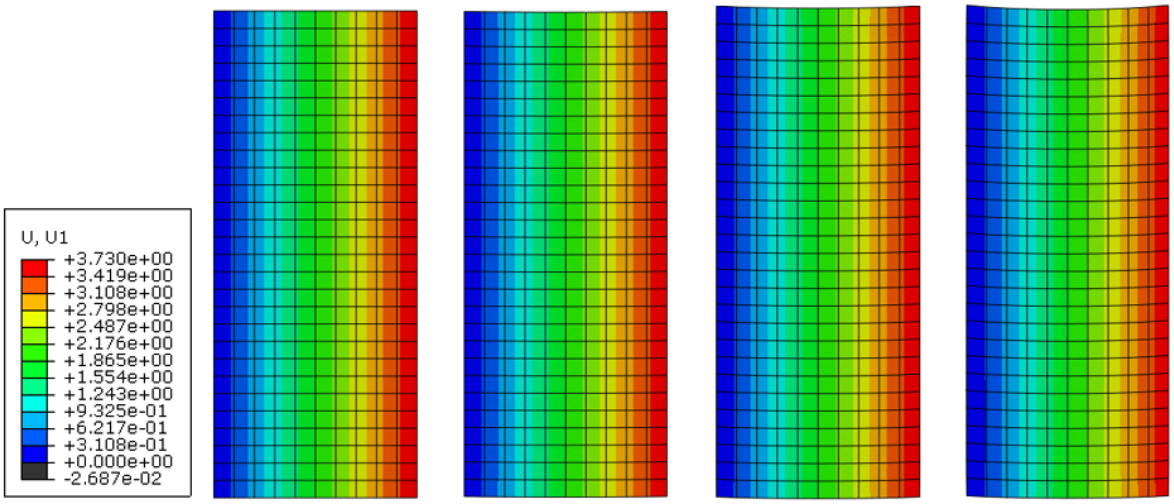

Figure C.25: Tangential expansion, deformation scale factor: 5,8 (Abaqus).

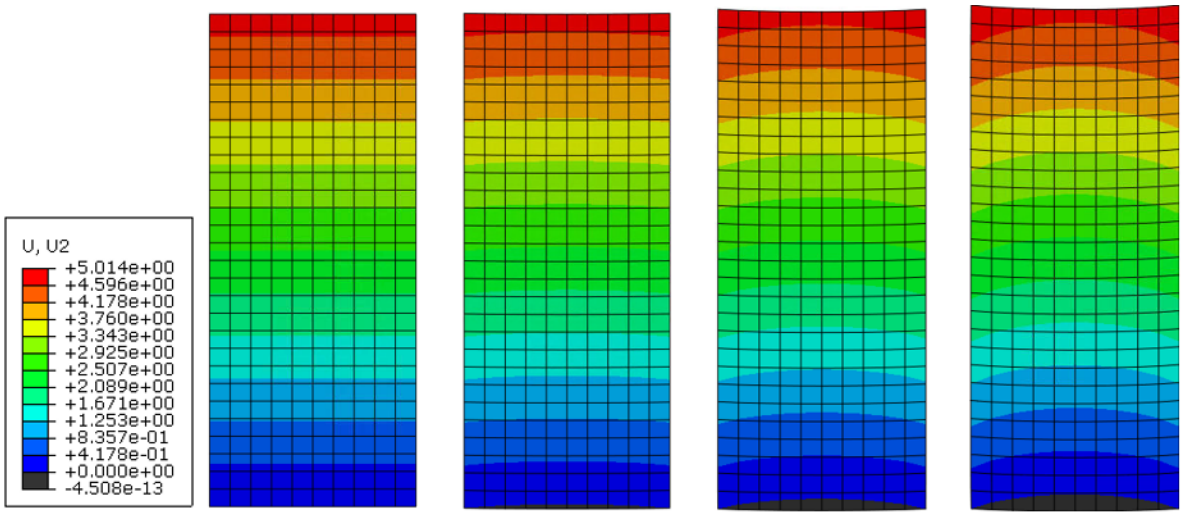

Figure C.26: Radial expansion, deformation scale factor: 5,8 (Abaqus).

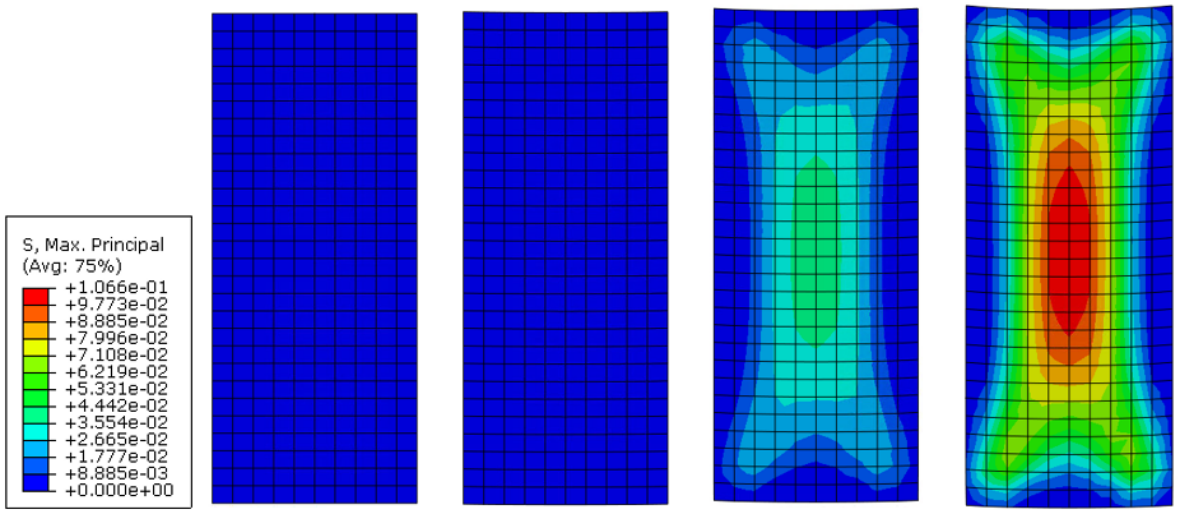

Figure C.27: Max. principal stresses, deformation scale factor: 5,8 (Abaqus).

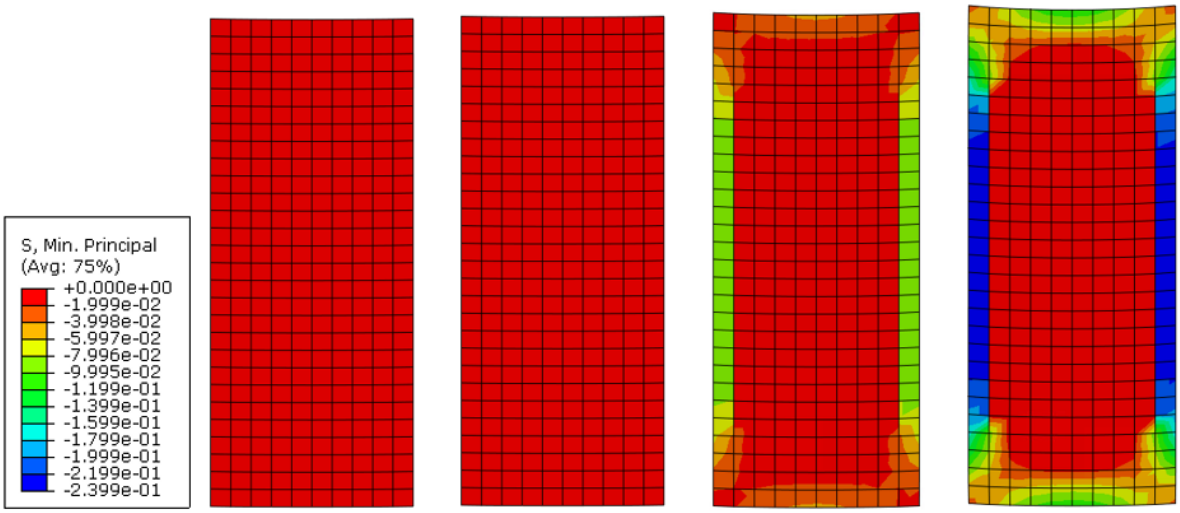

Figure C.28: Min. principal stresses, deformation scale factor: 5,8 (Abaqus).

For the modeling of joints in this research, only the 0° and 9° variants are used. Since the difference between the 0° and 3° variants cannot be observed in figures C.27 and C.28, the max. principal and min. principal stresses for the 3° variant are presented again in figure C.29 with a color scale tailored to these individual plots. The max. principal and min. principal stresses for the 0° variant are zero.

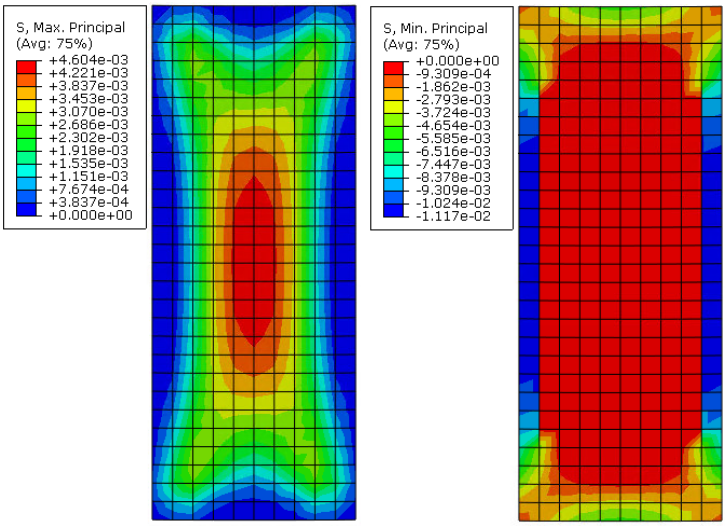

(a) Max. principal stresses. **(b)** Min. principal stresses.

Figure C.29: 3° variant with tailored color scales, deformation scale factor: 5,8 (Abaqus).

C.3. 3D verification

Models for verifying 3D parts. The 3D part will exhibit the same swelling behavior in the longitudinal direction in each plane as tested in 2D. However, the material has different properties in the longitudinal direction.

Tangential and radial swelling

Model for 3D verification of free swelling. The transition from 2D to 3D models involves an increase in the number of elements. To manage the computational running time, the element size for the 3D model was set to be twice that of the 2D model. The mesh size is now 20, reducing the number of elements per row in the tangential direction from 10 in the 2D model to 5 in the 3D model.

No analytical calculations were performed for this model. Table C.11 compares the numerical output of this model with the *2D tangential and radial swelling* test.

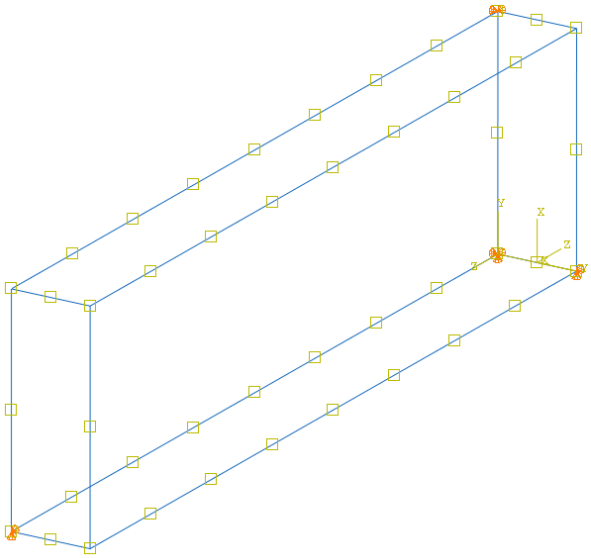

Figure C.30: Situation sketch (Abaqus).

Table C.11: Control model comparison verification.

		Control model: *2D tangential and radial swelling*	Numerical output	Difference
Tangential expansion (X)	[mm]	3,730	3,730	0,0
Radial expansion (Y)	[mm]	4,816	4,816	0,0
Longitudinal expansion (Z)	[mm]	-	0,0	-
Max. Principal	[N/mm^2]	0,0	0,0	0,0
Min. Principal	[N/mm^2]	0,0	0,0	0,0

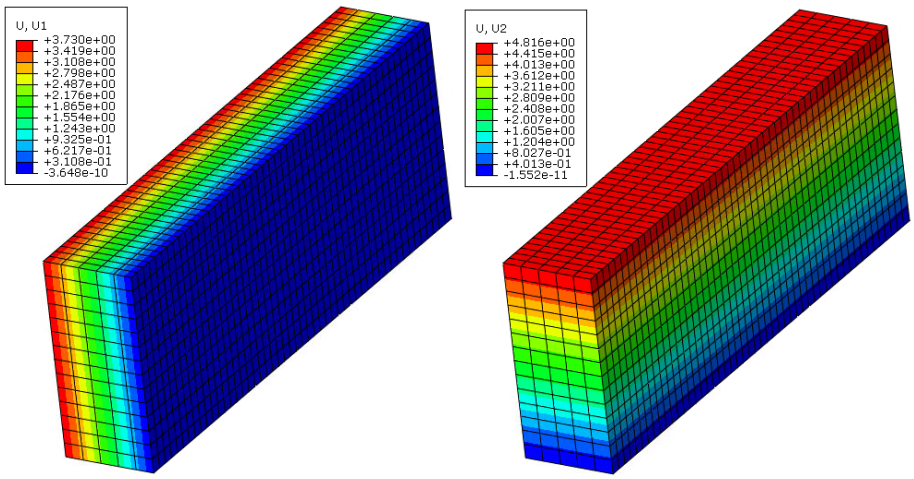

(a) Tangential expansion. **(b)** Radial expansion.

Figure C.31: Numerical output, deformation scale factor: 20,0 (Abaqus).

Tangential compressive stress

Model for verifying compressive stress in the tangential direction, created by rollers placed on the left and right side surfaces of the model, and by allowing the model to swell.

No analytical calculations were performed for this model. Table C.12 compares the numerical output of this model with the *2D tangential compressive stress* test.

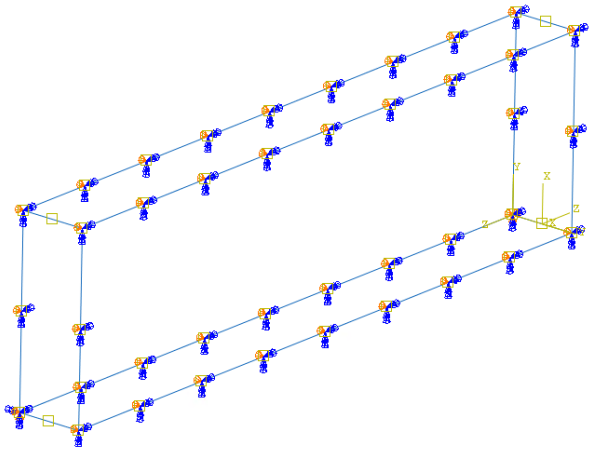

Figure C.32: Situation sketch (Abaqus).

Table C.12: Control model comparison verification.

		Control model: *2D tangential compressive stress*	Numerical output	Difference
Tangential expansion (X)	[mm]	0,0	0,0	0,0
Radial expansion (Y)	[mm]	4,828	4,828	0,0
Longitudinal expansion (Z)	[mm]	-	0,000185	-
S11 - tension (X)	[N/mm^2]	0,0	0,0	0,0
S22 - tension (Y)	[N/mm^2]	0,0	0,0	0,0
S33 - tension (Z)	[N/mm^2]	-	0,0	-
S11 - compression (X)	[N/mm^2]	11,19	11,19	0,0
S22 - compression (Y)	[N/mm^2]	0,0	0,0	0,0
S33 - compression (Z)	[N/mm^2]	-	0,0	-

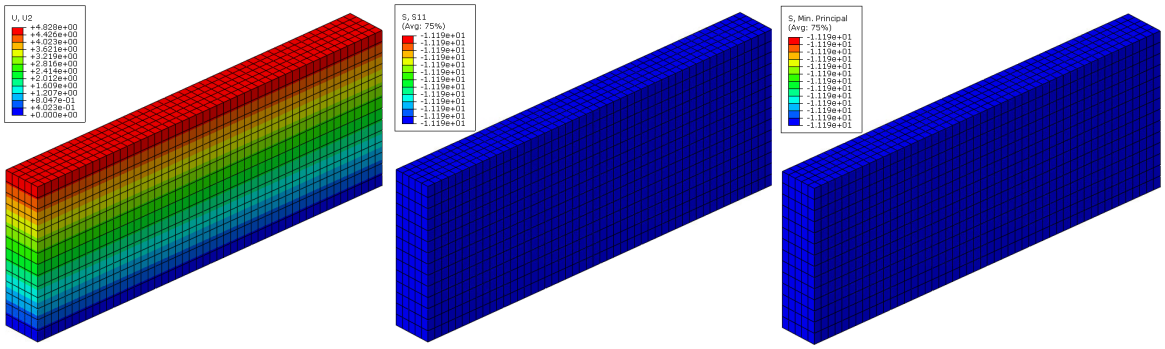

(a) Radial expansion. **(b)** Tangential stresses (S11). **(c)** Min. principal stresses.

Figure C.33: Numerical output, deformation scale factor: 20,0 (Abaqus).

Longitudinal compressive stress

Model for verifying compressive stress in the longitudinal direction, created by a uniform displacemnt in longitudinal direction with rollers on the other side surface, and by allowing the model to swell.

Table C.13 compares the analytical calculation with the numerical output.

$$u = L_0 \cdot \alpha \cdot \Delta T = L_0 \cdot \varepsilon$$

$$\sigma = E \cdot \varepsilon = E \cdot \frac{\Delta L}{L_0}$$

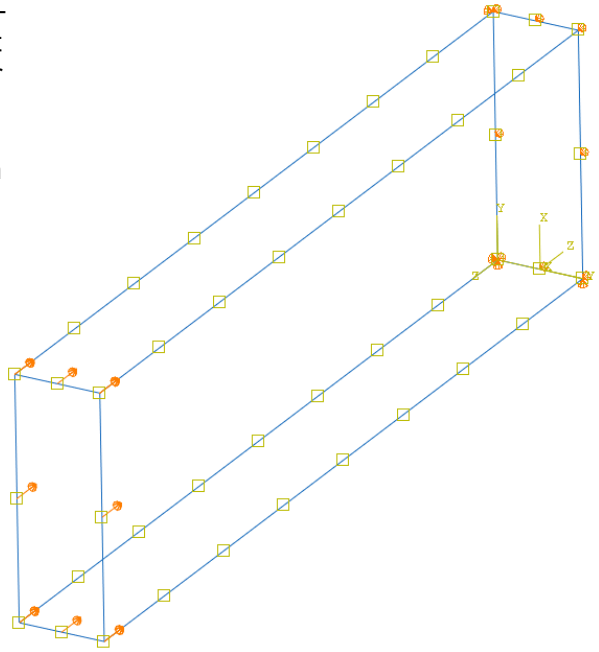

Figure C.34: Situation sketch (Abaqus).

Table C.13: Control model comparison verification.

		Analytical calculation	Numerical output	Difference
Tangential expansion (X)	[mm]	100*3,73% = 3,730	3,730	0,0
Radial expansion (Y)	[mm]	280*1,72% = 4,816	4,819	0,003
Longitudinal expansion (Z)	[mm]	20,0	20,0	0,0
S11 - tension (X)	[N/mm^2]	0,0	0,0	0,0
S22 - tension (Y)	[N/mm^2]	0,0	0,0	0,0
S33 - tension (Z)	[N/mm^2]	0,0	0,0	0,0
S11 - compression (X)	[N/mm^2]	0,0	0,0	0,0
S22 - compression (Y)	[N/mm^2]	0,0	0,0	0,0
S33 - compression (Z)	[N/mm^2]	10000*(20/1000) = 200,0	200,0	0,0

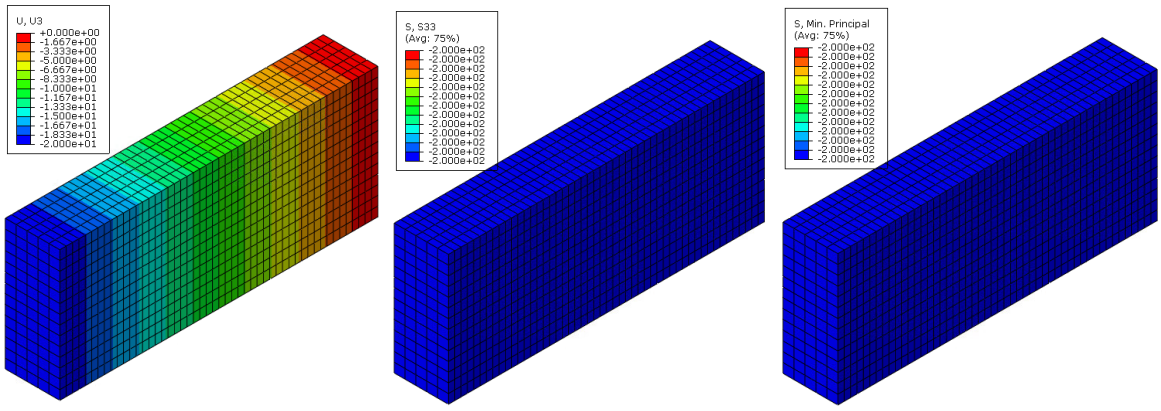

(a) Longitudinal expansion. **(b)** Longitudinal stresses (S33). **(c)** Min. principal stresses.

Figure C.35: Numerical output, deformation scale factor: 5,0 (Abaqus).

Volumetric dowel

Various tests were conducted to evaluate a volumetric dowel in a 3D element. For the surface interaction properties used, refer to Appendix C.4, ”Surface Interaction.” Figure C.36 illustrates a test setup without dowel heads including a upward force. Figure C.37 shows the output of this model. Figure C.38 shows the output of a swelling test model including dowel heads.

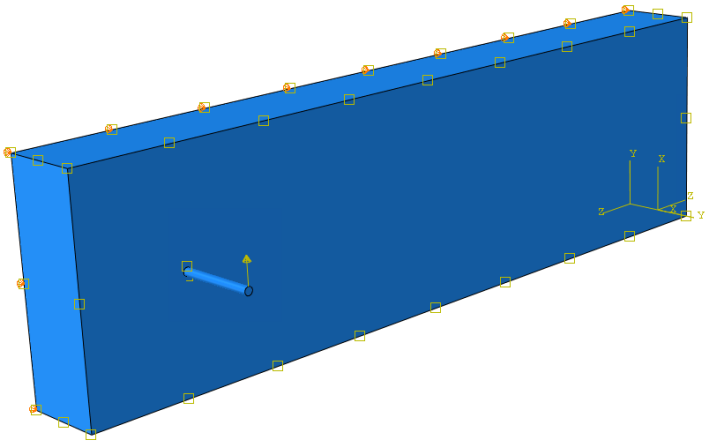

Figure C.36: Situation sketch (Abaqus).

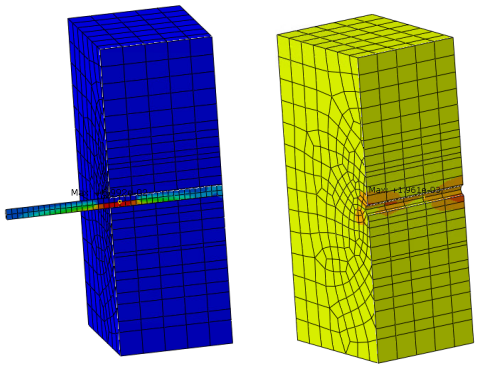

(a) Min. principal stresses dowel part.

(b) Min. principal stresses wood part.

Figure C.37: Numerical output of element cross-sectioned along dowel (Abaqus).

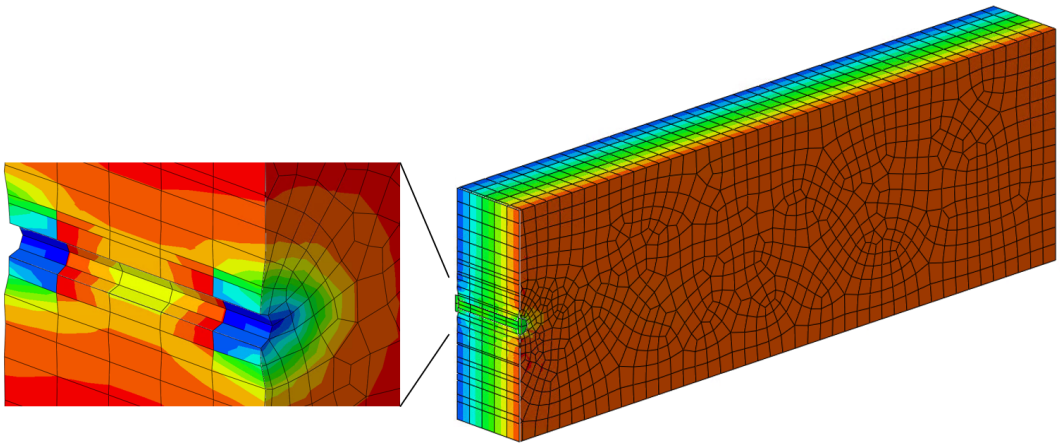

Figure C.38: Left: Min. principal. Right: Tangential expansion (Abaqus).

Curved swelling

Model for testing curved swelling (i.e. cupping) on a 3D part. This model contains a maximum curvature of 9°. The array of angular displacements applied to each horizontal row of this part is: [-9°, -3°, 0°, 3°, 9°].

In theory, the 2D part should behave similarly to the 3D part. However, the results differ by up to 53,96%. This can be explained by the generation of the results using a mesh structure that is twice as large.

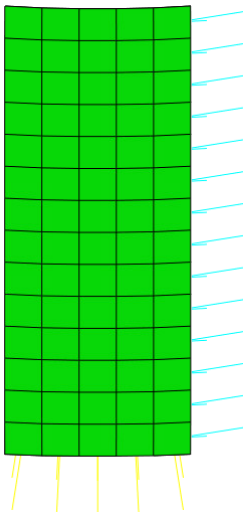

Figure C.39: Material orientation projected on deformed part (Abaqus).

Table C.14: Control model comparison verification.

		Control model: *2D 9° curved swelling*	Numerical output	Aboslut difference	Relative difference
Tangential expansion (X)	[mm]	3,708	3,701	-0,007	-0,19%
Radial expansion (Y)	[mm]	4,891	4,916	0,025	0,51%
Longitudinal expansion (Z)	[mm]	-	$5{,}571e^{-6}$	-	-
S11 - tension (X)	[N/mm^2]	0,009736	0,01499	0,005254	53,96%
S22 - tension (Y)	[N/mm^2]	0,04032	0,05392	0,0136	33,72%
S33 - tension (Z)	[N/mm^2]	-	$6{,}236e^{-5}$	-	-
S11 - compression (X)	[N/mm^2]	0,04445	0,04215	-0,0023	-5,17%
S22 - compression (Y)	[N/mm^2]	0,09275	0,07542	-0,01733	-18,68%
S33 - compression (Z)	[N/mm^2]	-	$8{,}909e^{-5}$	-	-
Max. principal	[N/mm^2]	0,04032	0,05398	0,01366	33,88%
Min. principal	[N/mm^2]	0,0951	0,07709	-0,01801	-18,94%
Horizontal elements count	-	10	5	-	-
Max. angle step ($\Delta\theta$)	°	3,89	6	-	-

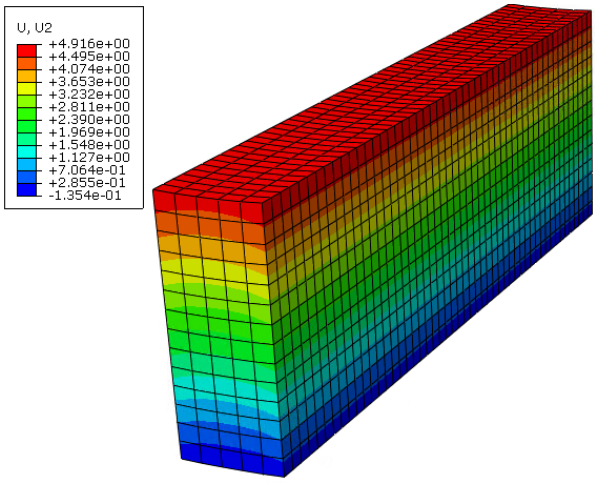

Figure C.40: Radial expansion, deformation scale factor: 10 (Abaqus).

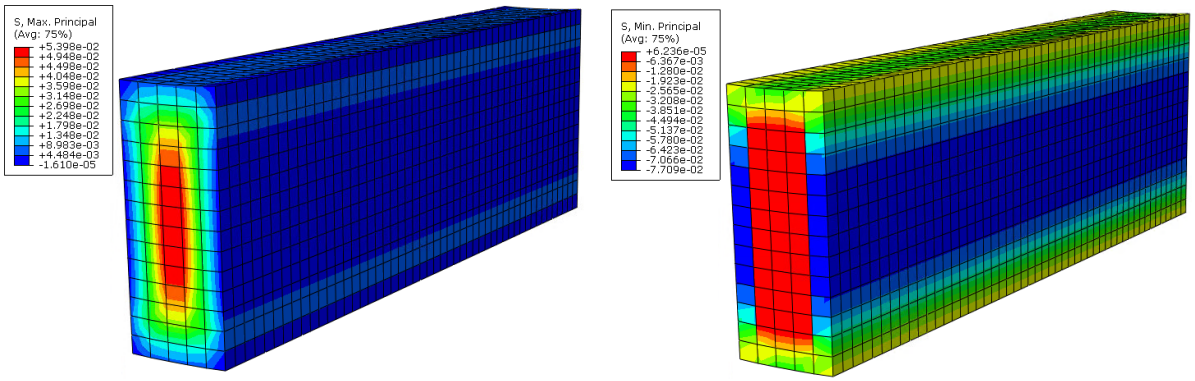

(a) Max. principal stresses

(b) Min. principal stresses

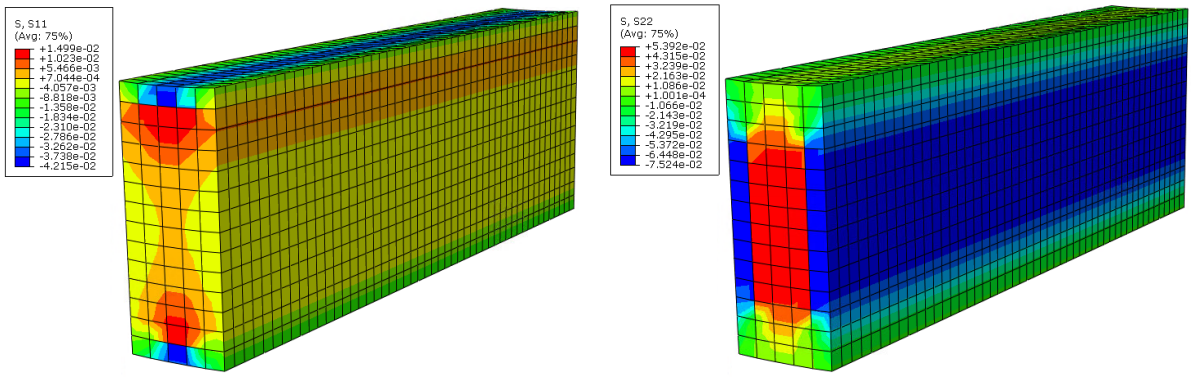

(c) Tangential stresses (S11)

(d) Radial stresses (S22)

Figure C.41: Numerical output, deformation scale factor: 10 (Abaqus).

C.4. Surface interaction

Surface interactions were tested for a wood-to-wood scenario. Table C.15 shows the interaction properties used for this model and the analysis models involving wood-on-wood contact. For steel-to-wood contact, a friction coefficient of 0,3 is applied.

Table C.15: Interaction properties wood-to-wood.

Friction coefficient	0,4
Max. elastic slip	0,005
Hard contact	-

This model shows the left wooden part swelling to a maximum angle of 9°. The right part does not swell. Rollers are applied to the right and left edge surfaces. In figure C.44, it can be seen that the parts do, as expected, not penetrate each other but lose contact at some places. Figures C.44 (a), (c) and (d) clearly show how the surfaces interact with each other and how shear stresses play a role here.

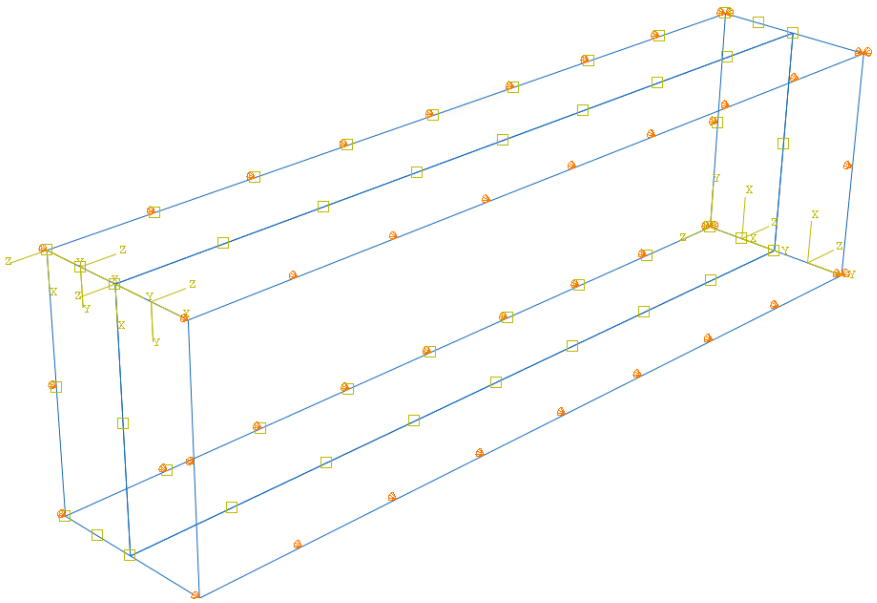

Figure C.42: Situation sketch (Abaqus).

Table C.16: Numerical output.

		Numerical output
S11 - tension (X)	[N/mm^2]	0,0
S22 - tension (Y)	[N/mm^2]	1,907
S33 - tension (Z)	[N/mm^2]	0,0
S11 - compression (X)	[N/mm^2]	3,919
S22 - compression (Y)	[N/mm^2]	2,488
S33 - compression (Z)	[N/mm^2]	0,0
Max. Principal	[N/mm^2]	1,954
Min. Principal	[N/mm^2]	4,030
S12 - shear (XY)	[N/mm^2]	-1,334 to +1,808

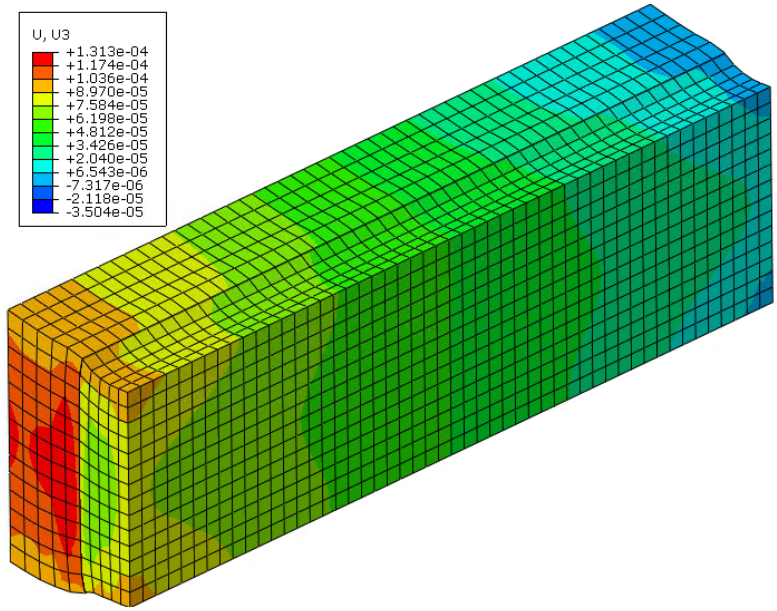

Figure C.43: Longitudinal expansion, deformation scale factor: 10 (Abaqus).

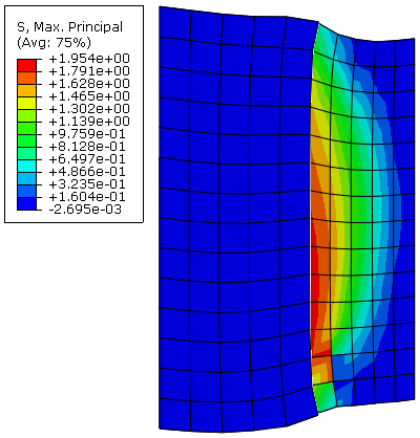

(a) Max. principal stresses

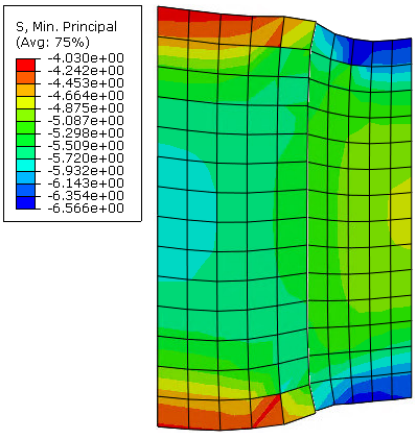

(b) Min. principal stresses

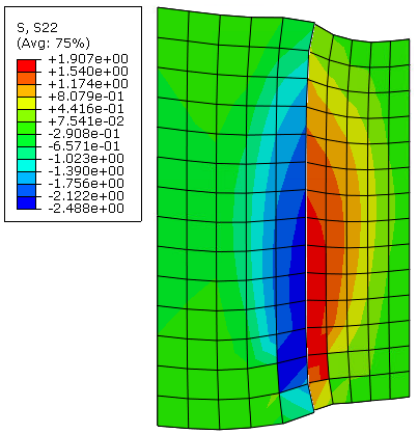

(c) Radial stresses (S22)

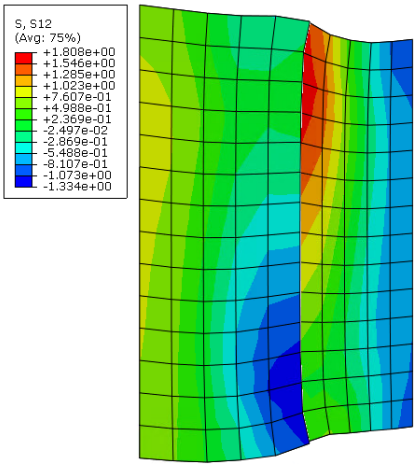

(d) Shear stresses (S12)

Figure C.44: Numerical output, deformation scale factor: 10 (Abaqus).